AFCRL-72-0075

A CENTER OF COMPETENCE IN SOLID STATE MATERIALS AND DEVICES

by

Fredrik A. Lindholm, Arthur J. Brodersen, Eugene R. Chenette,
Larry L. Hench, Sheng S. Li

Electrical Engineering Department
College of Engineering
University of Florida
Gainesville, Florida 32601

Contract No. F 19628-68-C-0058

Project No. 8627

Scientific Report No. 8
10 October 1971

Contract Monitor
Andrew C. Yong
Solid State Sciences Laboratory

Sponsored by

Advanced Research Projects Agency
ARPA Order No. 1060

Prepared
for

AIR FORCE CAMBRIDGE RESEARCH LABORATORIES
AIR FORCE SYSTEMS COMMAND
UNITED STATES AIR FORCE
BEDFORD, MASSACHUSETTS 01730

DISCLAIMER NOTICE

THIS DOCUMENT IS THE BEST QUALITY AVAILABLE.

COPY FURNISHED CONTAINED A SIGNIFICANT NUMBER OF PAGES WHICH DO NOT REPRODUCE LEGIBLY.

Program Code No. 1D10
Effective Date of Contract . . . . . 11 September 1967
Contract Expiration Date . . . . . 31 August 1972
Principal Investigator and Phone No. . . . . Dr. Fredrik A. Lindholm/904 392-0904
Project Scientist and phone no. . . . . Dr. Andrew C. Yang/617 861-2225

Unclassified
Security Classification

DOCUMENT CONTROL DATA - R&D

(Security classification of title, body of abstract and indexing annotation must be entered when the overall report is classified)

1. ORIGINATING ACTIVITY *(Corporate author)*
University of Florida
Engineering and Industrial Experiment Station
Gainesville, Florida 32601

2a. REPORT SECURITY CLASSIFICATION
Unclassified

2b. GROUP

3. REPORT TITLE
A CENTER OF COMPETENCE IN SOLID STATE MATERIALS AND DEVICES

4. DESCRIPTIVE NOTES *(Type of report and inclusive dates)*
Scientific Interim

5. AUTHOR(S) *(First name, middle initial, last name)*
Fredrik A. Lindholm
Arthur J. Brodersen
Eugene R. Chenette
Larry L. Hench
Sheng S. Li

6. REPORT DATE
10 October 1971

7a. TOTAL NO. OF PAGES
171

7b. NO. OF REFS
95

8a. CONTRACT OR GRANT NO.
F 19628-68-C-0058 ARPA Order No. 1060

b. PROJECT, TASK, WORK UNIT NOS.
8687 n/a n/a

c. DOD ELEMENT
61101D

d. DOD SUBELEMENT
n/a

9a. ORIGINATOR'S REPORT NUMBER(S)
Scientific Report No. 8

9b. OTHER REPORT NO(S) *(Any other numbers that may be assigned this report)*
AFCRL-72-0075

10. DISTRIBUTION STATEMENT
1 A - Approved for public release; distribution unlimited

11. SUPPLEMENTARY NOTES
This research was supported by
Advanced Research Projects Agency

12. SPONSORING MILITARY ACTIVITY
Air Force Cambridge Research
Laboratories (CR)
L. G. Hanscom Field
Bedford, Massachusetts 01730

13. ABSTRACT This report describes technical findings concerned with single-crystal semiconductors and devices and with the radiation sensitivity of amorphous semiconductors. Measured response times and noise equivalent powers suggest the potential of the photomagnetoelectric and Dember effects in Gold-doped silicon for photodetection. For Cr-doped gallium arsenite we describe the recombination and trapping behavior of photo-injected carriers. For n-type indium antiminide measurements of the PME and PC effects yields values for the carrier lifetimes and the hole mobility. Buried layers, in silicon transistors may cause the collector breakdown voltages to be considerably less than existing theory predicts; we describe an effect that accounts for the observed behavior. A method is described for incorporating systematic model selection into the simulation of semiconductor circuit behavior; applicability for radiation environments is discussed. For a KPO_3-V_2O_5 semiconducting glass the fast neutron irradiation damage threshold for structural dependent electronic processes is found to be 5×10^{16} nvt; the radiation behavior is interpreted by a theoretical model. The fast neutron irradiation sensitivity of electronic properties of heterogeneous semiconducting glasses containing crystallites is established at fluences from 1×10^{17} to 3×10^{17} nvt; based on these results and on softening point correlations, a prediction of the radiation sensitivity of other amorphous semiconductor systems is made.

DD FORM 1 NOV 65 1473

Unclassified
Security Classification

14. KEY WORDS	LINK A		LINK B		LINK C	
	ROLE	WT	ROLE	WT	ROLE	WT
semiconductors						
semiconducting glasses						
irradiation properties						
detectors						
transistors						

AFCRL-72-0075

A CENTER OF COMPETENCE IN SOLID STATE MATERIALS AND DEVICES

by

Fredrik A. Lindholm, Arthur J. Brodersen, Eugene R. Chenette,
Larry L. Hench, Sheng S. Li

Electrical Engineering Department
College of Engineering
University of Florida
Gainesville, Florida 32601

Contract No. F 19628-68-C-0058

Project No. 8687

Scientific Report No 8
10 October 1971

Contract Monitor
Andrew C. Yang
Solid State Sciences Laboratory

Sponsored by

Advanced Research Projects Agency
ARPA Order No. 1060

Prepared
for

AIR FORCE CAMBRIDGE RESEARCH LABORATORIES
AIR FORCE SYSTEMS COMMAND
UNITED STATES AIR FORCE
BEDFORD, MASSACHUSETTS 01730

Program Code No. 1D10
Effective Date of Contract . . . . . 11 September 1967
Contract Expiration Date . . . . . 31 August 1972
Principal Investigator and Phone No. . . . . Dr. Fredrik A. Linnholm 904 392-0904
Project Scientist and phone no. . . . . Dr. Andrew C. Yang 617 861-2225

ABSTRACT

This report describes technical findings concerned with single-crystal semiconductors and devices and with the radiation sensitivity of amorphous semiconductors. The potential of the photomagnetoelectric (PME) and Dember effects in Gold-doped silicon is suggested for photo-detection in the visible and near infra-red regions; measured response times and noise equivalent powers are reported. For Cr-doped gallium arsenide the development of a theoretical model and correlation with measurements of the PME and photoconductivity (PC) effects enables description of the recombination and trapping behavior of photo-injected carriers. For n-type indium antiminide a study of the PME and PC effects for temperatures between 4.2°K and 300°K yields values for the carrier lifetimes and the hole mobility and demonstrates the negligible influence of trapping processes. The presence of a buried layer in a bipolar silicon transistor may cause the value of the collector breakdown voltages to be considerably less than existing theory predicts; we describe an effect termed premature punch-through that accounts for the observed behavior. A method is described for the incorporation of systematic model selection into the computer simulation of semiconductor circuit behavior; applicability to the simulation of circuit behavior in a radiation environment is discussed. For a KPO_3-V_2O_5 semiconducting glass we establish the fast neutron irradiation damage threshold for atomic structural dependent electronic processes to be 5×10^{16} nvt and interpret the radiation behavior by a theoretical model based on cluster hopping processes. The fast neutron irradiation sensitivity of electronic properties of heterogeneous semiconducting glasses containing crystallites is established at fluences from 1×10^{17} to 3×10^{17} nvt; based on these results and on softening point correlations, a prediction of the radiation sensitivity of other amorphous semiconductor systems is made. A computer program is described which manipulates the approximately 12,000 data points generated in a combined dielectric and thermogravimetric absorption isotherm study.

SUMMARY

This report, for the eighth semi-annual period of contract support, describes technical findings in two main subject areas: single-crystal semiconductors and devices; and radiation sensitivity of amorphous semiconductors.

SINGLE-CRYSTAL SEMICONDUCTORS AND DEVICES:

We suggest the potential of the photomagnetoelectric and Dember effects in gold-doped silicon for photodetection in the visible and near I-R wavelength region. For a PME cell a response time t_r of 0.2 μsec and a noise equivalent power (NEP) of 6×10^{-10} watts are demonstrated; for a Dember cell, the corresponding data are $t_r < 0.03$ μsec and NEP = 2.5×10^{-10} watts.

A theoretical and experimental study is reported of the recombination and trapping processes governing the behavior of photoinjected carriers in semi-insulating Cr-doped GaAs. The experimental portion of the study consists in measuring the photomagnetoelectric (PME) and photoconductive (PC) effects between 80°K and 300°K. To interpret the data, we develop a theory of the PME and PC effects that takes into account the variation of carrier lifetimes with injected carrier density and the trapping of holes in the chromium levels. The theory predicts a power-law relationship between the PME short circuit current I_{PME} and the photoconductance ΔG, with different exponents in the power law applying for different injection ranges. Two well-defined ranges of injection were observed: For high injection, I_{PME} is directly proportional to ΔG, and for intermediate injection, I_{PME} varies in proportion as $\Delta G^{1.2}$. Numerical values of the lifetimes τ_n and τ_p are given as functions of ΔG. The results are in good agreement with the theoretical predictions.

A study of the photomagnetoelectric (PME) and photoconductive (PC) effects in N-type InAs single crystals is described for the temperature range between 4.2°K and 300°K under low injection conditions. For T > 77°K the PME open-circuit voltage varies in proportion to the magnetic induction and for T < 21°K the PME open-circuit voltage saturates at large magnetic induction. These observations agree with the predictions of large Hall-angle PME theory. For temperatures between 4.2°K and 300°K, carrier lifetimes are computed from the PME and PC data between 4.2°K and 300°K; the hole mobility is estimated from the PME data at 21°K and 4.2°K. The observed linear relationship between the PME open-circuit voltage and photoconductance at low light levels demonstrates that trapping contributes negligible effect over the entire temperature range from 4.2°K to 300°K.

The presence of a buried layer in a bipolar silicon transistor may cause the value of the collector breakdown voltages BV_{CES} and BV_{CBO} to be considerably less than existing theory predicts. We describe an effect termed premature punch-through that accounts for the observed behavior. Expressions are derived for the premature punch-through voltage BV_{PPT} and the thickness $(W_{EPI})_{OPT}$ of the epitaxial collector that maximizes this voltage and, hence, the usable region of device operation. The expression for BV_{PPT} is shown to be consistent with measurements taken on transistors fabricated in our laboratory.

We describe how systematic selection of transistor models can be incorporated into the computer simulation of semiconductor circuit behavior. The selection is so done that each model chosen provides the best accuracy-simplicity compromise for the circuit environment in which each transistor resides. Compared with other procedures now available, the method described here simplifies computation, saves computational cost, and enables simulation of larger circuits. Applicability to the simulation of circuit behavior in a radiation environment is discussed.

RADIATION SENSITIVITY OF AMORPHOUS SEMICONDUCTORS:

A fast neutron irradiation damage threshold for atomic structural dependent electronic processes in a KPO_3-V_2O_5 semiconducting glass is established as 5×10^{16} nvt. This radiation threshold depends neither upon thermal processing nor upon microstructure of the glasses. The radiation behavior is interpreted in terms of a cluster hopping model.

Fast neutron irradiation sensitivity of certain electronic properties of heterogeneous semiconducting glasses containing crystallites is established at fluences from $1\text{-}3 \times 10^{17}$ nvt. Relaxation loss spectra are appreciably changed by the irradiation. Presumably, this occurs because of disordering of the phase barriers which are responsible for interfacial polarization in the material. A prediction of the radiation sensitivity of other amorphous semiconductor systems is made based on these results and on softening point correlations.

A computer program is described which manipulates the approximately 12,000 data points generated in a combined dielectric and thermogravimetric adsorption isotherm study. Applications of this method to characterizing the surface dependent behavior of electronic materials are suggested.

TABLE OF CONTENTS :

III. Cont.

I. Introduction

The original general objective of this research program was to establish at the University of Florida a "Center of Competence in Solid State Materials and Devices." From the efforts expended in developing this center of competence have evolved technical findings: technical findings concerning such materials as glass ceramics, semiconducting glasses, magnetic films, degenerate materials and degenerate semiconductors; concerning devices made from these materials; concerning measurement techniques; and concerning methods of fabrication. The first of the findings in these various areas are described in seven previous scientific reports.[1-7] To Scientific Report No. 1 the reader is referred for a more detailed statement of the research objectives than given here and for a discussion of the means to be used in achieving these objectives.

In accordance with an agreement made with the contact monitor in January 1971, we have focussed the objectives of this research program to give greatest emphasis to the following problem areas:

1. The development of new types of detectors with stress given to utilizing the Dember and photomagnetoelectric effects in semiconductors and to utilizing new mask geometries compatible with conventional silicon technology.

2. Full static and dynamic characterization of bipolar and field-effect devices aiming both toward improved device design and toward improved circuit implementation. The characterization will deal with operation over a wide range of temperatures, with emphasis on the range between ordinary room temperature and cryogenic temperatures.

3. The incorporation of the effects of irradiation into the characterization of device behavior; junction field-effect devices will receive special attention. Emphasis will be placed on the development of characterizations enabling computer simulation and design of circuits.

4. Noise studies proceeding collaterally with each of the efforts listed above. Moreover, studies will continue dealing with the noise associated with Zener and avalanche phenomena in field-effect and bipolar devices.

5. Radiation studies of amorphous semiconductors.

To a large degree, the content of the present report reflects this change in emphasis. In the presentation to follow, Section II describes the results of research concerning single-crystal semiconductors and semiconductor devices, and Section III reports findings concerned with radiation effects in semiconducting glasses.

REFERENCES

1. F. A. Lindholm et al, Scientific Report No. 1, Contract #F 19628-68-C-0058, College of Engineering, University of Florida, 10 April 1968.

2. F. A. Lindholm et al, Scientific Report No. 2, Contract #F 19628-68-C-0058, College of Engineering, University of Florida, 10 October 1968.

3. F. A. Lindholm et al, Scientific Report No. 3, Contract #F 19628-68-C-0058, College of Engineering, University of Florida, 10 April 1969.

4. F. A. Lindholm et al, Scientific Report No. 4, Contract #F 19628-68-C-0058, College of Engineering, University of Florida, 10 October 1969.

5. F. A. Lindholm et al, Scientific Report No. 5, Contract #F 19628-68-C-0058, College of Engineering, University of Florida, 10 April 1970.

6. F. A. Lindholm et al, Scientific Report No. 6, Contract #F 19628-68-C-0058, College of Engineering, University of Florida, 10 October 1970.

7. F. A. Lindholm et al, Scientific Report No. 7, Contract #F 19628-68-C-0058, College of Engineering, University of Florida, 10 March 1971.

II. Single Crystal Semiconductors and Devices (A. J. Brodersen, E. R. Chenette, S. S. Li and F. A. Lindholm)

A. PHOTODETECTION USING PHOTOMAGNETOELECTRIC AND DEMBER EFFECTS IN GOLD-DOPED SILICON (H. F. Tseng and S. S. Li)

The first report on utilizing the photomagnetoelectric (PME) effect for light detection using Ge cell was made by Boatright and Mette.[1] Zitter[2] has subsequently developed an InSb PME detector capable of demodulating optical masers at wavelength up to 7 μm.

In this letter we report our study of the PME and Dember effect detectors made of gold-doped n- and p-type silicon wafers, operating between -20°C and +50°C. It is found that the detector's detectivity is limited by Johnson noise and the response speed is by RC time constant of the detector system.

In our recent work[3] we have developed a general theory to account for the PME and Dember effects in gold over-compensated silicon for the small signal case. The results are that the PME open circuit voltage is given by[3]

$$V_{PME} = B \cdot \frac{1+b}{\Gamma^{-1}+b} \left(\frac{n_o\Gamma^{-1}+p_o}{n_o b+p_o}\right)^{\frac{1}{2}} \left(\frac{D_n}{\tau_n}\right)^{\frac{1}{2}} \frac{\Delta G}{G_o} \qquad (1)$$

and the Dember voltage is

$$V_D = \frac{d(b-\Gamma^{-1})}{\mu_n(b+\Gamma^{-1})} \left(\frac{n_o b+p_o}{n_o\Gamma^{-1}+p_o}\right)^{\frac{1}{2}} \left(\frac{D_n}{\tau_n}\right)^{\frac{1}{2}} \frac{\Delta G}{G_o} \qquad (2)$$

where

V_{PME} is the PME open circuit voltage per unit sample length

V_D is the open circuit Dember voltage, d is the sample thickness

B denotes the magnetic flux density

μ_n, τ_n, D_n, n_o, p_o and b ($=\mu_n/\mu_p$) has the conventional meaning.

Γ is the ratio of excess electron and hole density ($\Gamma = \Delta n/\Delta p$).

ΔG and G_o are the photoconductance and dark conductance per unit sample width to length ratio, respectively.

The above two equations indicate that the V_{PME} and V_D are directly proportional to the photoconductance ΔG which in turn varies linearly with the light intensity for small signal case. This is experimentally observed for all the cells reported in this paper.

The reasons for using gold-doped silicon as detector material are two-fold: (1) gold-doped silicon has extremely short excess carrier lifetime and therefore fast response cell could be built. (2) High resistivity silicon could be achieved by gold doping and hence increases the sensitivity of the PME and Dember effects in silicon.

Gold-doped n- and p-type silicon PME and Dember cells with different gold density and shallow impurity concentrations were fabricated and tested. The typical cell's dimensions were 5x2x0.1 mm^3. The experimental data and calculated parameters for several cells are summarized in Table I for comparison. The spectral response of the PME and Dember cells are similar to the conventional silicon photodetectors with the peak response occurring near 0.6 μm, and the response is relatively flat ranging from 0.45 μm to 0.7 μm. The normalized PME open circuit voltage V_{PME} (with V_{PME} at 25°C as reference) as function of temperature between -20°C and +50°C for samples N-1-d, N-2-d, and N-4-d is shown in Fig. 1.

The result shows that for each cell there exists a peak sensitivity temperature, and the position of this peak shifts to the lower temperature side as the cell's resistivity decreases. The result also indicates that the temperature sensitivity of each cell around room temperature is independent of its resistivity. The change in PME response (V_{PME}) for these cells is two percent per °C around 25° ±10°C.

The noise measurement on PME detectors indicates that the $\frac{1}{f}$ noise dominates for frequencies below 1 KHz and the thermal noise is the only component for f>1 KHz. Further experiments indicate that the noise level does not change when the cell is exposed or removed from the light. This fact shows that thermal noise rather than g-r noise will constitute the lower limit for the detection of weak signal.

Our PME cell's response speed measurements indicate that the detector response time is controlled by the cell's RC time constant rather than by the excess carrier lifetimes. It is noted from Table I that for cells with high internal resistance the responsivity is high, while cells with low internal resistance have relatively low responsivity and short RC time constant. To fabricate a PME light detector of considerable sensitivity and fast response speed, it requires to compromise the doping concentration of gold and shallow impurities in silicon.

The general features of a Dember cell are analog to that of a PME detector. Table I summarized results of Au-doped n- and p- type cells. The measured sensitivity in both cells is two orders of magnitude lower than the value predicted by Eq. (2). This might be due to the fact that the photo-injected carriers have a very short diffusion length (of the order of few μm) and the large ohmic contact area which shortens a large part of the Dember voltage.

In summary, as a photodetector, a Dember cell has a compact structure with a faster response speed and lower sensitivity than a PME cell. However, a PME cell, aside from using it as a photodetector, can also be used as a Gaussmeter by incorporating it with a small GaAs light emitting diode.

REFERENCES

1. A. Boatright and H. Mette, Proc. of the 1962 Army Science Conf., West Point, New York, Vol. 1, pp. 31-46.
2. R. N. Zitter, Rev. of Sien. Instr., 35, 5, p. 594 (1964).
3. S. S. Li and H. F. Tseng, Phys. Rev. B., Vol. 4, pp. 490-497 (1971).

TABLE I Performance Characteristics of Au-doped Si PME/Dember Detectors at 300°K

A. PME Detector	Sample No.	Type	N_D or N_A cm^{-3}	N_{Au} cm^{-3}	R(Ω)	Responsivity ($mV/mW/cm^2$)	Response Time (sec)	RC Time Constant μ sec.	$NEP_{\frac{1}{2}}$ ($W/H_z^{\frac{1}{2}}$)
(1) measured at B = 10 kG	N-1-d	n	5×10^{15}	8×10^{16}	27×10^{6}	100	8.1×10^{-9}	40	6.7×10^{-11}
(2) capacitance for each sample is less than 1.5 pf.	N-2-d	n	10^{16}	8×10^{16}	2×10^{6}	13	8.7×10^{-9}	6	1.4×10^{-10}
	N-3-d	n	10^{16}	5×10^{16}	10^{6}	4	1.5×10^{-8}	1.5	3.2×10^{-10}
	N-4-d	n	1.5×10^{16}	2×10^{16}	0.125×10^{6}	0.7	1.2×10^{-7}	0.185	6.5×10^{-10}
(3) spectral response 0.4 ~ 1 μm	P-5-d	p	10^{15}	3×10^{16}	0.19×10^{6}	0.5	1.6×10^{-8}	0.28	1.12×10^{-9}
	P-6-d	p	10^{14}	10^{16}	0.25×10^{6}	1	1.6×10^{-7}	0.37	6.43×10^{-10}
B. Dember Detector	D-1-d	n	10^{16}	5×10^{16}	10^{3}	0.17	1.5×10^{-8}	<0.03	2.5×10^{-10}
	D-2-d	p	10^{14}	10^{16}	400	0.02	1.6×10^{-7}	<0.012	1.28×10^{-9}

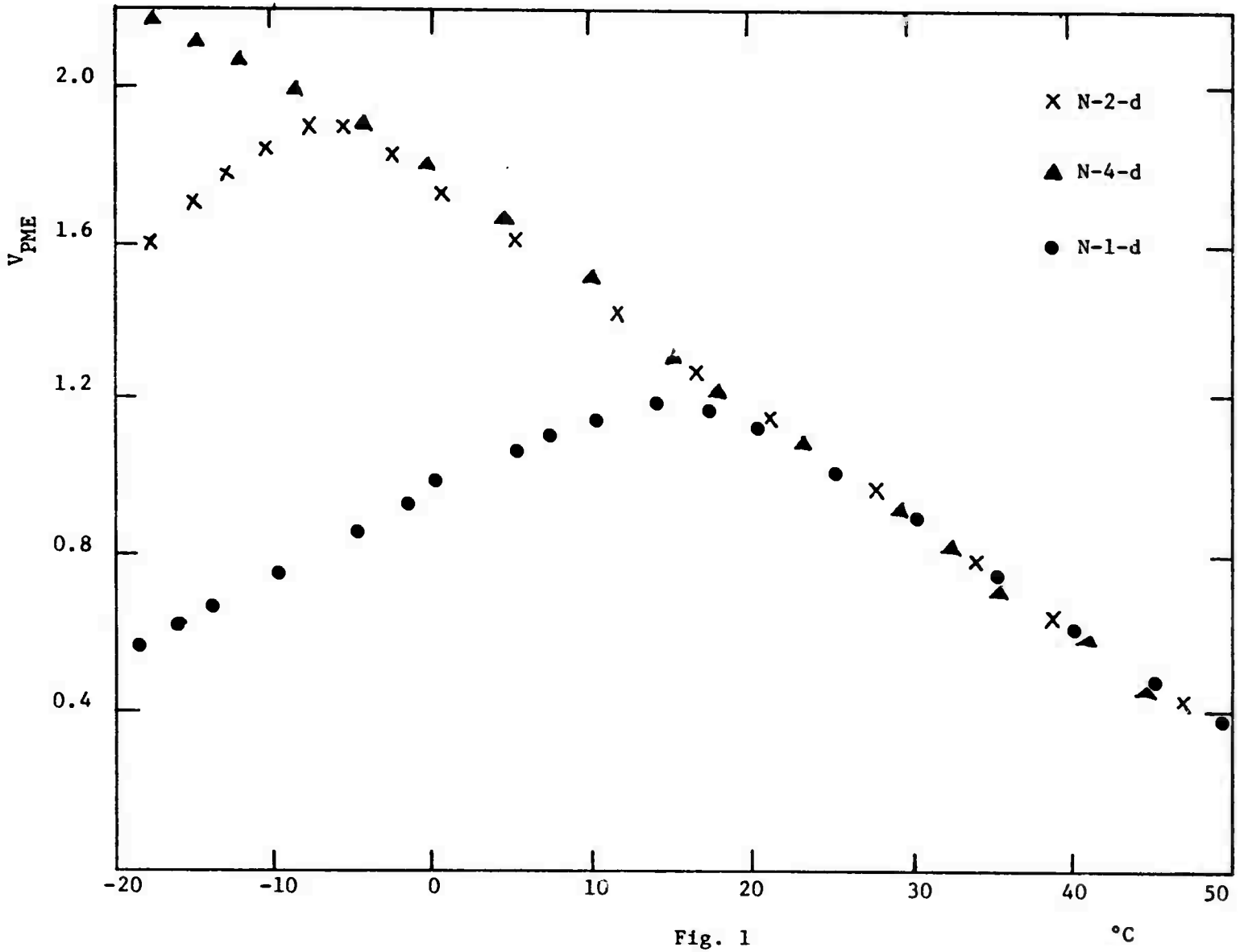

Fig. 1

Normalized V_{PME} (V_{PME}/V_{PME} at 25°C) versus temperature, T. for samples N-1-d, N-2-d and N-4-d.

B. INVESTIGATION OF THE RECOMBINATION AND TRAPPING PROCESSES OF PHOTO-INJECTED CARRIERS IN SEMI-INSULATING Cr-DOPED GaAs USING PME AND PC METHODS (S. S. Li and C. I. Huang)

I. Introduction

Photoconductivity (PC) and photomagnetoelectric (PME) effects in undoped semi-insulating and semiconducting GaAs single crystals were first reported by Holeman and Hilsum.[1] Hurd[2] reported the experimental results of the Dember and PME effects in O_2-doped GaAs between 140°K and 300°K. The photoelectronic analysis of high-resistivity n-type GaAs was given by Bube,[3] based on the recombination theory of Rose.[4] A more recent study on the photoconductivity of high resistivity GaAs and Cr-doped GaAs was reported separately by Broom,[5] and Milner-Brown and Fortin.[6] These authors analyzed the observed photoconductivity data mainly for the small injection conditions. In this paper we report the results of our measurement of the PME and PC effects in semi-insulating chromium-doped GaAs ($\rho \sim 10^8$ Ω-cm) at T = 80°K and 300°K. A generalized theory to account for the observed PME and PC effects in Cr-doped GaAs is developed by considering the carrier lifetimes as a function of injection and the effect of the trapping. Based on the theory, we are able to define different ranges of injections in which a power law relationship is obtained between the PME short circuit current, I_{PME} and the photoconductance, ΔG. This is verified by our PME and PC experiment, in which we observed two distinct and well-defined injection ranges.

II. Trapping and Recombination Processes

In steady state injection, the emission and capture of carriers by the impurity centers cause the charge in such centers to change from its equilibrium values. Therefore, the density of carriers trapped in the impurity states is a function of injected carrier densities. If the density of these traps is larger than the excess carrier density, the charge in them will play an important role in preserving the charge neutrality under steady state injection. This has been shown by Agraz and Li[7] in gold-doped silicon, where they observed that the charged impurity centers completely dominate in charge neutrality except at high injection. This theory has been verified by them from the results of PME and PC measurements in gold-doped silicon under small and intermediate injection conditions.[8-9]

The recombination model for the semi-insulating Cr-doped GaAs resembles that of gold-doped silicon due to the fact that chromium atoms introduce one single deep acceptor level in GaAs.[10] This level is located near the middle of the band gap, and is an effective recombination center for the excess carriers under illumination conditions. A very high resistivity n-type GaAs can be obtained by doping semiconducting n-type GaAs with chromium. This is

due to the auto-compensation effect of chromium impurity with the shallow donor impurities in GaAs.[5]

In order to understand the charge states in the chromium levels under dark and illumination conditions, an energy band diagram for the Cr-doped GaAs is presented in Fig. 1. In thermal equilibrium, the chromium levels are occupied by the conduction electrons (see Fig. 1(a)), and are in negatively-charged states. In steady state injection (e.g., by means of photoexcitation), the free holes in the valence band are captured by the negatively-charged chromium centers due to coulomb attractive potential. As a result, these trapped holes will tend to destroy the charge balance in the localized and band states. This is true for the case when the chromium density is much higher than the thermal equilibrium electron concentration. If the injection is increased subsequently, more and more negatively-charged chromium centers will become neutral as a result of hole trapping at that level. This is illustrated in Fig. 1(b), which corresponds to the situation of the intermediate injection case. In this range of injection, the excess carrier densities Δn and Δp can be correlated by a trapping constant Γ (where $\Gamma = \frac{\Delta p}{\Delta n} = \frac{\tau_p}{\tau_n} < 1$). In addition to the trapping effect, the carrier lifetimes may also depend on the injected carrier density (or incident photon flux density). This dependence can, in general, be expressed in terms of a powerlaw relationship between τ_n and Δn, namely $\tau_n = \kappa \Delta n^{\beta}$ (values of κ and β will be discussed later). In the high injection region, the injected carrier density exceeds the chromium concentration (i.e., $\Delta n = \Delta p > N_{cr}$) and the chromium acceptor levels are occupied by holes, being in neutral charge states. As a result, the charge states in localized and band states are essentially controlled by injected carrier densities (i.e., $\Delta n = \Delta p$), and the electron and hole lifetimes are equal and independent of injection. The trapping constant Γ, for this case, is equal to unity and $\beta = 0$. The corresponding energy band diagram for this range of injection is shown in Fig. 1(c).

The above simple physical model can be used in the development of the generalized theory for PME and PC effects in chromium-doped GaAs under large injection conditions.

III. Photoconductive and Photomagnetoelectric Effects

Since the experimental conditions for the PME and PC measurements on Cr-doped GaAs are such that the excess electron density, Δn, is always greater than n_o, the derivation of PME and PC theory will be made under the assumption of large injection conditions (i.e., $\Delta n >> n_o$ and $\Delta p >> p_o$).

The effect of trapping can be expressed by

$$\Delta p = \Gamma \Delta n \tag{1}$$

where $\Gamma = \tau_p/\tau_n < 1$ for hole trapping.
And the dependence of carrier lifetimes on the injected carrier density can be written as

$$\tau_n = \kappa \Delta n^{\beta} \tag{2}$$

With the help of Eqs. (1) and (2), the generalized expressions for the PME short circuit current and the photoconductance can be obtained as follows:

The photoconductance per unit sample length-to-width ratio is given by:[7]

$$\Delta G = q \int_o^d (\mu_n \Delta n + \mu_p \Delta p) dy$$

$$= q \mu_n \int_o^{\Delta n_o} (\Delta n + \frac{\Delta p}{b}) \frac{D \, d\Delta n}{\Gamma n} \Big/ \left[2 \int_o^{\Delta n_o} DK d\Delta n\right]^{\frac{1}{2}} \tag{3}$$

where

$$D = \frac{2D_n \Gamma}{(\Gamma+b)} \text{ is the effective diffusion constant} \tag{3-a}$$

$$\triangleq 2D_p \Gamma \text{ for } b >> \Gamma$$

and

$$R = \frac{\Delta n}{\tau_n} = \frac{\Delta n}{\kappa \Delta n^{\beta}} = \frac{1}{\kappa} \Delta n^{1-\beta} \text{ is the rate of recombination} \tag{3-b}$$

Since the electron-hole mobility ratio, b, in GaAs is much greater than unity (we use b = 20 in this paper)[13] and the trapping constant Γ is smaller than unity (we found that in the intermediate injection range, $\Gamma \sim 0.18$ at 300°K and $\Gamma \sim 0.084$ at 80°K), it is therefore adequate to assume that $b >> \Gamma$ in the derivations of ΔG and I_{PME}.

Solving Eqs. (3), (3-a) and (3-b), we obtain the general expression of photoconductance, ΔG

$$\Delta G \triangleq \left(\frac{2q\mu_n}{2+\beta}\right)\left[(2-\beta)D_p \Gamma \kappa\right]^{\frac{1}{2}} \Delta n_o^{\frac{2+\beta}{2}} \tag{4}$$

Eq. (4) is valid for different injection ranges so long as the conditions given by Eqs. (1) and (2) are satisfied. The values of β in Eq. (4) may change from one injection range to the other and can be determined from measurement of the slope of the I_{PME} versus ΔG plot. Δn_o in Eq. (4) denotes the excess electron densities at the illuminated surface, which is related to the incident photon flux density.

The PME short circuit current per unit width of the sample, I_{PME}, is given by[7]

$$I_{PME} = q\, u_p (1+b)\, B \int_0^{\Delta n_o} D\, d\Delta n \qquad (5)$$

Solving Eqs. (3-a) and (5), we obtain the general expression for the PME short circuit current:

$$I_{PME} = 2q\mu_p (1+b)\, D_p\, \Gamma B\, \Delta n_o \qquad (6)$$

The relationship between I_{PME} and ΔG can now be obtained from Eqs. (4) and (6) by eliminating Δn_o from these two equations. The result yields

$$I_{PME} \triangleq 2q\mu_p (1+b)\, B\, \Gamma D_p \left[\frac{(2+\beta)^2}{4(2-\beta)D_p \Gamma\kappa}\right]^{\frac{1}{2+\beta}} \left(\frac{\Delta G}{q\mu_n}\right)^{\frac{2}{2+\beta}} \qquad (7)$$

The general expression of I_{PME} versus ΔG given in Eq. (7) is rather important, since it provides a direct correlation between the two measurable parameters I_{PME} and ΔG, and allows us to make a direct comparison of the theoretical prediction with the experimental results.

The general expressions for I_{PME} and ΔG, given above, can be reduced to a very simple form under certain injection conditions such as in the high injection region in which these parameters are linearly related to one another. To be more specific, we have observed two well-defined injection regions in the PME and PC measurements for the Cr-doped GaAs. This will be discussed in detail as follows:

(1) <u>High injection region ($\Delta n = \Delta p >> n_o, N_{cr}$)</u>

In this injection region (see Fig. 1-c), the excess electron and hole densities are much higher than the thermal equilibrium carrier concentration n_o and the electrically active chromium density N_{cr}. The charge neutrality condition is essentially controlled by the excess electron and hole densities. The carrier lifetime is independent of light intensity (or injection)[11] and the effect of trapping is completely negligible. As a result, the conditions given by Eqs. (1) and (2) can be reduced to the forms that

$$\Delta n = \Delta p \quad (\text{i.e., } \Gamma = 1) \qquad (1\text{-a})$$

and

$$\tau_n = \tau_p = \tau_\infty \quad (\text{i.e., } \beta = 0) \qquad (2\text{-a})$$

where τ_∞ is the carrier lifetime at high injection as defined by Shockley and Read.[11]

With the help of Eqs. (1-a) and (2-a), the photoconductance for this case is obtained from Eq. (4) by setting $\beta = 0$ and $\Gamma = 1$, which yields

$$\Delta G = q\mu_p(1+b)\,(D_a\tau_n)^{\frac{1}{2}}\,\Delta n_o \qquad (8)$$

where $D_a = \frac{2D_n}{1+b} \triangleq 2D_p$ is the ambipolar diffusion constant.

The PME short circuit current is obtained from Eq. (6) for $\Gamma = 1$

$$I_{PME} = q\mu_p(1+b)\,D_a B\,\Delta n_o \qquad (9)$$

The relationship between I_{PME} and ΔG for this case is obtained from Eqs. (8) and (9). The result yields

$$I_{PME} = \left(\frac{D_a}{\tau_n}\right)^{\frac{1}{2}} B\,\Delta G \qquad (10)$$

Furthermore, the PME open circuit voltage per unit length is obtained from Eq. (10) using the relation:[12]

$$V_{PME} = \frac{I_{PME}}{\Delta G} = \left(\frac{D_a}{\tau_n}\right)^{\frac{1}{2}} B \qquad (11)$$

The above results are consistent with the PME theory derived by Van Roosbroeck[12] for the high injection case. In this range of injection, the I_{PME} varies linearly with ΔG, and the V_{PME} is independent of light intensity (or injection).

(2) Intermediate injection region ($\Delta n > n_o$, $\Delta n < N_{cr}$, $\Delta n \neq \Delta p$)

In this range of injection, the charge states in the chromium levels contribute a significant part in the charge neutrality condition. The free holes are trapped in the chromium levels. As a result, the relationship between Δn and Δp is given by Eq. (1).

In addition, the carrier lifetime in this range of injection may also depend on the injection (or light intensity). The value of β in Eq. (2), depending on the range of injection, can only be determined by the experimental observation such as from the I_{PME} versus ΔG plot (see Fig. 3). In the Cr-doped

In addition, the carrier lifetime in this range of injection may also depend on the injection (or light intensity). The value of β in Eq. (2), depending on the range of injection, can only be determined by the experimental observation such as from the I_{PME} versus ΔG plot (see Fig. 3). In the Cr-doped GaAs samples, we found that in the intermediate injection range, the value of β is equal to $-\frac{1}{3}$ and therefore the electron lifetime, τ_n, for this case is given by:

$$\tau_n = \kappa \Delta n^{-1/3} \qquad (2\text{-b})$$

With the help of Eqs. (1) and (2-b), the photoconductance for this case can be deduced from Eq. (4) by setting $\beta = -\frac{1}{3}$, which yields

$$\Delta G \triangleq \left(\frac{6}{5} q\mu_n\right) \left[\frac{7}{3} D_p \Gamma \kappa\right]^{\frac{1}{2}} \Delta n_o^{5/6} \qquad (12)$$

The expression of I_{PME} for this case remains the same as that of Eq. (6).

The I_{PME} in terms of ΔG is obtained by substituting $\beta = -\frac{1}{3}$ into Eq. (7). The result yields:

$$I_{PME} \triangleq 2q\mu_p(1+b)\, B \left[\frac{27 D_p^2 \Gamma^2}{343\, \kappa^3}\right]^{\frac{1}{5}} \left[\frac{5\Delta G}{6q\mu_n}\right]^{\frac{6}{5}} \qquad (13)$$

Eq. (13) predicts that I_{PME} varies as $\Delta G^{1.2}$, if other parameters on the right-hand side are independent of injection. This is observed for sample S-1 at 80°K and sample S-2 at 80°K and 300°K in the intermediate injection range.

IV. Experimental Details

Two slices of rectangular bar were cut from a Cr-doped GaAs single crystal wafer (total chromium density, 1-3 x 10^{17} cm^{-3}) made by zone-melting method. The sample dimensions are 0.5 x 1 x 0.1 cm^3 for sample # (S-1) and 0.4 x 0.8 x 0.1 cm^3 for sample # (S-2). The samples were mechanically lapped on all six faces and chemically etched on the illuminated surface by using a solution mixed with $3H_2SO_4:H_2O_2:H_2O$. Ohmic contact was made by indium alloying. Resistivity, Hall effect and Photo-Hall effect measurements were made on both samples at 80°K and 300°K.

The dark resistivity for sample # S-1 is 1.2 x 10^8 ohm-cm and 3 x 10^8 ohm-cm for sample # S-2 at 300°K. The Hall mobility was found to be about 250 cm^2/V-sec at 300°K. The low Hall mobility is attributed to the mixed conduction in Cr-doped

GaAs, occurring at room temperature, as pointed out by Inoue and Ohyama.[13] The electron mobility can be calculated from the conductivity expression given in reference 13, and the result for the present case is found to be $\mu_n \triangleq 1000$ cm^2/V-sec at 300°K. The slight difference in resistivity between # S-1 and # S-2 implies that the chromium densities are not equal in both samples. Presumably, sample #S-1 contains slightly lower chromium impurity density than that of # S-2. The Photo-Hall effect measurements over two samples indicate that the Hall mobility is a slow varying function of light intensity in measured injection ranges of our PME and PC experiments. For sample # 2, it is found $\mu_H \triangleq 150 \pm 30$ cm^2/V-sec at 300°K and $\mu_H \triangleq 450 \pm 50$ cm^2/V-sec at 80°K, in the intermediate injection range.

The technique for measurements of the PME and PC response is described in detail by Li[14] and will not be repeated here. A high intensity tungsten light source is used for the PME and PC measurements.

V. Results and Analysis

In Section IV we have reported the results of resistivity, Hall effect and photo-Hall effect measurements on two samples. In this section, we will present the results of PME and PC measurements at T = 300°K and 80°K.

The PME open circuit voltage (V_{PME}), the I_{PME} and ΔG are measured as functions of incident radiant power density, I_o, for T = 80°K and 300°K. The results are interpreted in terms of the theory developed in Section III. Comparisons between the theory and the experimental data are made for both samples. Important parameters such as τ_n and τ_p are deduced from the present results. It is noted that the results indicate that the effect of hole trapping in sample # S-1 is less severe than in sample # S-2. This is consistent with the data of resistivity and Hall effect measurements in which we have found that the chromium density is slightly lower in sample # S-1 than in sample # S-2. Figs. 2 through 4 show the results of the PME and PC measurements, which will be discussed subsequently, as follows:

(a) The PME open circuit voltage (V_{PME})

The PME open circuit voltage, V_{PME}, as a function of magnetic field, B, for sample # S-1 at T = 80°K and 300°K, for different light intensity, I_o, is shown in Fig. 2. The linear dependence of V_{PME} on B at 300°K for different light intensity is in accord with the theoretical prediction of Eq. (13). Deviation from linearity at 80°K is due to the increase in electron mobility with decreasing temperatures. Saturation of V_{PME} with increasing light inten-

sity as shown in Fig. 2 provides the evidence that experiments are indeed performed at high injection regions.

(b) The PME short circuit current versus photoconductance (I_{PME} versus ΔG)

In order to correlate the experimental results with the theory developed in the previous section, we plot I_{PME} versus ΔG for T = 80°K and 300°K for both samples, and the result is shown in Fig. 3. It is interesting to note that two-well-defined regions are obtained in the I_{PME} versus ΔG plots. In region I (high injection), I_{PME} is directly proportional to ΔG; this is observed for sample # S-1 at T = 300°K. In region II (intermediate injection), I_{PME} varies with $G^{6/5}$; this is observed for both samples at 80°K and for sample # S-2 at 300°K. To interpret this result, the generalized theory developed in the previous section is used for this purpose.

The high injection linear region observed for sample # S-1 at 300°K is in accord with the theoretical prediction of Eq. (11). The electron and hole lifetimes are equal and independent of light intensity. In the intermediate injection region (region II), the effect of hole trapping at the chromium acceptor levels and the dependence of τ_n on $\Delta n^{-1/3}$ leads to the observed dependence of I_{PME} on $\Delta G^{6/5}$ for both samples at 80°K and for sample # S-2 at 300°K. This is predicted by Eq. (13), derived in the previous section under the assumption that $\tau_n = \kappa \Delta n^{-1/3}$ and $\Delta p = \Gamma \Delta n$. The dependence of carrier lifetimes on the injected carrier densities has been cited by several authors,[1,11] although no explicit form has so far been proposed in the literature. In fact, the power law dependence of τ_n on Δn^{β} can be established for different injection ranges. The values of β may vary from material to material and the ranges of injection as well. (Li[14] has observed τ_n varies with $\Delta n^{-\frac{1}{2}}$ in silicon at low temperatures).

(d) Carrier lifetimes versus photoconductance

We have shown in the previous section that the lifetimes of holes and electrons are equal and independent of light intensity under high injection conditions. This is observed for sample # S-1. However, in the intermediate injection, the electron and hole lifetimes are, in general, functions of injection. In order to determine the electron and hole lifetimes as functions of injection, it is necessary to define an apparent lifetime τ_a, in the I_{PME} expression. This can be achieved by rewriting Eq. (13) in the form that

$$I_{PME} = \left(\frac{D_a}{\tau_a}\right)^{\frac{1}{2}} B\,\Delta G \tag{14}$$

where

$$\tau_a = \left(\frac{42}{25}\right)\left[\frac{7D_p\kappa^6}{3\Gamma^4}\right]^{1/5}\left(\frac{5\Delta G}{6q\mu_n}\right)^{-2/5} \tag{15}$$

is the PME apparent lifetime. Eq. (14) resembles Eq. (10) for the high injection case, with τ_n replaced by τ_a.

Eq. (15) predicts that the apparent lifetime τ_a is proportional to the $\Delta G^{-2/5}$ in the intermediate injection range.

With the help of Eq. (14) and Fig. 3, the apparent lifetime τ_a is computed as a function of ΔG and the results are shown in Fig. 4. The result of τ_a versus ΔG plot yields a slope of $-\frac{2}{5}$, which is in accord with the theoretical prediction of Eq. (15). Note that τ_a is equal to τ_n and τ_p in the high injection region.

In the intermediate injection region where trapping of holes at the chromium acceptor levels is essential, the electron lifetime is expected to be longer than the hole lifetime (i.e., $\Gamma < 1$). This is because the negatively-charged chromium acceptor levels have a larger capture cross section for holes than for electrons. To deduce the electron and hole lifetimes from the PME apparent lifetimes, we make use of the following relation in the presence of trapping:[15]

$$\tau_a = \frac{\Delta p\tau_n + \Delta n\tau_p}{\Delta n + \Delta p} = \frac{\tau_p + \Gamma\tau_n}{1 + \Gamma} \triangleq 2\tau_p \tag{16}$$

where we assume $\Gamma = \tau_p/\tau_n < 1$.

In essence, the PME apparent lifetime, τ_a is a parallel sum of τ_n and τ_p, and is controlled by the shorter of the two lifetimes, namely, τ_p. With the help of Eq. (15), τ_p is deduced from Eq. (16) and the results are shown in Fig. 4.

The remainder of the parameters τ_n, Γ and κ can be deduced subsequently by using Eqs. (15), (2-b) and Fig. 3, and the relation that $\Delta n = \Delta G/q\mu_n d$ (where d is the thickness of the sample). It is worth noting that the computed values of Γ and κ are fairly constant over the entire intermediate injection range. The value of Γ is found equal to 0.18 at 300°K and 0.084 at 80°K for sample # S-2, which shows that the ratio of τ_n/τ_p is about 5.5 at 300°K and is about 12 at 80°K for sample # S-2. The results are in good

agreement with the statement by Holeman and Hilsum [1] in that they predicted a ratio of $\tau_n/\tau_p < 10$ for semi-insulating GaAs. The present results show that the effect of hole trapping in the chromium levels is not too severe even at 80°K in the intermediate injection region, and can be ignored at high injection.

The decrease of electron and hole lifetimes (see Fig. 4) with increasing injection indicates that more and more chromium acceptor centers are converted from the originally hole-trapped centers to effective recombination centers for electrons as injection is increased. This is consistent with the recombination model proposed in Fig. 1.

VI. Conclusions

Photomagnetoelectric (PME) and photoconductive (PC) effects in semi-insulating chromium-doped GaAs have been investigated at T = 80°K and 300°K. Using a simple recombination and trapping model, a generalized theory has been developed for the PME and PC effects, taking into account the effect of trapping and the dependence of the carrier lifetimes on the injection, under large injection conditions. Good agreement between theory and experiment is obtained for two well-defined injection ranges; one region is characterized by a linear dependence of I_{PME} on ΔG and constant lifetime ($\tau_n = \tau_p = 2.5 \times 10^{-10}$ sec. at 300°K for sample # 3-1), and the other region is characterized by a nonlinear dependence of I_{PME} on ΔG (i.e., I_{PME} varies as $\Delta G^{1.2}$). Numerical values of τ_n, τ_p, ΔG and I_{PME} as functions of injection are given for both samples.

References

1. B. R. Holeman and C. Hilsum, J. Phys. Chem. Solids, vol. 22, 19 (1961).
2. C. M. Hurd, Proc. Phys. Soc., vol. 79, 42 (1962).
3. R. H. Bube, J. Appl. Phys., vol. 31, 315 (1960).
4. A. Rose, Phys. Rev., 97, 322 (1955).
5. R. F. Broom, J. Appl. Phys., vol. 38, 3483 (1967).
6. H. Milner-Brown and E. Fortin, Canadian J. Phys., vol. 47, 2790 (1969).
7. J. Agraz and S. S. Li, Phys. Rev. B, vol. 2, 4966 (1970).
8. J. Agraz and S. S. Li, Phys. Rev. B, vol. 2, 1847 (1970).
9. S. S. Li and H. F. Tseng, Phys. Rev. B, to be published (1971).
10. R. Cronin and R. W. Haisty, J. Electrochem. Soc. 111, 874 (1964).
11. W. Shockley and W. T. Read, Jr., Phys. Rev. 87, 835 (1952).
12. W. van Roosbroeck, Phys. Rev. 101, 1713 (1956).
13. T. Inoue and M. Ohyama, Solid State Comm., vol. 8, 1309 (1970).
14. S. S. Li, Phys. Rev. 188, 1246 (1969).
15. R. N. Zitter, Phys. Rev. 112, 852 (1958).

Figure Captions

Fig. 1 Energy band diagram for Cr-doped GaAs in thermal equilibrium and under steady state illumination

Fig. 2 The PME open circuit voltage, V_{PME} versus magnetic flux density, B, for different light intensities

a) I_o = 100 mW/cm^2, b) 40 mW/cm^2, c) 22 mW/cm^2, d) 11 mW/cm^2,

e) 4 mW/cm^2, f) 2 mW/cm^2

a') I_o = 256 mW/cm^2, b') I_o = 100 mW/cm^2, c') I_o = 40 mW/cm^2.

Fig. 3 The PME short circuit current per unit width of sample, I_{PME}, versus photoconductance, ΔG, for samples #S-1 and #S-2, at 80°K and 300°K. In region (I), I_{PME} is proportional to ΔG, and in region (II), I_{PME} varies with $\Delta G^{1.2}$ ($B = 0.1\ Wb/m^2$).

Fig. 4 The PME apparent lifetime τ_a, the electron lifetime, τ_n and the hole lifetime τ_p versus ΔG in the intermediate injection region (region II) for sample #S-2 at 80°K and 300°K. The slope of τ versus ΔG is - 2/5.

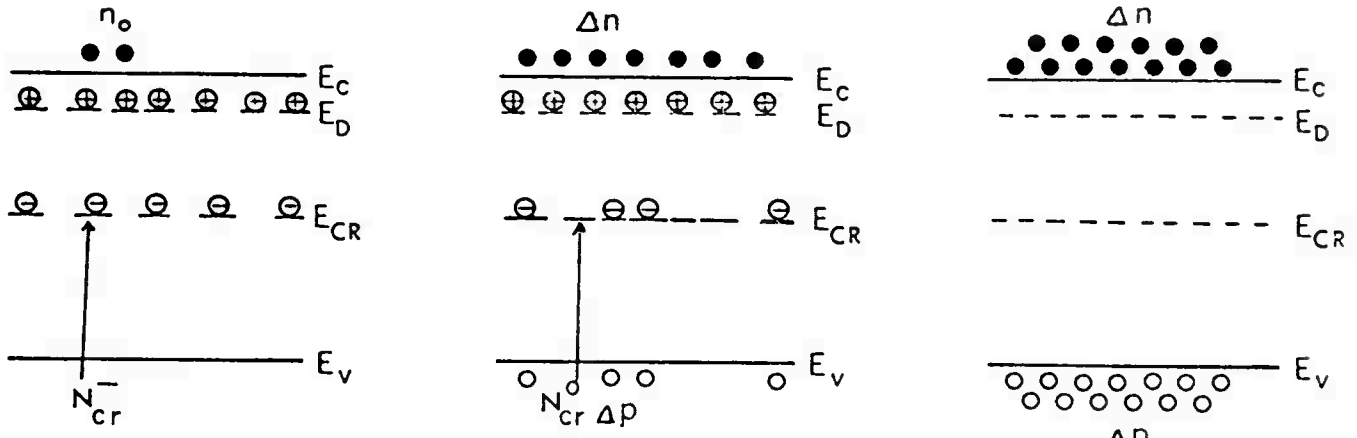

(a) In thermal equilibrium

(b) Intermediate injection

$\Delta p = \Gamma \Delta n \quad (\Gamma << 1)$

$\tau_n = \kappa \Delta n^{-1/3}$

$\tau_p = \Gamma \tau_n \ , \Delta n < N_{cr}$

(c) High injection

$\Delta n = \Delta p > N_{cr}$

$\tau_n = \tau_p = \tau_\infty$

FIG. 1

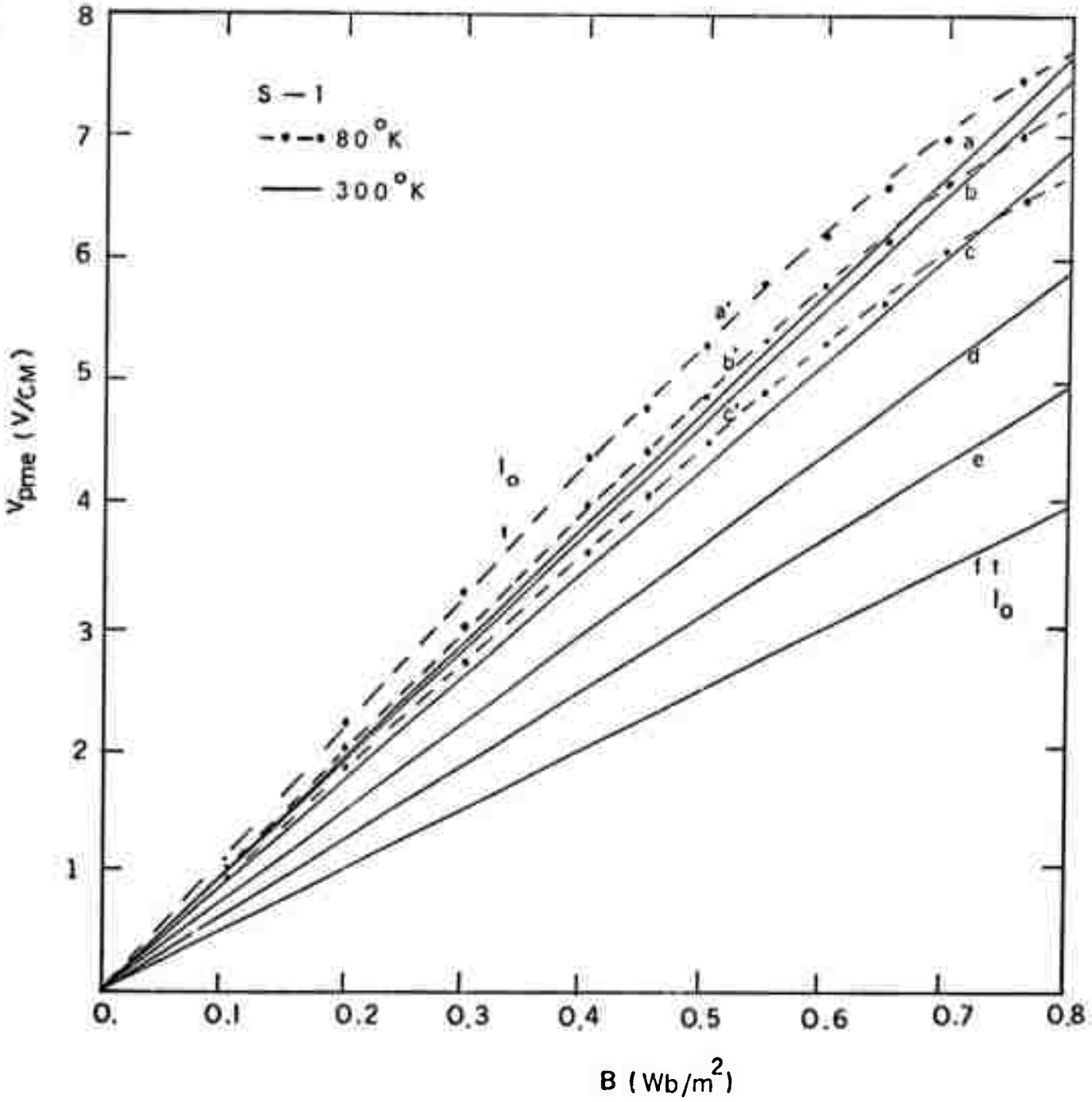
S — 1
80°K
300°K
a'
b'
c'
a
b
c
d
e
f
I_o
I_o
V_{pme} (V/CM)
B (Wb/m^2)
0.
0.1
0.2
0.3
0.4
0.5
0.6
0.7
0.8
1
2
3
4
5
6
7
8

FIG. 2

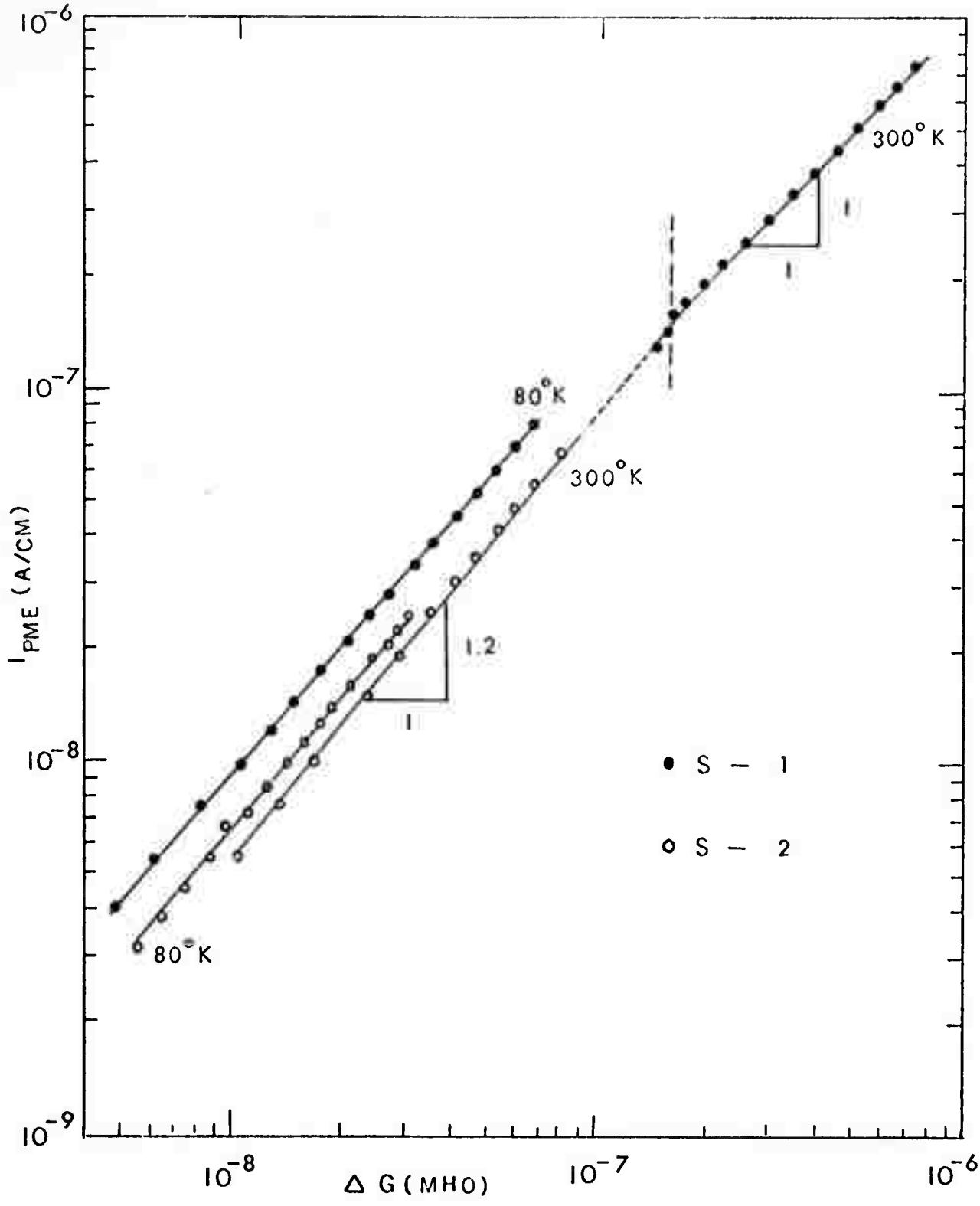
10^{-6}
10^{-7}
10^{-8}
10^{-9}
I_{PME} (A/CM)
300° K
80° K
300° K
80° K
1.2
1
1
1
• S — 1
o S — 2
10^{-8}
Δ G (MHO)
10^{-7}
10^{-6}

FIG. 3

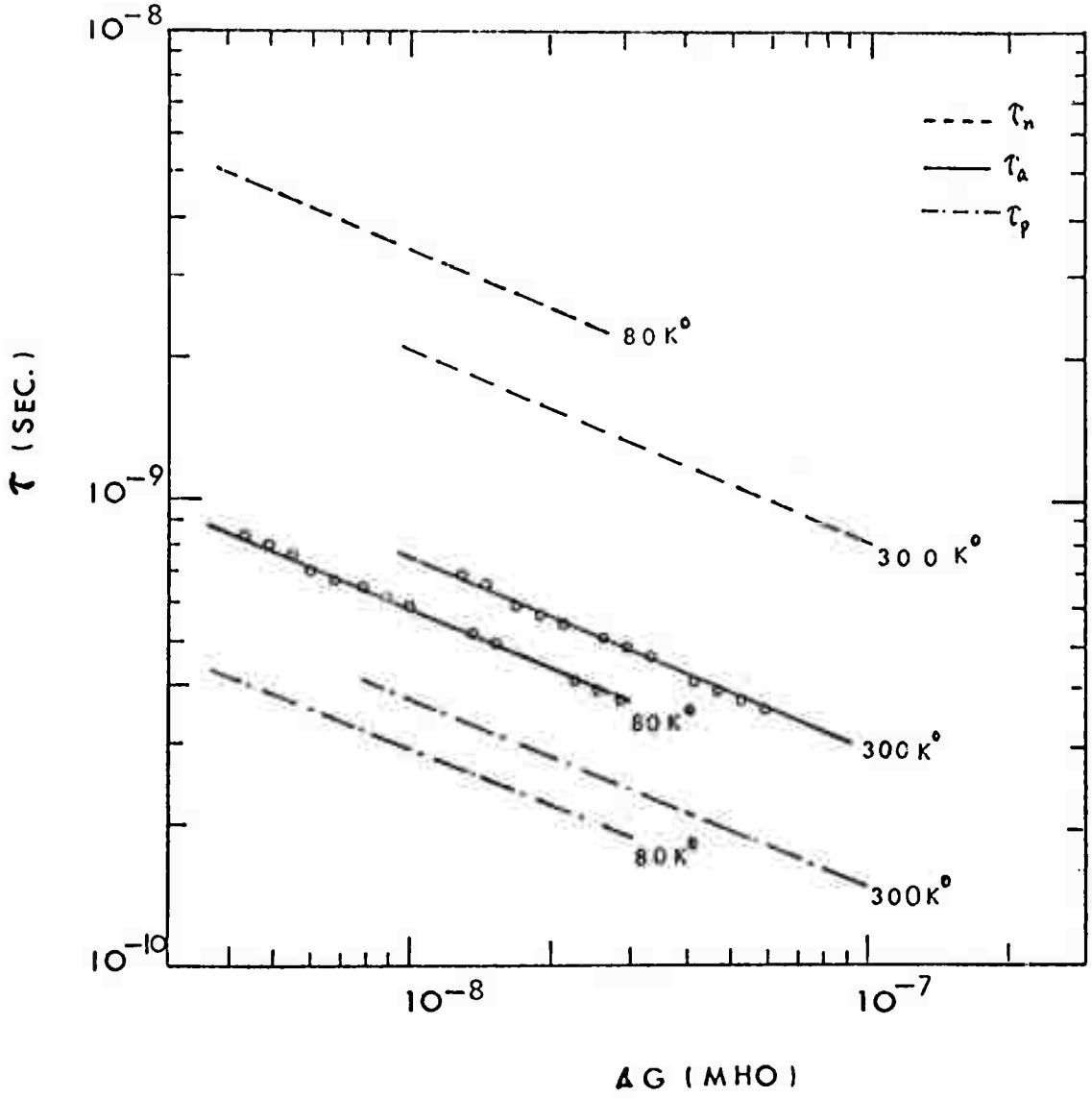
10^{-8}
10^{-9}
10^{-10}
τ (SEC.)
τ_n
τ_a
τ_p
80 K°
300 K°
80 K°
300 K°
80 K°
300 K°
10^{-8}
10^{-7}
ΔG (MHO)

FIG. 4

C. LOW TEMPERATURE PHOTOMAGNETOELECTRIC AND PHOTOCONDUCTIVE EFFECTS IN N-TYPE InAs (S.S. Li and C.I. Huang)

Introduction

The room temperature photomagnetoelectric (PME) effect in both n- and p-type InAs was reported previously by Dixon.[1] The results were interpreted in terms of the large Hall angle PME theory[2] for p-type samples and of the small Hall angle PME theory[3] for n-type samples.

In the present work we extended the experimental study of the PME and PC effects in single crystal n-type InAs from room temperatures down to 4.2°K. Incorporating the two measurements with resistivity and Hall effect experiments would allow us to determine the carrier lifetimes as well as electron and hole mobilities at low temperatures. The carrier lifetimes were computed from the PME and PC data, and the electron and hole mobilities were deduced from the Hall effect and the PME data between 4.2°K and 300°K.

Experimental

Undoped n-type InAs grown by the Czochralski method with electron concentration of 2.4×10^{16} cm^{-3} was used in the present work. The sample was cut into rectangular form by using a diamond saw. The dimensions of the sample, after being mechanically lapped by SiC powder and chemically etched by CP_4, were $1.3 \times 0.4 \times 0.04$ cm^3. The sample was then mounted onto the cryotip of the AC-310 refrigeration system. The resistivity and Hall effect measurements were performed by using the a-c method, similar to that described in Reference 1. The tungsten lamp light source was chopped at 400 cps, and the PME and PC signals picked up from the sample were passed through amplifiers and a wave analyzer. The system provides a gain of 10^5, which would allow us to measure a relatively small signal.

Results and Discussion

The resistivity and Hall effect were measured between 4.2°K and 300°K. The results showed that the electron concentration was nearly constant over the entire temperature range, and the Hall mobility (assuming equal to electron mobility) reached a peak value at 77°K. The results are summarized in Table I.

The PME open-circuit voltage and the photoconductance as functions of magnetic induction and light intensity were measured between 300°K and 4.2°K. The results for $T > 77$°K were in accord with the small Hall angle PME theory, and for $T < 21$°K, the large Hall angle PME theory predicted the observed PME data. This will be discussed separately in the following subsections:

A. Results for 77°K < T < 300°K.

In this temperature range, the small-signal PME and PC data are shown in Figs. 1 and 4. Fig. 1 shows the PME open-circuit voltage V_{PME} versus the

magnetic induction, B, for T = 300°K and 77°K, with light intensity, I_o, as a parameter. The results are in accord with the small Hall angle PME theory given by Van Roosbroeck,[3] which reads

$$V_{PME} = \left(\frac{D_p}{\tau_p}\right)^{\frac{1}{2}} B \frac{\Delta G}{G_o} \tag{1}$$

where D_p is the hole diffusion coefficient, τ_p is the hole lifetime, G_o is the dark conductance and ΔG is the photoconductance. The linear relationship between V_{PME} and B, observed at 77°K and 300°K, indicates that the hole mobility is low in this temperature range. Assuming that the electron mobility equals the Hall mobility, and electron-hole mobility ratio of 100, the hole mobility was estimated at 300°K and 77°K (see Table I). The hole lifetime (which is equal to electron lifetime for the present case) is deduced from Eq. (1) and the PME data shown in Fig. 4. The carrier lifetime estimated at 300°K ($\tau = 3.7 \times 10^{-8}$ sec) is in good agreement with that reported previously by Dixon.[1] The substantial increase in the photoconductance at 77°K (as compared with value at 300°K) is due to the fact that both the carrier mobility and the carrier lifetime are increased substantially at 77°K.

B. Results for 4.2°K < T < 21°K

In this temperature range, the V_{PME} saturates at high magnetic field strength, indicating that the hole mobility is greatly increased at low temperatures. To interpret the observed V_{PME} versus B plot as shown in Fig. 2, the large Hall angle PME theory is used. The theory predicts that[4]

$$V_{PME} = \left(\frac{D_p}{\tau_p}\right)^{\frac{1}{2}} \frac{B}{(1 + \mu^2 B^2)^{\frac{1}{2}}} \frac{\Delta G}{G_o} \tag{2}$$

where $\mu = (\mu_n \mu_p)^{\frac{1}{2}}$ is the effective carrier mobility. Eq. (2) predicts that the V_{PME} is proportional to B at low magnetic field and is independent of B at high magnetic field. The results shown in Fig. 2 for T = 21°K and 4.2°K are in accord with the prediction given by Eq. (2). To estimate effective mobility μ and hole lifetime τ_p from Eq. (2) and Fig. 2, a plot of $(B/V_{PME})^2$ versus B^2 is shown in Fig. 3. The intercept of the straight lines shown in Fig. 3 with the ordinate yields the hole lifetime and the slope of these lines yields the effective carrier mobility. The computed values of μ and τ_p at 21°K and 4.2°K from Fig. 3, are summarized in Table I. The electron mobility is deduced from resistivity and Hall effective measurements, and the hole

mobility is computed from $\mu_p = \mu^2/\mu_n$. The results show that the electron and hole mobility ratio changes drastically from assumed value of 100[1] at 300°K to the value of b = 5 (computed value) at 4.2°K. This is indeed consistent with the observed V_{PME} versus B data for T at 300°K and 4.2°K. The change in mobility ratio with temperature has also been observed in InSb.[5]

Fig. 4 illustrates the plot of (V_{PME}/B) versus $\Delta G/G_o$ for T = 300°K, 77°K, 21°K and 4.2°K. The results (slope of this plot is one) at all temperatures, show that no trapping effect is involved in the entire temperature range.[6,7] It is noted in Fig. 3 that the deviation from linearity (as is predicted by Eq. 5) at higher magnetic field is due to the fact that the photoconductance becomes magnetic field dependence as B is increased.

Conclusions

Experimental study of the PME and PC effects in n-type InAs single crystals has been extended from room temperature down to 4.2°K. The results are in good agreement with the theory developed previously. Carrier lifetimes and mobilities are deduced from the present results. Measurements of the PME and Hall effect at low temperatures enable us to determine both the majority and minority carrier mobilities in n-type InAs. Study of the PME and PC effects show that no trapping is involved in the entire temperature range for the present samples.

References

1. J. R. Dixon, Phys. Rev. 107, 374 (1957).

2. S. W. Kurnick and R. N. Zitter, J. Appl. Phys. 27, 278 (1956).

3. W. van Roosbroeck, Phys. Rev. 101, 1713 (1956).

4. S. S. Li, Phys. Rev. 188, 1246 (1969).

5. R. N. Zitter, A. J. Strauss and A. E. Attard, Phys. Rev. 115, 266 (1959).

6. S. S. Li and H. F. Tseng, Phys. Rev. (to be published) (1971).

7. There will be a non-linear relationship between the V_{PME} versus G/G_o plot in the presence of trapping of excess carriers. (See, for example, J. Agraz and S. S. Li, Phys. Rev. B, 2, 1847 (1970).)

Table I Transport and Recombination Parameters for n-type InAs

T	$\rho(\Omega\text{-cm})$	$R_H(cm^3/coul)$	$n_o = \frac{1}{R_H e}\ (cm^{-3})$	μ_n* $(\frac{cm^2}{V\text{-sec}})$	$b(\frac{\mu_n}{\mu_p})$	$\mu_p(\frac{cm^2}{V\text{-sec}})$	τ(sec)
300 K	0.0114	263	2.38×10^{16}	2.3×10^4	100	230	3.7×10^{-8}
78 K	0.00583	310	2.02×10^{16}	7.37×10^4	100	737	1.8×10^{-7}
21 K	0.0063	310	2.02×10^{16}	4.93×10^4	15	3290	2.1×10^{-8}
4.2 K	0.01	310	2.02×10^{16}	3.10×10^4	5	6200	4.75×10^{-9}

* Assuming $r_H = 1$, $\mu_H = \mu_n$

Figure Captions

Fig. 1 PME open circuit voltage per unit sample length, V_{PME}, versus magnetic induction, B, with light intensity I_o as a parameter, for T = 300°K and 77°K.

Curve a) I_o = 430 mW/cm^2 b) 270 mW/cm^2 c) 81 mW/cm^2
d) 430 mW/cm^2 e) 224 mW/cm^2 f) 129 mW/cm^2

Fig. 2 PME open circuit voltage per unit sample length, V_{PME}, versus magnetic induction, B, with light intensity I_o as a parameter, for T = 21°K and 4.2°K.

Curve a) I_o = 430 mW/cm^2 b) 224 mW/cm^2 c) 81 mW/cm^2
d) 350 mW/cm^2 e) 156 mW/cm^2 f) 106 mW/cm^2

Fig. 3. $(B/V_{PME})^2$ versus B^2 with light intensity I_o as a parameter for T = 21°K and 4.2°K. The intercept of this plot with ordinate is equal to $(\frac{\tau_p}{D})$ and the slope of this plot yields $(\frac{\tau_p}{D})\mu^2$.

Curve a) I_o^p = 106 mW/cm^2 b) 224 mW/cm^2 c) 430 mW/cm^2
d) 106 mW/cm^2 e) 224 mW/cm^2

Fig. 4. PME open circuit voltage, V_{PME}, versus photoconductance ratio, $\frac{\Delta G}{G_o}$ for T = 300°K, 77°K, 21°K and 4.2°K. The slope of these plots is unity.

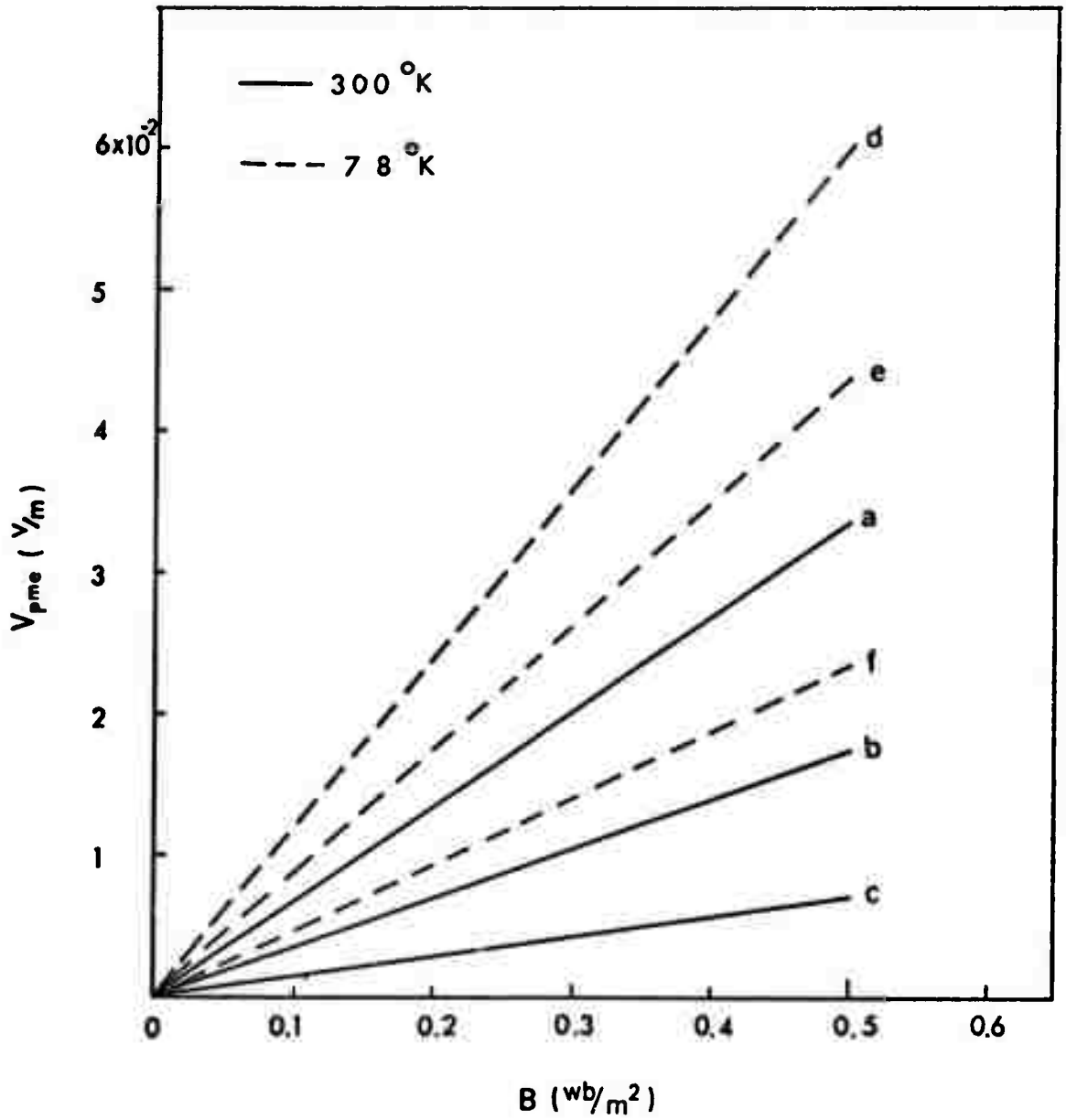

Fig. 1

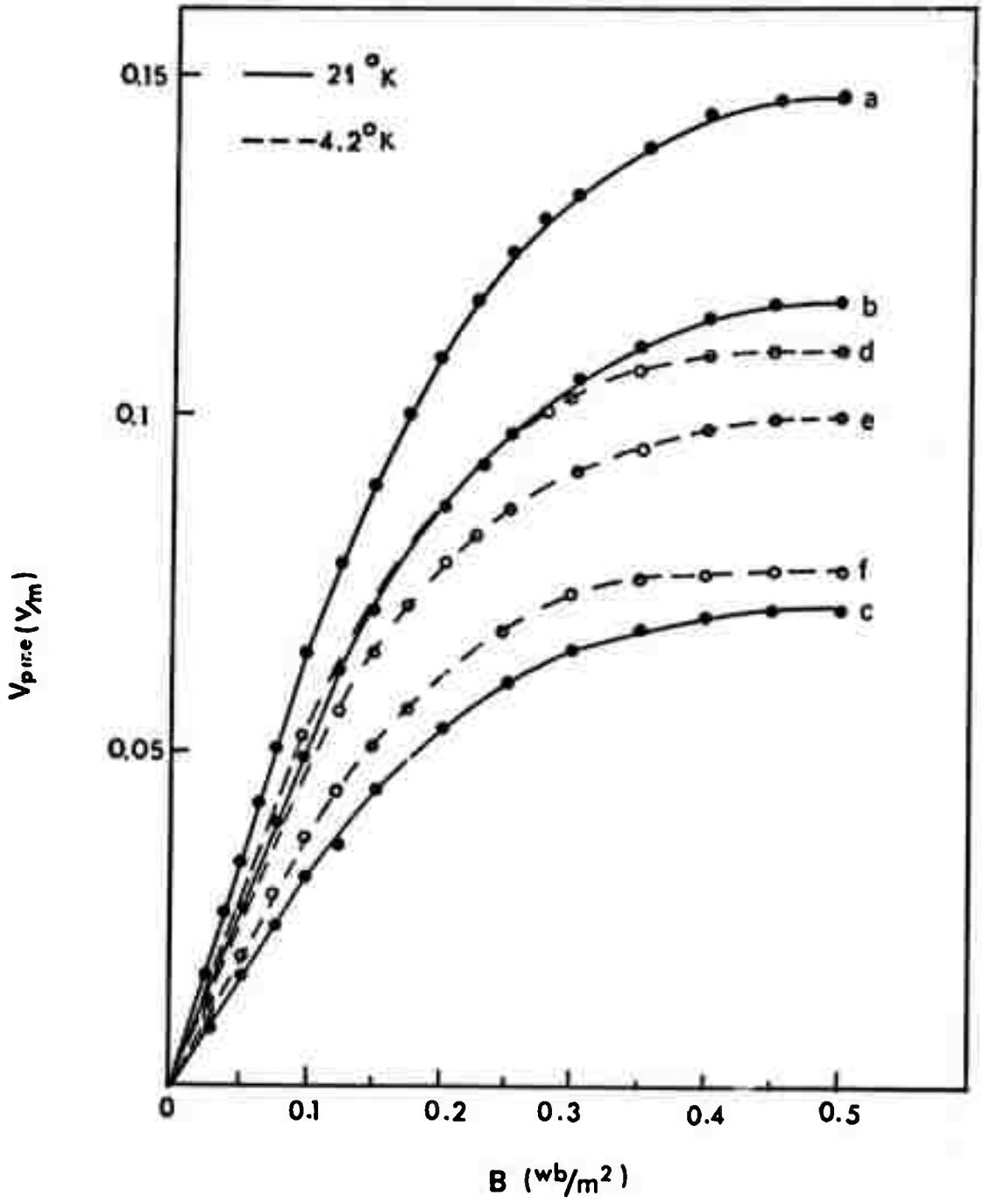

Fig. 2

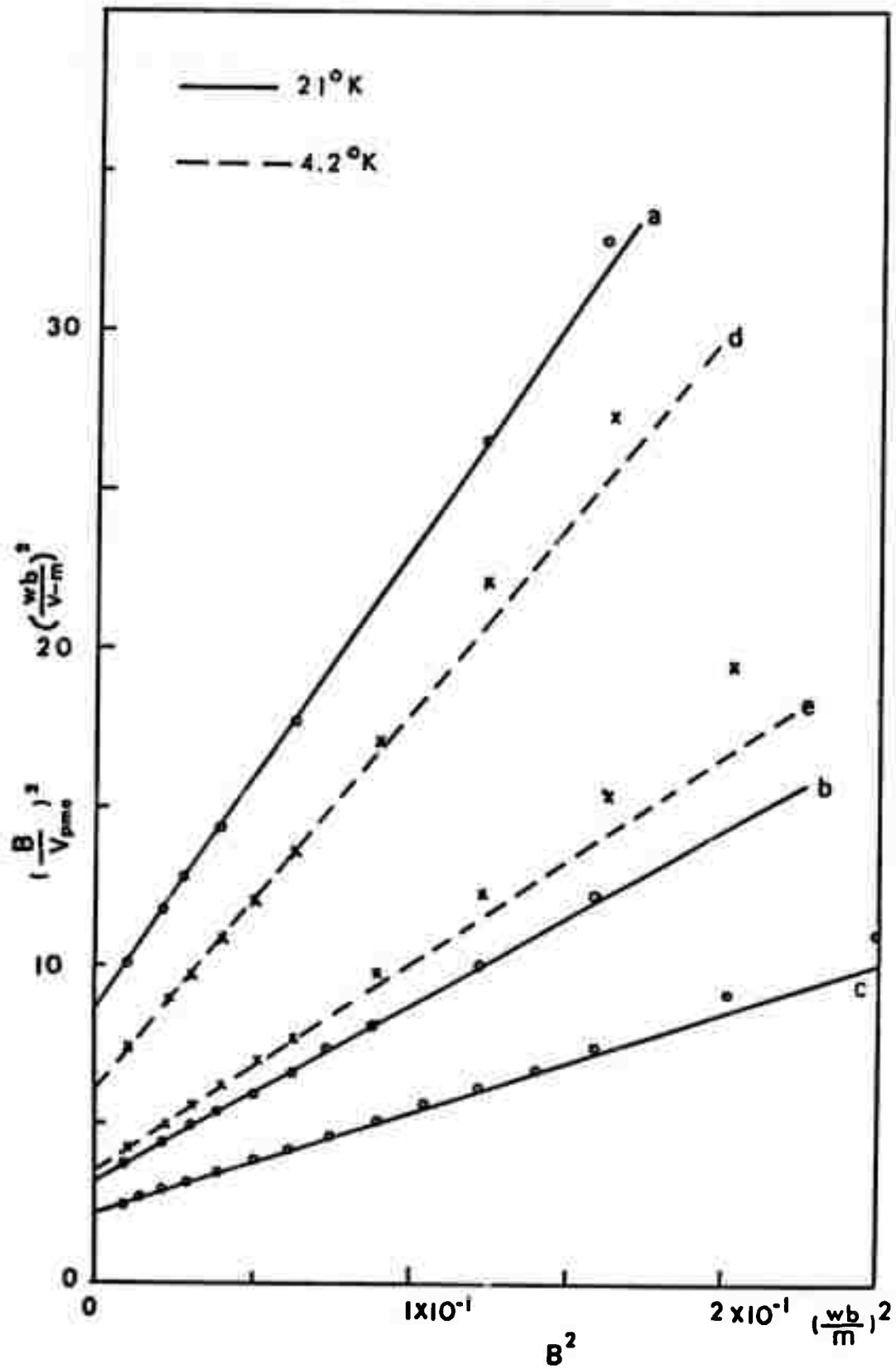

Fig. 3

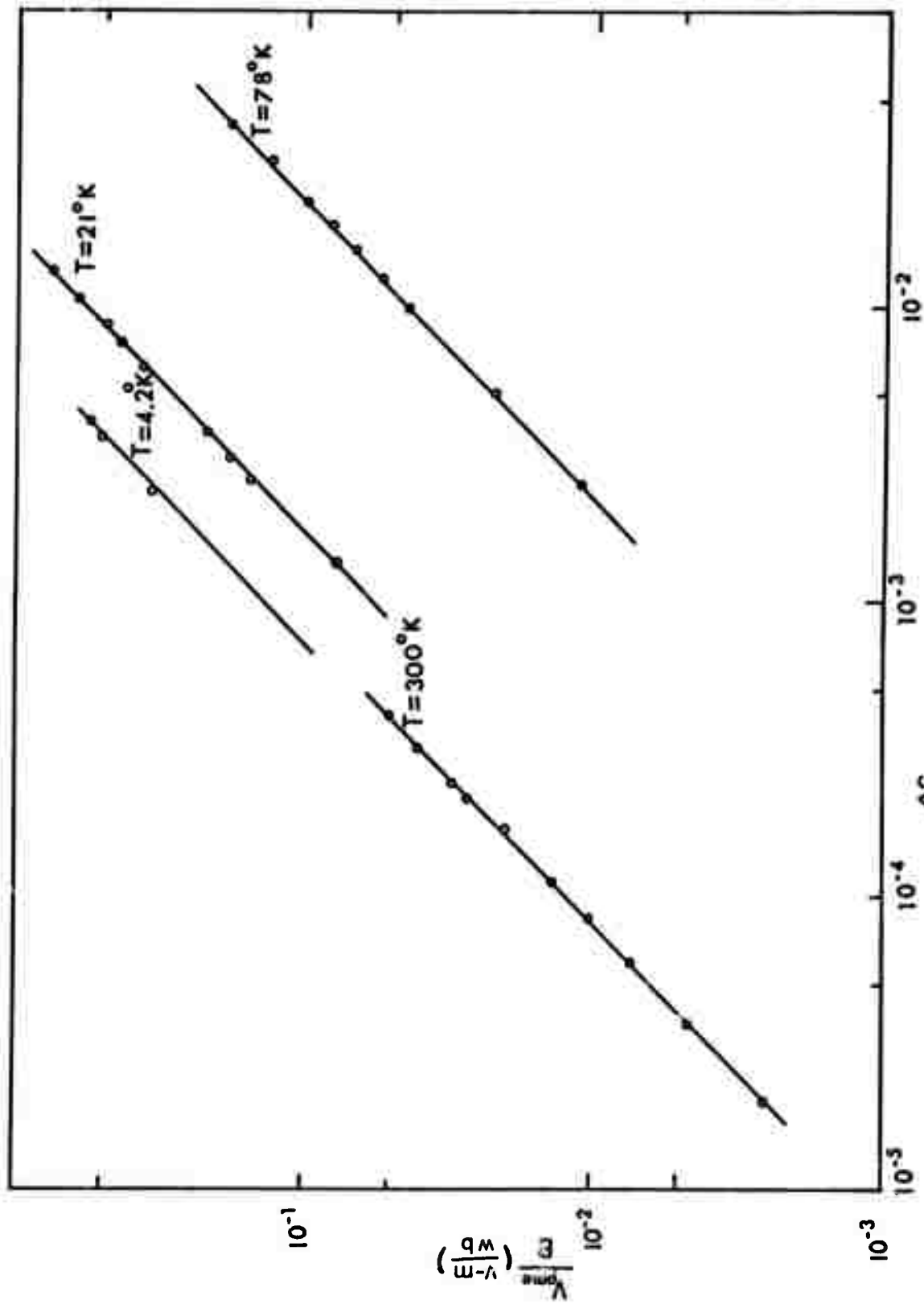
T=78°K
T=21°K
T=4.2°K
T=300°K
10^{-1}
10^{-2}
10^{-3}
10^{-3}
10^{-4}
10^{-3}
10^{-2}
$\frac{\Delta G}{G_0}$
$\frac{V_{rms}}{E}\left(\frac{\sqrt{-1}}{wb}\right)$

Fig. 4

D. THE EFFECT OF A BURIED LAYER ON THE COLLECTOR BREAKDOWN VOLTAGES OF BIPOLAR JUNCTION TRANSISTORS (F.W. Hewlett, Jr., F.A. Lindholm and A. J. Brodersen)

I. Introduction

Bipolar transistors designed for high-frequency or high-speed applications are very shallow structures. For example, devices used for small-signal microwave amplification may have emitter and collector junctions that lie within 5000 Angstrom units from the surface; typically, the devices are fabricated by successive diffusions into N/N^+ epitaxially grown silicon [1]. The N-type epitaxial material is made thin, less than 10 microns, to reduce collector series resistance. Similar devices are used commonly in high-speed digital integrated circuits.

In this paper, we describe a premature punch-through effect occurring in this type of transistor that can lower the collector breakdown voltages below the values predicted by existing theory. We express the premature punch-through voltage BV_{PPT}, which characterizes the effect, in terms of parameters of the fabrication processing, and from this derive an expression for the thickness of the epitaxial collector that maximizes BV_{PPT} and, hence, the usable region of device operation. Measurements are presented that support the theoretical predictions.

Punch-through occurs when the space charge layer of a reverse biased PN junction contacts the space charge layer of a nearby PN junction. Reach-through occurs when the depletion region of a reverse biased junction contacts the boundary between the P-type or N-type material and that of a nearby layer of the same but higher conductivity type. The punch-through condition may occur in shallow bipolar transistors whose doping in the collector is comparable with that in the base. The reach-through condition may occur

in PN junctions fabricated on high conductivity buried layers. In this case, premature avalanche breakdown due to reach-through takes place.

In the premature punch-through effect, a sufficiently large reverse bias placed on the collector base junction can cause the collector base depletion region to reach through the lightly-doped collector to the N^+ buried layer. Further increase of the collector base voltage acts to widen the collector depletion region mainly on the base side, forcing it to punch through the base into the emitter space charge region. This occurrence results in a large current flow, or breakdown, if the emitter and base are short-circuited.

In Section II, we summarize the existing theory for punch-through [2] and reach-through [3] and present a theory which is new for premature punch-through. Section III contains experimental evidence which substantiates the theory presented in Section II.

II. Theory

A. PUNCH-THROUGH IN TRANSISTORS

In this part, we present a method, discussed in Phillips [2], which enables one to distinguish between breakdown resulting from punch-through in the base and that resulting from avalanche multiplication in the collector. The discussion herein is qualitative and yields relations between the breakdown voltages of a bipolar transistor valid for both punch-through and premature punch-through.

If breakdown is due to avalanche multiplication in the collector space charge region, we may determine this as follows. One measures the breakdown voltage from emitter to collector with the base shorted to the emitter, BV_{CES}, and the breakdown voltage from collector to base with the emitter open BV_{CBO}. If avalanche multiplication in the collector is causing breakdown, then

$$BV_{CES} = BV_{CBO}. \tag{1}$$

Thus, avalanche breakdown and the ensuing heavy current do not depend on the constraint applied at the emitter lead. Large currents flow at the same value of base collector voltage both when the emitter is shorted to the base and when the emitter is open circuited.

Next, consider a device in which the breakdown voltage is punch-through limited. Here, the breakdown voltage, BV_{CBO}, is related to the punch-through voltage BV_{PT}, by

$$BV_{CBO} = BV_{PT} + BV_{EBO} \tag{2}$$

where BV_{EBO} is the breakdown voltage applied between emitter and base with the collector open circuited. This relation may be explained as follows. As the collector base reverse bias is increased, the collector transition region punches through into the emitter space charge region. If the emitter is open circuited, this condition will not result in a large current flow. A further increase in voltage is necessary to cause avalanche breakdown of the emitter-base sidewall, which then results in the flow of heavy current from the base lead. Thus, BV_{CBO} for a device limited by punch-through is equal to the voltage necessary to cause the collector transition region to punch through the base plus the breakdown voltage of the emitter base sidewall.

In the measurement of BV_{CES}, one shorts the emitter to the base. In this case, when punch through occurs, we have two layers of N-type material separated by a layer of space charge. It is not necessary to breakdown the emitter side wall since the shorted emitter lead provides a current path. The energy band diagrams for three values of V_{CB} are shown in Figure 1. Figure 1(a) represents a thermal equilibrium situation. The energy band of Figure 1(b) illustrates a reverse biased collector junction. Figure 1(c) shows the punch-through condition. For $V_{CB} = BV_{PT}$ the potential barrier has been reduced so that electrons, supplied by the shorted emitter lead, can overcome the barrier and slide down the potential "hill." As V_{CB} is increased above BV_{PT}, space-charge-limited flow ensues [4].

Therefore,

$$BV_{CES} = BV_{PT}. \tag{3}$$

for a transistor in which punch through determines the breakdown characteristics; and, from equations (2) and (3),

$$BV_{CBO} = BV_{CES} + BV_{EBO}. \tag{4}$$

Phillips [2] gives a theoretical expression for BV_{PT} in terms of fabrication parameters applicable to a uniform base alloy transistor:

$$BV_{PT} = \frac{qN_A W_B^2}{2K_S \varepsilon_0} \tag{5}$$

where N_A is the acceptor concentration in the base region, and W_B is the width of the base region. Figures 2(b) and 2(c) illustrate the electronic

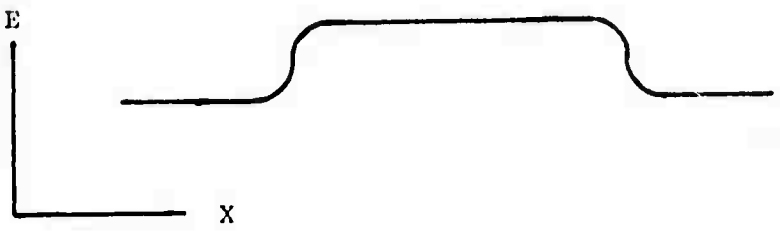

(a) Thermal equilibrium.

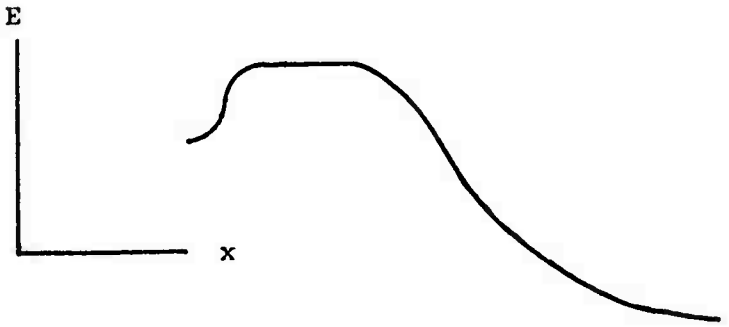

(b) The collector reverse biased.

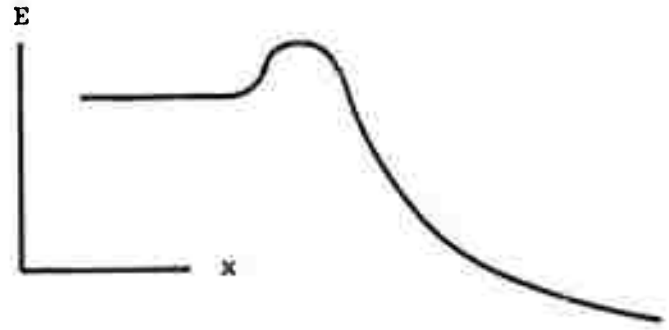

(c) Onset of space charge limited flow.

Figure 1 Energy band diagram for an NPN transistor with various applied collector voltages. Only the conduction band edge is shown.

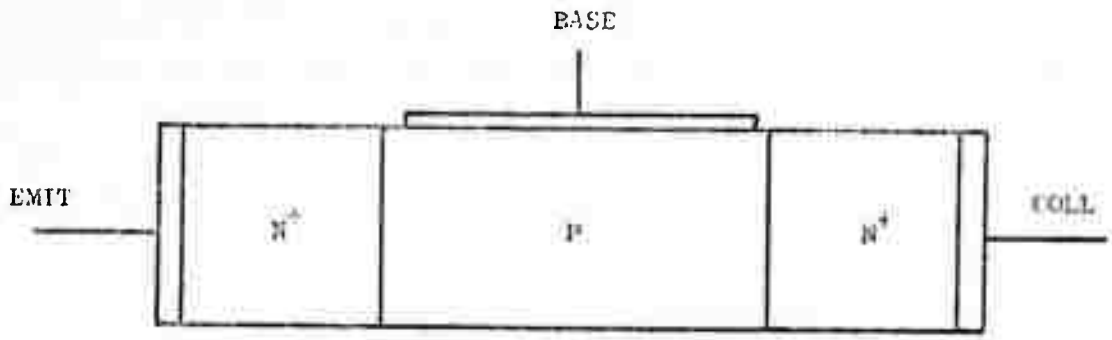

(a) Intrinsic structure

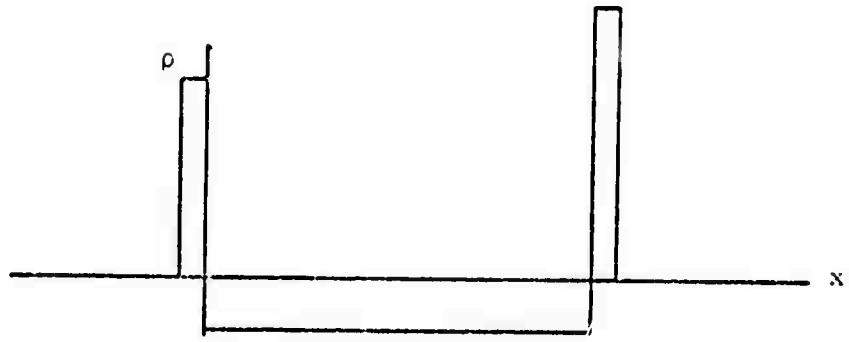

(b) Electronic charge distribution

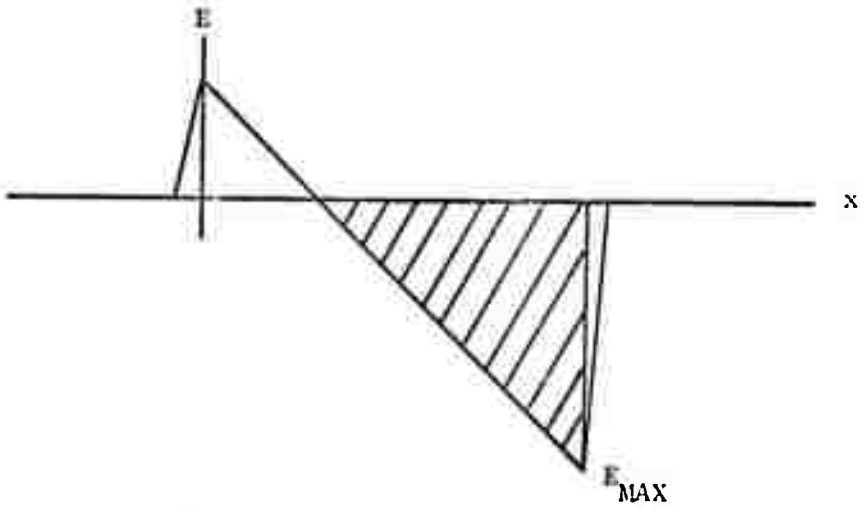

(c) Electrostatic field distribution.

Figure 2 Illustration of an N^+PN^+ alloy transistor in the punch-through condition.

charge and electrostatic field distributions at the punch-through condition. Equation (5) assumes that the collector base junction is asymmetrical, the collector being much more heavily doped than the base. Therefore, approximately all the voltage difference appears on the base side of the collector transition region. The collector base voltage at punch-through is approximated by the area of the shaded triangle in Figure 2(c).

For a double diffused structure, one may obtain an approximate value for BV_{PT} from the Lawrence and Warner curves [5], using an iterative procedure. However, when space charge region widths become comparable with the quasi-neutral base width, a computer solution may be necessary.

B. REACH-THROUGH IN DIODES

Reach-through is an effect which can limit the breakdown voltage of P^+N junction diodes fabricated on N/N^+ epitaxial material, of the type shown in Figure 3(a). An increase of the reverse voltage widens the transition or space-charge region, which extends primarily into the lightly doped N region. For a particular value of reverse bias, the space charge region extends to the buried layer. Further increase in reverse voltage causes uncovering of immobile ion charge in the N^+ layer, as shown in Figure 3(b). This produces a sensitive dependence on reverse voltage of the maximum electric field E_{MAX}, which grows until it reaches the critical field for avalanche multiplication E_{CRIT}. This critical field supplies conduction electrons with sufficient energy to impact ionize valance electrons, resulting in heavy current flow. The charge and electrostatic field distributions at breakdown are illustrated in Figures 3(b) and 3(c).

Grove's expression for the breakdown voltage due to reach-through BV_{RT} in terms of the critical field and fabrication parameters is [3]

$$BV_{RT} = E_{CRIT}\, W_{EPI} - \frac{qN_D\, W_{EPI}^2}{2K_S\, \varepsilon_0} \qquad (6)$$

Here N_D is the donor concentration in the epitaxial silicon and W_{EPI} is the width in epitaxial material measured from the metallurgical P^+N step junction to the buried layer. Equation (6) is an approximation for the shaded area indicated in Figure 3(c). It is a good approximation for a single diffused P^+NN^+ diode.

This development assumes a step function change in collector doping as one moves from the lightly doped collector toward the buried layer.

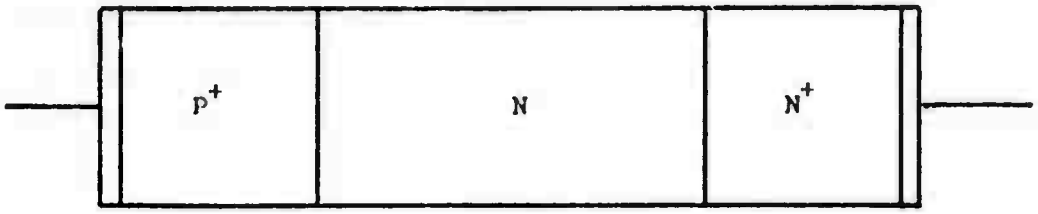

(a) Intrinsic structure.

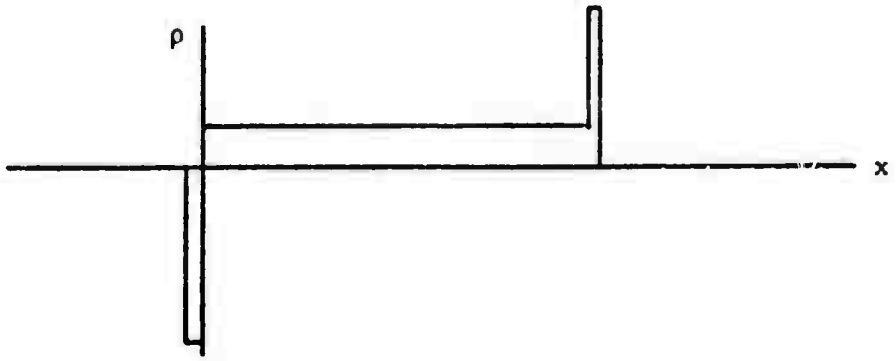

(b) Electronic charge distribution

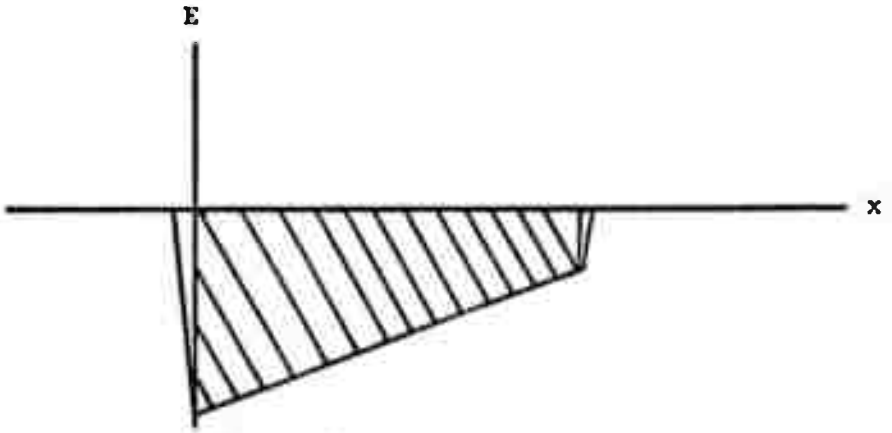

(c) Electrostatic field distribution.

Figure 3 Illustration of a P^+NN^+ diode in the reach-through condition.

In reality, the out-diffusion of the substraight impurity during epitaxial growth and subsequent heat treatments may cause BV_{RT} to be less than the value predicted by equation (6). A similar reduction of the breakdown voltage resulting from the out-diffusion of the substrate impurity also holds for the premature punch-through effect in junction transistors, which we are now prepared to examine.

C. PREMATURE PUNCH-THROUGH IN TRANSISTORS

The breakdown of the P^+NN^+ diode, illustrated in Figure 3 results from avalanche multiplication in the P^+N junction transition region. The maximum field, E_{MAX}, attains the value of the critical field prematurely because of the presence of the buried layer. The presence of another transition region creates an alternative mechanism for the occurrence of large current flow. This possibility exists in $NPNN^+$ bipolar structures. For simplicity of discussion, we deal first with a one dimensional structure with homogeneous base doping which is illustrated in Figure 4(a).

In this type of shallow device, the emitter and collector transition regions are separated by a narrow distance, typically less than one micron. Thus, the collector space charge region, broadening with increasing reverse voltage, may punch through the quasi-neutral base into the emitter space charge region before the critical field for avalanche multiplication in the collector is reached. The charge and electric field distributions are illustrated in Figures 4(b) and 4(c), respectively, for a transistor with uniform doping in the collector and base. The breakdown voltages of a structure experiencing premature punch-through obey equation (4).

To obtain an expression for the breakdown voltage due to premature punch-through, BV_{PPT}, we must include the voltage drops in both the base and the collector as represented by the shaded area of Figure 4(c). This area may be expressed as the sum of the areas of Figure 2(c) and 3(c), which corresponds to replacing E_{CRIT} by E_{MAX} in equations (5) and (6). Thus, an approximate expression for the breakdown voltage due to premature punch-through may be written as

$$BV_{PPT} = E_{MAX} W_{EPI} - \frac{qN_D W_{EPI}^2}{2K_S \varepsilon_0} + \frac{qN_A W_B^2}{2K_S \varepsilon_0} \qquad (7)$$

where

$$E_{MAX} = \frac{qN_A W_B}{K_S \varepsilon_0} \qquad (8)$$

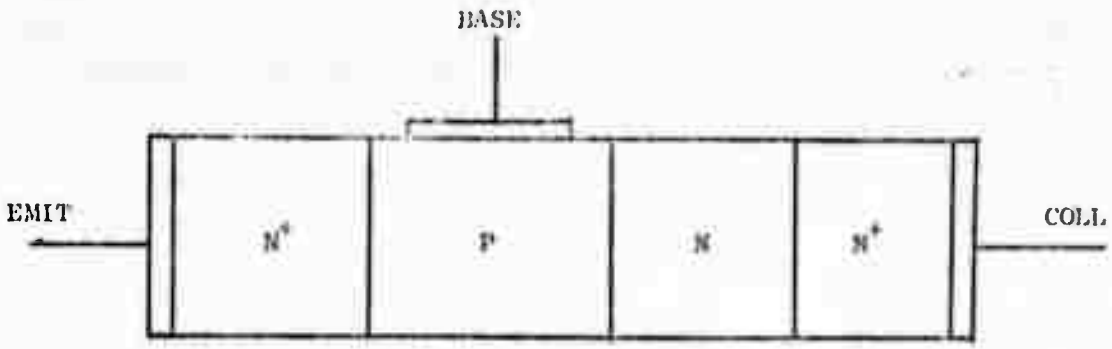

(a) Intrinsic structure.

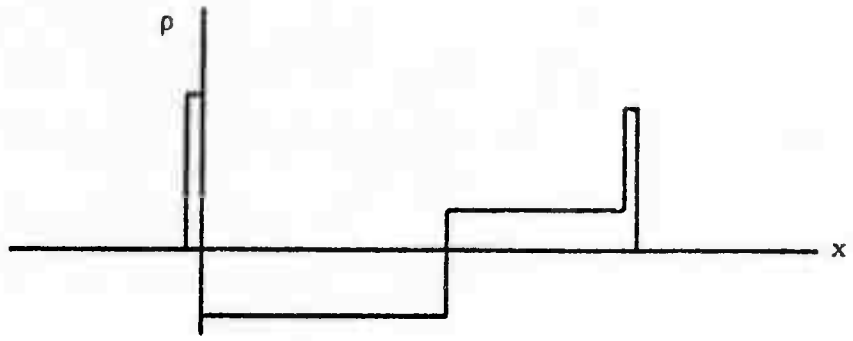

(b) Electronic charge distribution

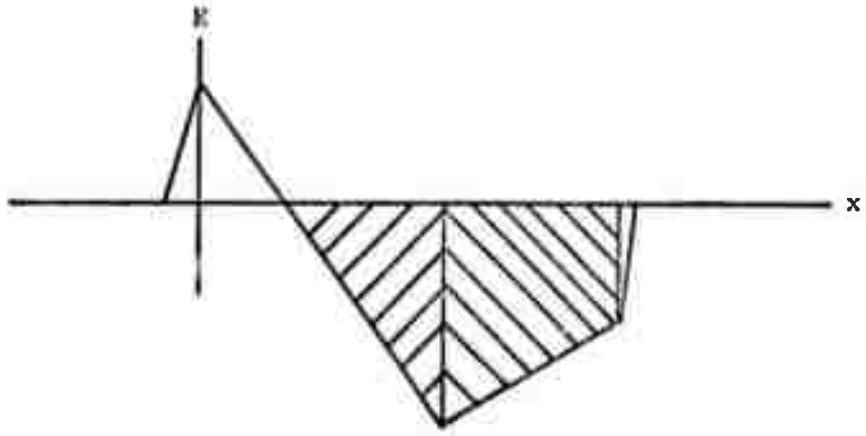

(c) Electrostatic field distribution.

Figure 4 Illustration of an N^+PNN^+ transistor in the premature punch-through condition.

when the punch-through condition occurs.

This development applies for a homogeneous base transistor. However, one may approximate the value of BV_{PPT} for a double diffused device by combining equations (7) and (8),

$$BV_{PPT} = \frac{q}{K_S \varepsilon_0} \left(N_A W_B W_{EPI} - \frac{N_D W_{EPI}^2}{2} + \frac{N_A W_B^2}{2} \right) \tag{9}$$

and by noting that the product of N_A and W_B which appears in equation (9) is Gummel's number N_B for a homogeneous base transistor. Therefore, as an approximation to BV_{PPT} for the double diffused structure we write

$$BV_{PPT} = \frac{q}{K_S \varepsilon_0} \left(N_B W_{EPI} - \frac{N_D W_{EPI}^2}{2} + \frac{N_B W_B}{2} \right) \tag{10}$$

where N_B may be determined via terminal measurements [6] and W_B may be determined by the groove and stain method [7].

Equation (10) indicates that, for a device whose breakdown voltages are limited by premature punch-through, there is a value of W_{EPI} which gives a maximum value of BV_{PPT}. Differentiating equation (10), we find the optimum epitaxial thickness, $(W_{EPI})_{OPT}$, is

$$(W_{EPI})_{OPT} = \frac{N_B}{N_D}. \tag{11}$$

Thus, BV_{PPT} will be the largest for a particular fabrication process when the epitaxial thickness is equal to Gummel's number (in atoms/cm^2) divided by the doping concentration of the lightly doped collector (in atoms/cm^3).

The next section contains data on bipolar structures that experience premature breakdown resulting from reach-through and from punch-through induced by reach-through. For comparison, it also shows the breakdown voltage, BV_{CES}, of a related device which experiences neither effect.

III. Experimental

We have designed and fabricated two runs of bipolar transistors whose fabrication parameters and profiles were similar but whose values of BV_{CES} and BV_{CBO} were considerably different. The feature which distinguished the two runs was that one of them employed a buried layer. These devices were designed to avoid punch through of the base in the usual sense. The purpose of the experiment was to investigate the effect of a buried layer on the breakdown characteristics of these $NPNN^+$ transistors.

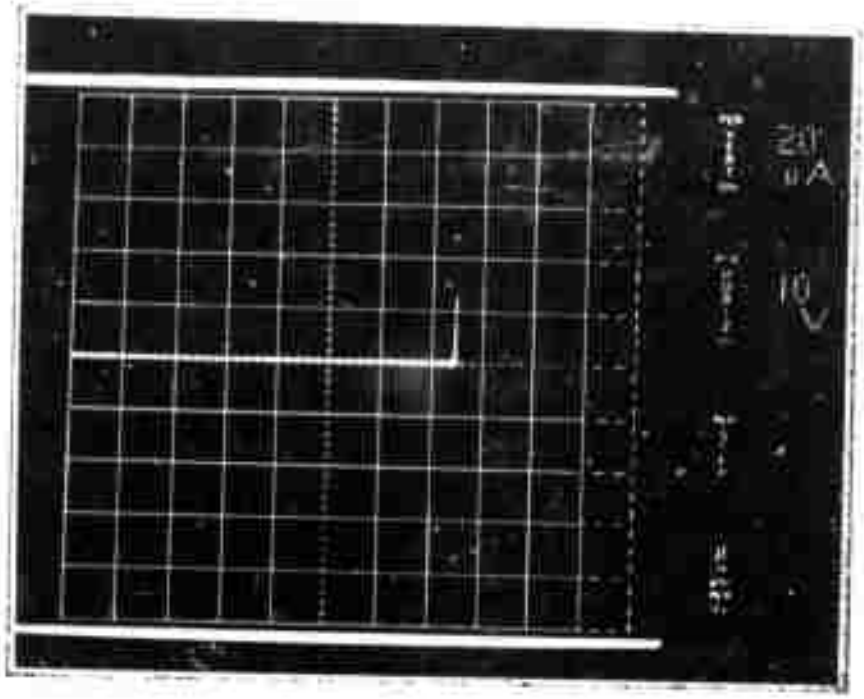

Figure 5(a) Photograph of BV_{CES} for test unit #1-4L.

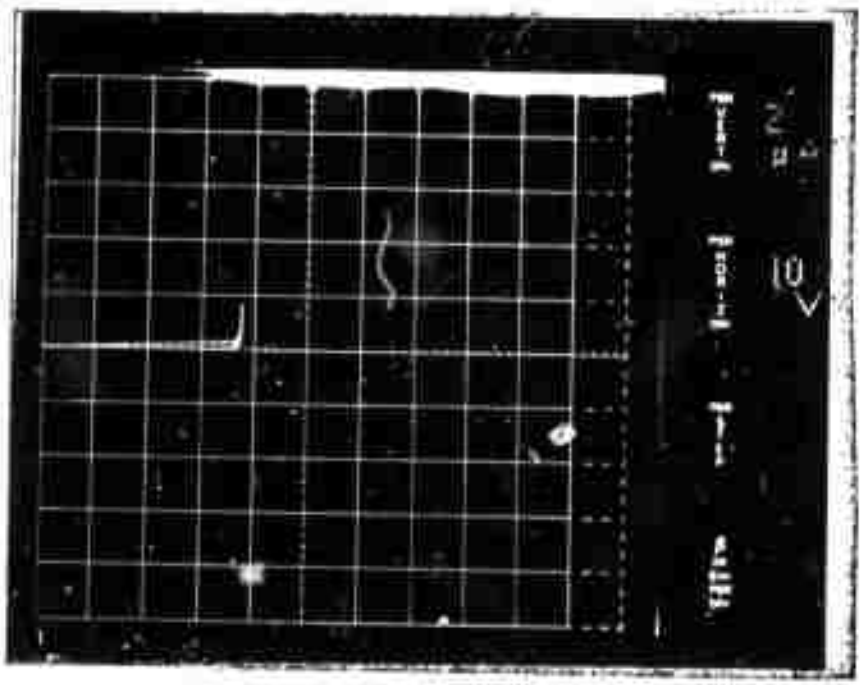

Figure 6(a) Photograph of BV_{CES} for test unit #3-4L.

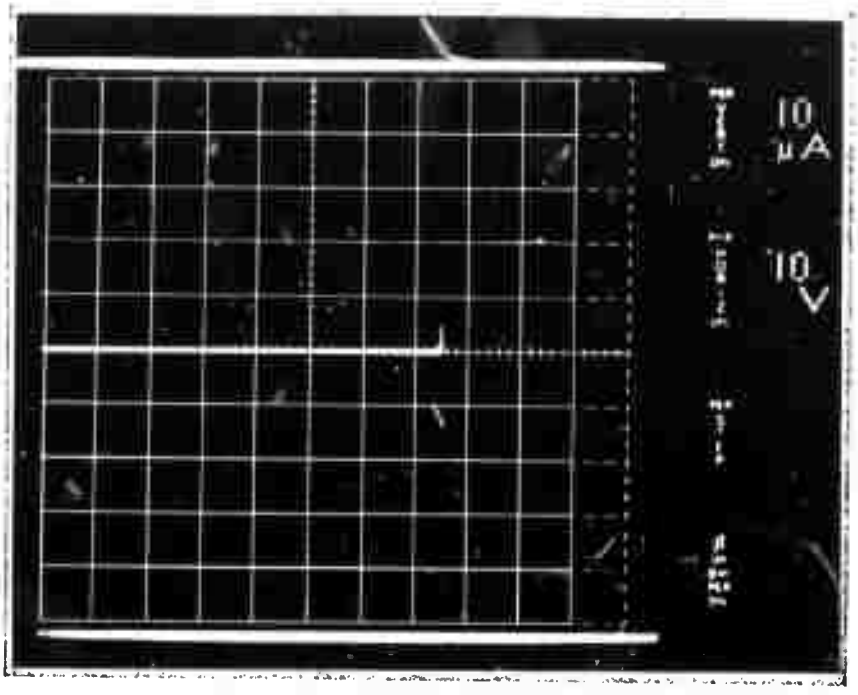

Figure 5(b) Photograph of BV_{CBO} for test unit #1-4L.

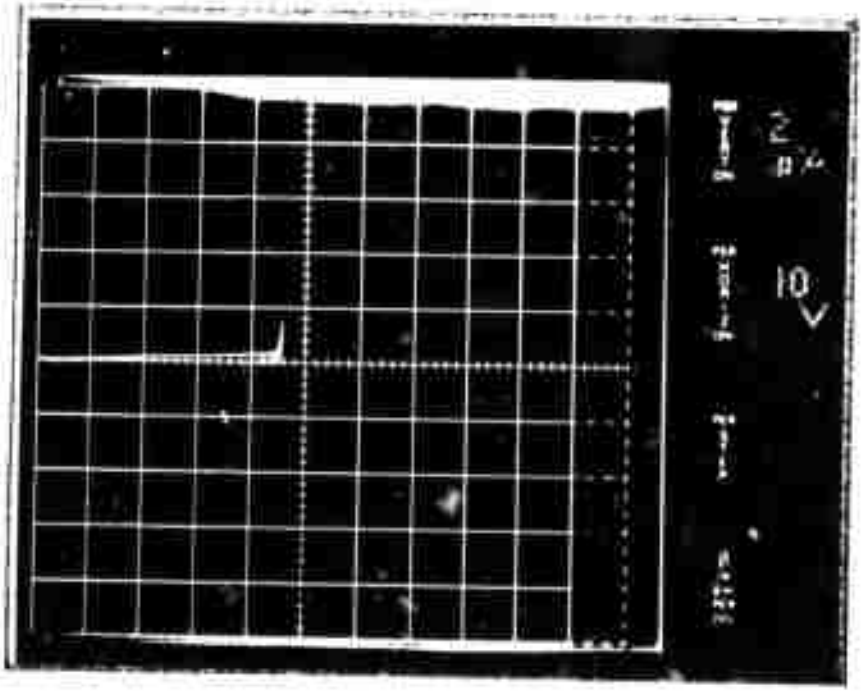

Figure 6(b) Photograph of BV_{CBO} for test unit #3-4L.

Data taken from the bipolar transistors fabricated are contained in Table 1. Test unit #1-4L was fabricated on N-type material without a buried layer. For this device BV_{CES} is equal to BV_{CBO} (equation (1)) which indicates that avalanche multiplication in the collector transition region causes the large current flow. BV_{CES} and BV_{CBO} for this device are pictured in Figure 5 (a) and (b), respectively. The other test units in Table 1 were fabricated on N/N^+ epitaxial material. Test units #3-2L and #3-3L exhibit breakdown due to premature avalanche multiplication in the collector transition region caused by reach-through. BV_{CES} is equal to BV_{CBO} for these test units. Test units #3-4L and #3-6L are limited by premature punch-through. Figure 6(a) shows a photograph of BV_{CES} for test unit #3-4L. Figure 6(b) shows a photograph of BV_{CBO} for this test unit which is greater than BV_{CES} by the value of BV_{EBO} obeying equation (4). The values of N_B and I_{ES} were determined by measurement using the method described by Gummel [6].

Test unit #3-3L, which has a higher value of N_B and hence more impurities in the base layer per unit area, $5.6 \times 10^{+12}$ cm^{-2}, than test unit #3-2L, $4.7 \times 10^{+12}$ cm^{-2}, breaks down in the collector at lower voltages. However, #3-6L, which has a larger value of N_B than #3-4L, breaks down at correspondingly higher values of BV_{CES} and BV_{CBO}. Thus, the addition of more impurities in the base increases $BV_{CES} = BV_{PPT}$ for test units #3-4L and #3-6L, in which premature punch through dominates, and decreases BV_{CES} for units #3-3L and #3-2L, in which the dominant mechanism is avalanche multiplication induced by reach-through.

IV. Summary and Conclusions

We have combined existing theory for punch-through and reach-through to obtain an expression for the premature punch-through breakdown voltage, equation (10). Device characteristics which show premature punch through are presented and compared with those which show the usual avalanche breakdown in the collector.

Equation (11) gives in terms of fabrication parameters the thickness of the epitaxial layer which maximizes the breakdown voltages (both BV_{CES} and BV_{CBO}) of a device limited by premature punch-through.

Experimental results indicate that large variations in the breakdown voltages of devices fabricated on the same thin epitaxial layer may be expected (37 to 50 volts). These variations likely result from two causes:

TABLE 1

BREAKDOWN VOLTAGES

Test Unit	BV_{CES} (volts)	BV_{CBO} (volts)	BV_{EBO} (volts)	N_B cm^{-2}
#3-2L	48.	48.		$4.7 \times 10^{+12}$
#3-3L	46.	46.		$5.6 \times 10^{+12}$
#3-4L	37.	45.	8.	$2.3 \times 10^{+12}$
#3-6L	42.	50.	8.	$3.1 \times 10^{+12}$
#1-4L	75.	75.		$2.9 \times 10^{+12}$

(1) because of nonuniformities in the diffusion process and the fact that the base widths were determined by the tails of two diffusions result in variations in the number of impurities in the base, and, therefore, in the breakdown voltages; (2) because of nonuniformities in the epitaxial layer thickness, W_{EPI}. More important, the fact that both premature, punch-through and reach-through occur in different devices taken from the same wafer causes wide variations in the values of BV_{CES}.

Gummel's number N_B is interpreted in equation (10) as the net number of impurities per unit area in the base layer. In certain shallow transistors, this interpretation is no longer valid [8]. In these devices, N_B is the number of holes per unit area in the transistor [8,9]. Therefore we would not expect equation (10) to accurately reflect BV_{PPT} for those devices for which the conventional interpretation of N_B is not valid. For such devices a computer solution may be required.

REFERENCES

1. Harry F. Cooke, Microwave Transistors: Theory and Design," Proc. IEEE, Vol. 59, No. 8, pp. 1163-1181, Aug. 1971.

2. A. B. Phillips, Transistor Engineering, New York: McGraw-Hill, 1962.

3. A. S. Grove, Physics and Technology of Semiconductor Devices, New York: Wiley, 1967.

4. For a general discussion of space-charge-limited flow, see: A. van der Ziel, Solid State Physical Electronics, New Jersey: Prentice Hall, 1968.

5. The Lawrence and Warner curves may be found in ref. #2 above (A.B. Phillips).

6. H. K. Gummel, "Measurements of the Number of Impurities in the Base Layer of a Transistor," Proc. IRE, Vol. 49, p. 834, April 1961.

7. F. W. Hewlett, Jr., "Junction Depth Measurements Via the Grove and Stain Method," Proc. Letters, in preparation.

8. F. W. Hewlett, Jr., "Computer vs. Conventional Analysis of Shallow Bipolar Transistors," Ph.D. Dissertation, University of Florida, 1971.

9. H. K. Gummel, "A Charge Control Relation for Bipolar Transistors," BSTJ, Vol. 49, pp. 115-120, January 1970.

E. DEVICE CHARACTERIZATION FOR COMPUTER ANALYSIS OF LARGE SEMICONDUCTOR CIRCUITS (F. A. Lindholm)

I. Introduction

From a general viewpoint, the starting point in complex microcircuit design is the processing (diffusion of impurities, mask generation, etc.) used in fabrication. The end point is a circuit that meets specifications in system performance and cost. In between are four modeling problems, each involving abundant use of computer calculation as the flow chart of Fig. 1 illustrates.

The first of these problems seeks to describe the relationship between processing and resulting physical make-up (spatial distribution of impurities and defects, corresponding distribution of the pertinent material parameters, etc.) of each device in the circuit. In the second modeling problem one solves the relevant partial differential equations, often by numerical methods, to relate the physical make-up to the spatial and temporal dependence of such internal variables as free carrier densities, quasi-Fermi levels, charge density, and current density. Response is sought for excitation pertinent to the proposed system application. The understanding thus gained is useful in designing the devices comprising the circuit. In the third modeling problem, one tries to link the physical make-up and the current voltage behavior of each device at its terminals. The vehicle for describing this behavior is usually called a circuit model or an equivalent circuit. The availability of adequate circuit models is essential in the design of any circuit.

Past research in device characterization has focussed nearly exclusively on these three modeling problems. This paper deals with the fourth problem indicated in Fig. 1, which is concerned with selection of models.

The maximum size of semiconductor circuit amenable to computer analysis and the efficiency of the analysis are both determined substantially by

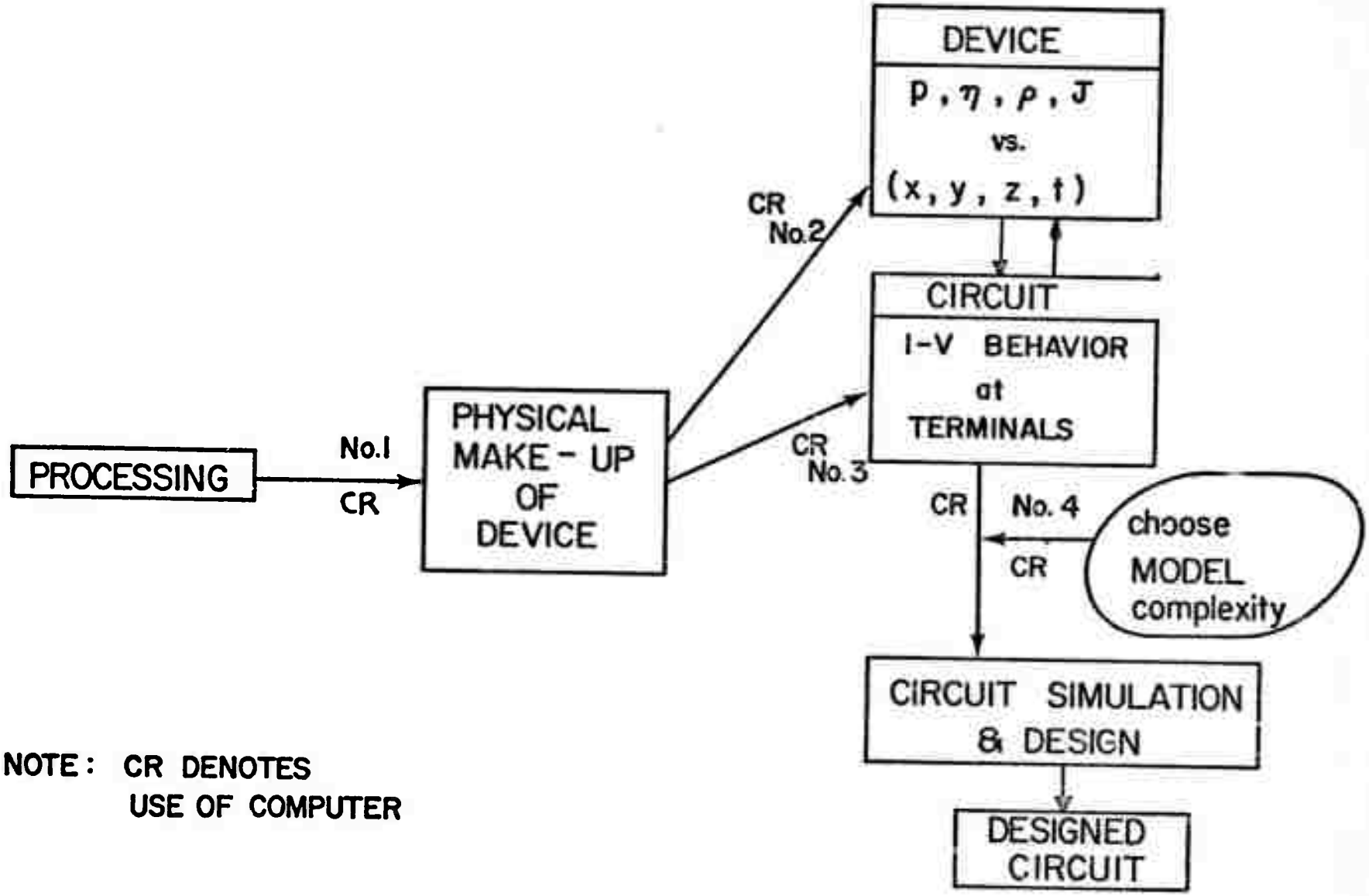

Fig. 1 Four modeling problems involved in modern circuit design.

the complexity of model selected to present each device in the circuit. The choice of model for active devices such as the bipolar transistor is particularly crucial. Since the invention of the bipolar transistor in 1949, many different circuit models have been proposed to account for the various phenomena that combine to determine transistor performance. But the related problem of systematically selecting the most appropriate model to represent each transistor in a given circuit environment has as yet received scant attention. The present paper describes a method for systematic model selection. For dc circuits operating in ordinary environments, it has proved capable of substantial savings in cost of analysis, and it potentially enables simulation of larger circuits than hitherto possible.[1,2] Application of this method to the simulation of irradiated circuits requires extensions, some of which are suggested.

II. Reservoir of Available Models

To provide perspective, we review certain of the transistor models available for selection. First, there exist the classical models: the Ebers-Moll model[3] and its equivalents.[4] In this paper the term, Ebers-Moll model, will mean the model in the original sense,

$$\begin{bmatrix} I_E \\ I_C \end{bmatrix} = \begin{bmatrix} (1 + \frac{1}{\beta_F})\, I_S & -I_S \\ -I_S & (1 + \frac{1}{\beta_R}) \end{bmatrix} \begin{bmatrix} \exp\,(\frac{qV_{EB}}{kT}) - 1 \\ \exp\,(\frac{qV_{CB}}{kT}) - 1 \end{bmatrix} \tag{1}$$

$$I_E + I_B + I_C = 0,$$

in which the slope factors associated with the exponential terms are unity and in which the parameters of the square matrix are constants, independent of the current or voltages at the device terminals. In Eq. (1), kT/q denotes the thermal voltage and β_F and β_R denote the forward and reverse current gains, respectively. This form of the Ebers-Moll model is termed its transport version, which exhibits certain advantages in representing modern transistors relative to its so-called injection version.[5]

The Ebers-Moll model is the simplest of the available dc transistor models, and this is its main attribute. Risk lies in its use, however, for it may not embody enough accuracy to yield a realistic simulation. To avoid

such risk, workers who developed package computer analysis programs[6-8] derived more accurate models by retaining the form of the Ebers-Moll model but letting the parameter values depend on current and voltage. The dependence was determined by measurements at the device terminals. Though this curve-fitting procedure gave greater accuracy, it did so at the cost of increased complexity and its consequent disadvantages: increased memory requirement and cpu time, and severe limitations of the size of circuit amenable to simulation. Recently, Gummel and Poon proposed a model that retains much of the accuracy of the curve-fitting approach, yet is mathematically more compact.[9,10] Moreover, the Gummel-Poon formulation contains a set of models that facilitates trading between accuracy and simplicity. This is a highly desirable attribute.[11]

III. Model Selection

The foregoing models constitute a basic part of the reservoir of available models from which theanalyst can choose. Our objective is to choose from this reservoir for each transistor in a circuit under study the simplest model that will give adequate accuracy. Thereby we avoid the severe limitation on circuit size and the excessive cpu time and memory requirements associated with representing each transistor by the most complex model available as well as the risk and the prohibitive cost of experimental cut and try associated with representing each transistor by the simplest model available. The following method accomplishes this objective:

1. Read in the network configuration using the Ebers-Moll model (with parasitic resistances) to represent each transistor.
2. Analyze the network using an analysis program of choice.
3. Determine for each transistor whether the computer currents and voltages at its terminals are consistent with the approximations underlying the model. This self-consistency check is accomplished by comparing the computed terminal currents and voltages with onset parameters, defined below, which describe the onset of failure of the approximations.
4. Increase model complexity where failure occurs in accord with which of the onset parameters is violated.
5. Analyze the network again.
6. Continue this procedure until self-consistency prevails for each transistor in the network.

IV. Model Failure and Onset Parameters

Implementation of this method requires specification of the onset parameters, which characterize the onset of model failure. This we now do for

the Ebers-Moll model. For simplicity this discussion will limit consideration to transistors operating in the static, forward-active model; moreover, we ignore for now the effects of a radiation environment. For these conditions the Ebers-Moll model fails because of six phenomena neglected in its formulation:

(1) High injection in the base[12,13]

(2) Emitter crowding[14,15]

(3) High current modes in the collector[16-24]

(4) Breakdown[4,25-28]

(5) Dominance of net recombination in junction transition regions and at surfaces[29,30]

(6) Early effect (base-width modulation)[31]

The Early effect can be easily incorporated in the Ebers-Moll formulation by the addition of a single parameter.[32] This parameter, termed the Early voltage, is defined by the intersection of the extrapolations of the forward-active $I_C - V_{CE}$ characteristics. The Early effect differs from the other phenomena listed above in that it occurs for all currents and voltages in the forward-active region of transistor operation. In contrast, the other five phenomena occur only over certain ranges of currents and voltages; consequently the onset of these phenomena can be described by specifying pertinent critical voltages or currents, which are the onset parameters referred to earlier. For example, the usual measurements[26] employed to characterizepunch through, avalanche or Zener breakdown will determine the critical voltage that signals the onset of breakdown. Further, the critical current below which dominance occurs of net recombination in the junction transition region or at surfaces can be easily found from the slopes appearing on the log I_B-V_{BE} characteristics.[29,30] The onset parameters for the other three phenomena will now be described.

A. High Injection in the Base

High injection in the base sets in when the charge injected in the base reaches some sizeable fraction F_{HIB} of the net ion charge present there in thermal equilibrium. Expressing this statement by charge-control theory gives the onset parameter $I_{C\text{-}HIB}$ as

$$I_{C\text{-}HIB} = F_{HIB}\, q\, A_E\, N_B/\tau_f \qquad (2)$$

in which A_E denotes the emitter area, N_B is Gummel's number,[33] and τ_f is the forward charge-control time constant.[5] The constant F_{HIB} is chosen at the analyst's discretion in accord with the maximum error tolerable in assessing model adequacy;[2] typically one selects values of 1, 0.5, or 0.25. If the collector current exceeds $I_{C\text{-}HIB}$, the phenomena normally associated with high injection set in: degradation of emitter efficiency and current gain; diminishing of base resistance; current dependence of internal variables such as lifetime and electric field; and alteration of the Boltzmann relation between barrier voltage and injected carrier density.

To illustrate the procedure of model updating, suppose that the initial computer analysis shows for a particular transistor model that the collector current exceeds $I_{C\text{-}HIB}$ but that no other onset parameter is violated. We then replace the errant model with the Gummel-Poon model, but abbreviated to contain only those parameters necessary to account for high injection in the base. Other models are similarly updated where necessary, the network is then again analyzed, and the method outlined earlier is followed until self-consistency everywhere prevails.

B. Emitter Crowding

According to present theory,[14,15] emitter crowding begins to set in when the collector current reaches approximately

$$I_{C\text{-}CR} = F_{CR} \frac{2kT/q}{R_B/m\beta_f} \tag{3}$$

in which F_{CR} again denotes a constant chosen as for high injection at the analyst's discretion, kT/q is the thermal voltage, R_B is the transverse base resistance, m is a constant depending on the stripe geometry, and β_f is the forward current gain. If the collector current exceeds $I_{C\text{-}CR}$, the effects associated with emitter crowding start to become severe: the thresholds of high injection in the base and high current modes in the collector are hastened, with accompanying degradation of Beta and f_T, and the base resistance diminishes.

To update a model to represent emitter crowding, one can use a version of the Gummel-Poon model abbreviated to contain only enough complexity to account for crowding. The resulting model is moderately complicated, however, because the Gummel-Poon formulation is based on the assumption of

one-dimensional flow. It accomplishes a first-order modeling of the effects of multi-dimensional flow, such as those accompanying crowding, by curve-fitting one of the so-called "push-out" parameters.[10] Thus computational advantage and improved accuracy both may derive from use instead of a model patterned after the work of Ghosh.[15] At the present, insufficient empirical and computational evidence exists to suggest which method of updating for crowding is superior.

C. High Current Modes in the Collector

Two basically different mechanisms have been put forward to explain the degradation of Beta and f_T that occurs in epitaxial transistors because of high currents in the collector region. In the first mode of operation, one assumes that increasing current gives rise to quasi-saturation following collapse of the collector space-charge region.[16,20-23] In the second, one assumes that increasing current leads to conditions under which space-charge-limited flow is avoided by the occurrence of either base widening or lateral spreading or both.[17,18]

The origin of these two different modes lies in the two opposing tendencies indicated in Fig. 2 that accompany high currents in the collector region. On the one hand, increasing collector current reduces the effective voltage applied across the collector space-charge region; thereby this region tends to collapse as current rises, leading ultimately to quasi-saturation. On the other hand, increasing collector current implies the existence of mobile electrons whose charge tends to cancel that of the donor ions; thus the collector space-charge region tends to widen with increasing current, producing eventually the mode associated with space-charge-limited flow.

Which mode predominates[24] is characterized by the onset parameter

$$V_{crit} \simeq \frac{v_{sat}}{\mu_{no}} W_C \qquad (4)$$

in which v_{sat} denotes the scatter-limited velocity of mobile electrons in the collector region, μ_{no} denotes the low-field mobility there, and W_C denotes the thickness of the low-conductivity epitaxial layer. For

$$V_{crit} < V_{CB}$$

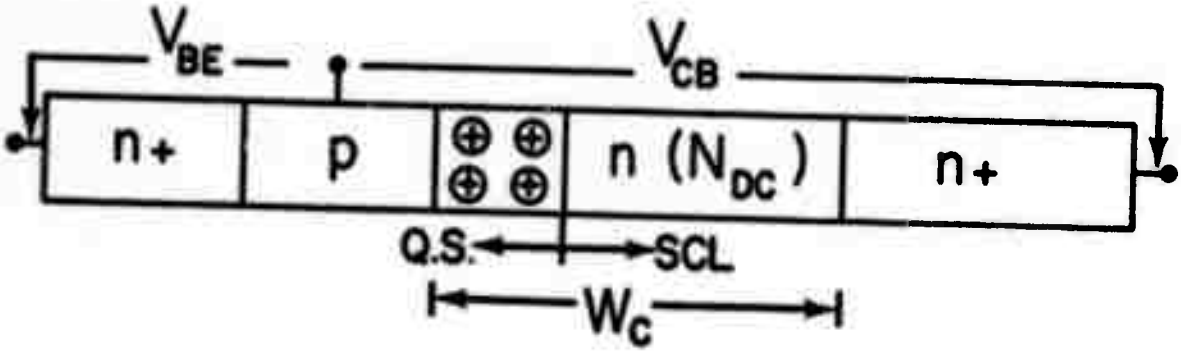

Fig. 2 Depending on the value of the collector voltage relative to the value of the onset parameter V_{crit}, the collector space-charge region will either tend to collapse of to widen, as indicated by the arrows. Collapse leads toward the mode of quasi-saturation, and widening leads toward the mode associated with space-charge-limited flow.

quasi-saturation occurs; otherwise space-charge-limited flow tries to start.

When the collector current approaches the onset parameters

$$I_{C\text{-}HCC} = F_{HCC}[q\ N_{DC}\ A_E\ \mu_{no}/W_C]\left[\frac{v_{sat}}{v_{sat} + (V_{CBT}/W_C)\mu_{no}}\right]\ V_{CBT} \qquad (5)$$

either quasi-saturation or the mode associated with space-charge-limited flow will begin.[2,24] The mode that prevails is found by the test involving V_{crit}. Here again F_{HCC} is an adjustable constant chosen subject to the maximum error tolerable in assessing model adequacy.[2] The first term in brackets in Eq. (5) denotes the conductance of the high-resistivity portion of the collector, taken apart from the rest of the transistor. The second term in brackets accounts for the field dependence of mobility. By V_{CBT} we mean the total voltage (applied plus contact potential) across the collector.

In updating models to account for the presence of high current modes in the collector, one should carefully note which mode prevails. If the collector current exceeds $I_{C\text{-}HCC}$ and the test with V_{crit} implies the presence of the mode associated with space-charge-limited flow, then base resistance, beta and f_T all diminish with increasing current. Evidence presently available[17] suggests that the functional dependences describing this diminution result from a combination both of base widening and lateral spreading. This mode therefore requires that the model used in updating account for the effects of multi-dimensional flow. As was discussed earlier in connection with emitter crowding, the presence of multi-dimensional flow raises questions concerning the adequacy of the Gummel-Poon formulation which the present dearth of experimental and computational experience leaves unsettled. If, on the other hand, the self-consistency test implies the existence of the quasi-saturation mode, the associated one-dimensional flow suggests that one can update with confidence using an appropriately abbreviated version of the Gummel-Poon model.

V. Epilogue

A reservoir of transistor models exists from which one can select. The purpose of this paper has been to describe how systematic selection can be incorporated into the computer simulation of circuit behavior in such a way that the models selected best fit the circuit environment in which

each transistor resides. The essence of the method involves a self-consistency test for the assessment of model adequacy. In this test an initial simulation yields currents and voltages which are compared with onset parameters. Violation of any onset parameter calls for an updating of the pertinent model. The model used as the replacement in the next simulation is not the most complex model available, but rather a model only complicated enough to represent the phenomena implied by the violated onset parameters. Thus the method puts complexity only where needed and only as much as needed. In this way it leads to the selection, for each transistor in a circuit being simulated, of the model of least complexity that will give adequate accuracy. Benefits follow: basically the method simplifies computation, saves computational cost, and potentially enables the simulation of larger circuits than hitherto possible.

It is sensible that any modeling techniques be conceived and tried for conventional circuits before subjecting them to the additional difficulties imposed by a radiation environment. The applicability of the method described here to the simulation of irradiated circuit behavior has yet to be demonstrated. But some comment about potential applicability can be made.

The method of model selection applies directly to the dc simulation of transistor circuits suffering permanent radiation damage. The likely dominance of net recombination current from the transition regions can be included by use of the Gummel-Poon formulation, appropriately abbreviated. To describe the transient behavior of a circuit exposed to time-varying radiation, however, one must generalize both the reservoir of available models and the self-consistency test for model adequacy. One needs a hierarchy of models of different accuracies and complexities that embodies the displacement currents that flow and the photocurrents generated in the intrinsic and extrinsic portions of the transistor. The test for model adequacy must be generalized to assess whether the transient components of the computed currents and voltages are consistent with the approximations underlying each model used in a simulation.

REFERENCES

1. F. A. Lindholm and S. W. Director, "Assessing model adequacy in integrated-circuit simulation," 1971 IEEE International Solid State Circuits Conference: Technical Digest, pp. 42-43, Feb. 1971.

2. F. A. Lindholm, S. W. Director, and D. L. Bowler, "Assessing model adequacy and selecting model complexity in integrated-circuit simulation," IEEE Journal of Solid State Circuits, Vol. SC-6, pp. 213-223, August 1971.

3. J. J. Ebers and J. L. Moll, "Large signal behavior of junction transistors," Proc. IRE, vol. 42, pp. 1773-1784, Dec. 1954.

4. D. J. Hamilton, F. A. Lindholm, and J. A. Narud, "Comparison of large-signal models for junction transistors," Proc. IEEE, vol. 52, pp. 239-248, March 1964.

5. J. Logan, "Characterization and modeling for statistical design," Bell Syst. Tech. J., vol. 50, pp. 1105-1147, April 1971.

6. A. F. Malmberg and F. N. Cornwell, "NET-1 Network Analysis Program LA-3119," Los Alamos Scientific Laboratory, Sept. 1964.

7. L. D. Milliman, W. A. Massena, and R. H. Dickhaut, "CIRCUS, A digital computer program for transient analysis of electronic circuits - User's guide," Harry Diamond Laboratories, 346-1, Jan. 1967.

8. J. C. Bowers and S. R. Sedore, SCEPTRE: A Computer Program for Circuit and Systems Analysis, Prentice Hall 1971, pp. 111-154.

9. H. K. Gummel and H. C. Poon, "A compact bipolar transistor model," 1970 ISSCC Technical Digest, vol. 13, pp. 78-80, Feb. 1970.

10. H. K. Gummel and H. C. Poon, "An integral charge control model of bipolar transistors," BSTJ, vol. 49, pp. 827-852, May-June 1970.

11. F. A. Lindholm, "Device modeling for computer-aided analysis and design of integrated circuits," Solid State Electronics, vol. 12, pp. 831-840, Nov. 1969.

12. a. A. S. Grove, Physics and Technology of Semiconductor Devices. New York: Wiley, 1967.
b. A. K. Jonscher, Principles of Semiconductor Device Operation. New York: Wiley, 1960.
c. P. E. Gray, D. DeWitt, A. R. Boothroyd, and J. F. Gibbons, Physical Electronics and Circuit Models of Transistors. New York: Wiley, 1964.

13. L. E. Clark, "High current-density beta diminution," IEEE Trans. Electron Devices, vol. ED-17, pp. 661-667, Sept. 1970. (Contains extensive review of prior work.)

14. J. R. Hauser, "The effects of distributed base potential on emitter current injection density and effective base resistance for stripe transistor geometries," IEEE Trans. Electron Devices, ED-11, pp. 238-242, May 1964.

15. H. N. Ghosh, "A distributed model of the junction transistor and its application in the prediction of the emitter-base diode characteristic, base impedance, and pulse response of the device," IEEE Trans. Electron Devices, vol. ED-12, pp. 513-531, Oct. 1965.

16. C. T. Kirk, Jr., "A theory of transistor cutoff frequency (fr) falloff at high current densities," IRE Trans. Electron Devices, vol. ED-9, pp. 164-174, Mar. 1962.

17. R. J. Whittier and D. A. Tremere, "Current gain and cutoff frequency falloff at high currents," IEEE Trans. Electron Devices, vol. ED-16, pp. 39-57, Jan. 1969.

18. A. van der Ziel and D. Agourides, "The cutoff frequency falloff in UHF transistor at high current," Proc. IEEE (Lett.), vol. 54, pp. 411-412, Mar. 1966.

19. H. C. Poon, H. K. Gummel, and D. L. Scharfetter, "High injection in epitaxial transistors," IEEE Trans. Electron Devices, vol. ED-16, pp. 455-458, May 1969.

20. L. E. Clark, "Characteristics of two-region saturation phenomena," IEEE Trans. on Electron Devices, vol. ED-16, pp. 113-116, January 1969.

21. L. A. Hahn, "The effect of collector resistance upon the high current capability of transistors," IEEE Trans. on Electron Devices, vol. ED-16, pp. 654-656, July 1969.

22. J.R.A. Beale and J.A.G. Slatter, "The equivalent circuit of a transistor with a lightly-doped collector operating in saturation," Solid State Electronics, vol. 11, pp. 241-252, 1968.

23. C.W. Gwyn, G. G. Summers, and W. T. Corbett, "Modeling of the saturation characteristics of high voltage transistors," IEEE Trans. Nuclear Science, vol. NS-17, pp. 63-69, Dec. 1970.

24. D. L. Bowler and F. A. Lindholm, "High current in epitaxial transistors," 1971 IEEE International Electron Devices Meeting, Washington, D. C., Oct. 1971.

25. R. M. Warner, Jr., and J. N. Fordemwalt, Integrated Circuits: Design Principles and Fabrication. New York: McGraw-Hill, 1965.

26. A. B. Phillips, Transistor Engineering. New York: McGraw-Hill, 1962.

27. S. M. Sze, Physics of Semiconductor Devices. New York: Wiley, 1969.

28. F. van de Wiele, R. van Overstraeten, and H. de Man, "Graphical method for the determination of junction parameters and of multiplication parameters," Solid-State Electron., vol. 13, pp. 25-36, Jan. 1970.

29. J. D. Meindl, Micropower Circuits. New York: Wiley, 1969.

30. a. C. T. Sah, R. N. Noyce, and W. Shockley, "Carrier generation and recombination in p-n junctions and p-n junction characteristics," Proc. IRE, vol. 45, pp. 1228-1243, Sept. 1957.

b. C. T. Sah, "Effect of surface recombination and channel on p-n junction and transistor characteristics," IRE Trans. Electron Devices, vol. ED-9, pp. 94-108, Jan. 1962.

31. J. M. Early, "Effects of space charge layer widening in junction transistors," Proc. IRE, vol. 46, pp. 1141-1152, Nov. 1952.

32. F. A. Lindholm and D. J. Hamilton, "Incorporation of the early effect in the Ebers-Moll model," IEEE Proceedings Letters, to appear September 1971.

33. H. K. Gummel, "Measurement of the number of impurities in the base layer of a transistor," Proc. IRE, vol. 49, pp. 834-835, 1961.

FIGURE CAPTIONS

Fig. 1 The four modeling problems involved in modern circuit design.

Fig. 2 Depending on the value of the collector voltage relative to the value of the onset parameter V_{crit}, the collector space-charge region will either tend to collapse or to widen, as indicated by the arrows. Collapse leads toward the mode of quasi-saturation, and widening leads toward the mode associated with space-charge-limited flow.

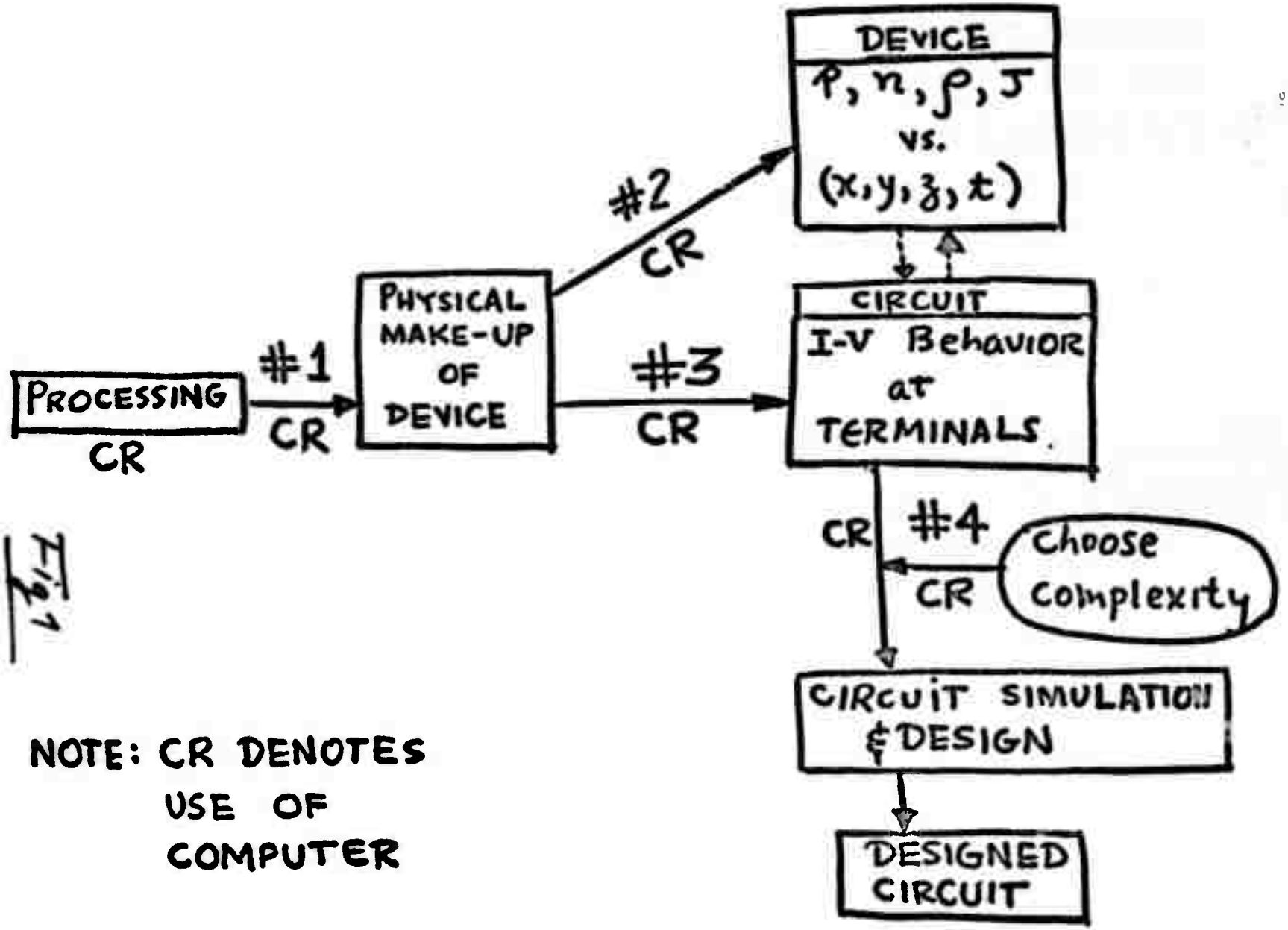

Fig. 1

NOTE: CR DENOTES USE OF COMPUTER

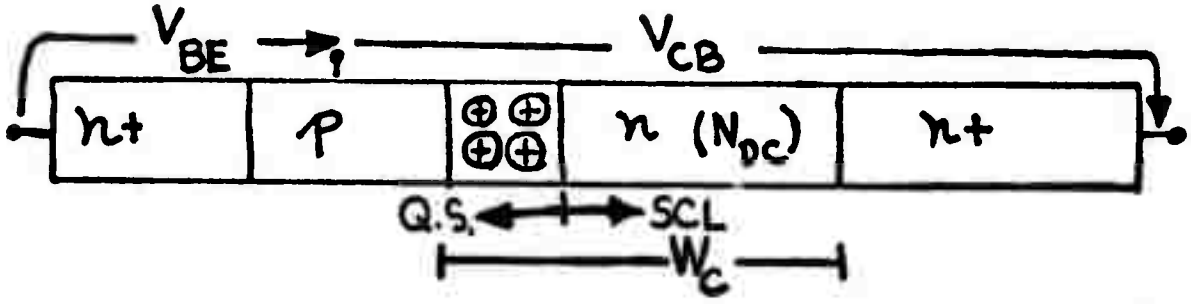

Fig 2

III. Radiation Sensitivity of Amorphous Semiconductors (L.L. Hench)

A. STRUCTURAL EFFECTS ON FAST NEUTRON RADIATION SENSITIVITY OF SEMICONDUCTING GLASSES

(H. F. Schaake, A. E. Clark and L. L. Hench)

Introduction

Because of the high degree of structural disorder in a glass, amorphous semiconductors are materials whose electrical properties should be relatively insensitive to high energy radiation. The fact that a certain amount of structural organization is present, however, suggests that a suitably high radiation dosage may affect the electrical conductivity.

The structural organization in a glass may be considered from both the atomic level and from the microscopic level. In the first class, recent pair function distribution analyses of amorphous x-ray diffraction studies have shown a high degree of structural correlations as far as the seventh-neighbors[1] in glasses.[1,2] Geometrical arguments,[3,4] coupled with the requirement for dense packing, have suggested that there is even more organization in the glass than is indicated by interpreting the pair function distributions as random arrays of bond lengths and angles. That is, the above arguments suggest that the existence of a particular-atomic coordination at one point in the glass results in a very high probability that in nearby regions the coordination is predictable, i.e., often the same.

Conventional heterogeneities constitute the second class of organization in glasses. Heterogeneities may result from 1) microcrystallization during quenching of bulk or thin films; 2) glass-glass phase separations; 3) nucleation and growth of crystals from a glassy phase; and 4) compositional fluctuations. Such features are extraordinarily difficult to avoid in-toto during the fabrication, annealing, and measuring of most amorphous semiconductors.[5]

It is proposed that when a high energy radiation dosage is sufficiently large to alter either the atomic structural organization in the glass or the microstructural features, changes in the electrical properties will be observed. Such changes have been observed in heterogeneous semiconducting glasses previously reported.[5,6,7]

In the present study, the effect of fast neutron irradiation on the electrical properties of 33 mole% K_2PO_3-67 mole% V_2O_5 semiconducting glasses has been investigated. The degree of structural organization has been varied by subjecting the glasses to different thermal treatments before irradiation. A correlation between various structural features and fast neutron damage thresholds is considered and irradiation dependent changes in electrical conduction mechanisms are proposed.

Measurements and Analysis

The conductivity as a function of frequency of a series of samples was measured before and after various fast neutron (70.1 MeV) radiation doses. Details of sample preparation, conductivity bridge measurements and irradiation techniques are given elsewhere.[5,6,7] The 67% V_2O_5-33% K_2PO_3 samples were melted in Pt crucibles in air and rapidly quenched in steel molds. The samples analyzed in this study were in the as-quenched condition, heat treated one-half hour at 288°C, and heat treated 30.8 hours at 288°C. As previously reported, these thermal treatments produce a glass-in-glass phase separation and microcrystallization, respectively.[5]

There is evidence of the formation of some sort of barrier at the electrode-sample interface giving rise to a low frequency relaxation mechanism.[8] It is impossible to distinguish between interfacial and heterogeneous relaxation mechanisms on the basis of overall conductivity measurements alone.[9] Furthermore, if both interfacial and heterogeneous relaxation mechanisms are present, then the interpretation of the low frequency conductivity will be complicated by the intermixing of these effects. Complicating the situation further is the fact that the conductivities and dielectric constants of the constituent phases are frequency dependent, leading to an even more complex overall behavior.

A degree of simplification can be achieved if certain conditions are met. The conductivity for both heterogeneous and electrode barrier mechanisms will be given by an equation:[9]

$$\sigma(\omega) = \sigma' + \frac{(\varepsilon_s - \varepsilon_\infty)\omega^2 \tau_R}{1+\omega^2 \tau_R^2} \qquad (1)$$

If $\omega >> 1/\tau_R$, then Eq. (1) becomes

$$\sigma(\omega) = \sigma' + \frac{(\varepsilon_s - \varepsilon_\infty)}{\tau_R} = \sigma_o \qquad (2)$$

i.e., a plateau is reached in the frequency vs. conductivity curves (assuming that σ', ε_s, ε_∞ and τ_R are independent of frequency in this range). If only electrode barrier effects are present, σ_o is the D.C. conductivity of the sample in the absence of the barrier. If there are heterogeneous effects, then σ_o is as given in Eq. (2) with the parameters as defined in Reference 9. A plateau was always observed in the present measurements (see Fig. 1).

Changes in the conductivity at still higher frequencies will be due to changes in the conductivities and dielectric constants of the phases present. The A.C. conductivity defined by

$$\sigma_{AC}(\omega) = \sigma_{Meas}(\omega) - \sigma_o \qquad (3)$$

therefore is due to frequency dependent mechanisms operating within the phases.

The analysis of the radiation dependent conductivity changes will center largely around $\sigma_{AC}(\omega)$ and σ_o. In all cases the conductivity could be represented by an equation of the form

$$\sigma(\omega) = A \exp(-E_0/kT) + B\omega^n \exp(-E_1/kT) + C\omega^2 \exp(-E_2/kT) \quad (4)$$

The first term is σ_o; the second two terms comprise $\sigma_{AC}(\omega)$. In the present as well as in previous investigations n had a value from 0.8 to 1.3.

Experimental Results

In the quenched glass (Fig. 2) a dose of 1×10^{17} nvt produces no change in the $\omega^{0.8}$ conductivity, while the ω^2 contribution decreases. Further irradiation to a dose of 2.1×10^{17} nvt results in the complete destruction of the ω^2 conductivity in the observed frequency range and an increase in the $\omega^{0.8}$ conductivity by a factor of ~3.

In the glass heat treated for one-half hour at 288°C, a dose of 5×10^{16} nvt leaves the A.C. conductivity unchanged (Figs. 3 and 4). The activation energy for the $\omega^{0.8}$ conductivity remains at 0.1 ev, while that for the ω^2 conductivity remains at 0.05 ev. σ_o, on the other hand, increases by 5%, while the activation energy decreases slightly from ~0.21 ev to ~0.19 ev (Fig 5). The results of higher dosages on a similar glass is shown in Fig. 6, After a dosage of 1×10^{17} nvt, the $\omega^{0.8}$ conductivity increases by a factor of 3, while the ω^2 conductivity increases by a factor of almost 13. Further irradiation to a dose of 2.7×10^{17} nvt results in the $\omega^{0.8}$ conductivity decreasing to 1.5 times the original and the ω^2 conductivity decreasing to 10 times the original. At the same time, σ_o behaves as follows:

Pre-irradiation	1.43×10^{-4}
1×10^{17} nvt	1.65×10^{-4}
2.7×10^{17} nvt	0.29×10^{-4}

The data for the glass heat treated 30.8 hours is shown in Fig. 7. There is no detectable $\omega^{0.8}$ conductivity in any samples. A dose of 1×10^{17} nvt causes the ω^2 conductivity to increase by a factor of 2. Further radiation to a level of 2.1×10^{17} results in no change in the ω^2 conductivity, but does introduce a new low frequency dependence proportional to $\omega^{1.3}$. As recently discussed,[7] the behavior of σ_o is as follows:

Pre-irradiation	5.2×10^{-3}
1×10^{17} nvt	6.8×10^{-3}
2.1×10^{17} nvt	5.85×10^{-3}

Discussion

The data presented suggests that the detectable threshold for neutron irradiation alteration of electrical properties in the 33 KPO_3-67 V_2O_5 glass is 5×10^{16} nvt. In the glass heat treated for one-half hour, this dosage resulted in no change in the A.C. conductivity, and a small increase in σ_o. In the quenched glass and in the glass heat treated for 30.8 hours, this threshold is under 1×10^{17} nvt; examination of the data suggests that it, too, is about 5×10^{16} nvt. Since the 30.8 hour glass contains ~0.4 volume fraction crystals, this means that over a range of from ~0 to ~0.4 volume fraction crystals, the radiation damage threshold is 5×10^{16} nvt.

Considering the controvery which apparently exists over the source of the ω^2 behavior of the A.C. conductivity at higher frequencies,[10] the present data is very interesting. Of particular interest is the fact that the $\omega^{0.8}$ and ω^2 conductivity possess different activation energies, both of which are smaller than the σ_o activation energy. It is also seen that

the $\omega^{0.8}$ and ω^2 conductivities change by different amounts with sufficiently high radiation, indicating that they are in fact due to different mechanisms.

In this research, ω^2 A.C. conductivity has been observed in every vanadate glass and glass-ceramic measured, while it has never been observed in a variety of ionically conducting glasses and glass-ceramics investigated with the same dielectric facility.

An ω^2 A.C. conductivity dependence is not predicted by a random hopping center model.[11] However, as discussed in the Introduction, a glass is not a random array of atoms, but contains regions of equivalent ionic coordination. The ω^2 conductivity can be attributed to the regions of structural equivalence. An ω^2 dependence will be observed if there exists in the glass a considerably larger number of short relaxation times than would be present in a random array of hopping centers (the hops between centers randomly distributed gives rise to the $\omega^{0.8}$ A.C. conductivity). Such a situation appears to be possible in a real glass due to the high degree of short range order.

To demonstrate this, we shall digress briefly to consider the case of amorphous silicon. This digression is necessary because of the lack of structural information on the vanadate glasses. Pair function analyses of any three or four element glass has not been reported. However, considerable structural information has been amassed for amorphous silicon. Grigorovici and others[3] have argued that the "mistake" in silicon which leads to an amorphous rather than a periodic structure is the occurrence of adjacent Si_4 tetrahedra in the eclipsed (cis-) rather than the correct, staggered (trans-) configuration, i.e., a rotation of 60°. This is an error in third nearest neighbors in the radial distribution function; first and second neighbor distances remain unchanged. Looking at these molecular units, the ground state energy in the cis-Si will be higher than in trans-Si. The cis-configuration forces the wave-function to

have more than the trans-configuration curvature; hence the kinetic energy, and by the virial theorem, the total energy is higher.

Grigorovici has also argued that these mistakes do not occur randomly; in order to achieve a high density of packing the mistakes occur in groups -- that is, the existence of a cis-grouping about one Si atom occasions the existence of one or more cis-groupings about nearby Si atoms. In the extreme case of grouping of these structural mistakes, we are led to the Vornoi dodecahedron. Amorphous silicon may therefore be described as a mixture of clusters of mistakes and regions of crystalline-coordinated Si. We shall now make the following assumption: That the energy of the first excited state of the cis-configuration is lower than the first excited state of the trans-configuration. (The validity of this assumption is currently being tested by direct calculation; it certainly seems reasonable.) Thus, when we investigate the wavefunctions of the conduction states in the glass, those in the conduction band or localized just below it, we will find that those having the lowest energy have large contributions from the cis-grouping "molecular" wavefunctions, and small contributions from the trans-grouping "molecular" wavefunctions. Thus, if the above assumption is correct, the localized states at the bottom of the conduction band are localized on clusters of mistakes.

Two types of hops may occur for a carrier located in the localized states at the bottom of the conduction band*: it may

---

*NOTE: When the overlap potential energy ($J_{ij} = \langle i|r_i|j\rangle$ for a simple one-electron model) between two states in the same cluster sufficiently exceeds the electron-lattice binding energy E_i for a single state $E_i \approx 1/2Kr_{ii}$, where K is the dielectric constant and r_{ii} is the radius of static ($r_{ii} = \langle i|r|i\rangle$), then the electron will be localized on both sites; i.e., the minimum energy wavefunction is $|i+j\rangle$. However, a transition to $|i-j\rangle$ may still take place, since the dipole moment $\langle i-j|x|i+j\rangle$ is not zero, and the following argument is valid.

hop to another cluster, or it may hop to another site in the same cluster.

For a hop through a given distance, the former process will result in a longer relaxation time than the latter. This is because the overlap between localized states on different clusters is considerably smaller than the overlap between two states on the same cluster. Therefore, as the hopping distance, d, decreases, the average relaxation time, $\tau(d)$, decreases, first in agreement with the random-center distribution model, then more rapidly, since the probability is that shorter hops occur within a mistake cluster. This results in a larger number of hops with short relaxation times, and a smaller number of hops with moderate relaxation times, and hence to ω^2 and $\omega^{0.8}$ conductivity. The $\omega^{0.8}$ conductivity may be attributed to hops between different clusters of mistakes, while ω^2 conductivity results from hops within a cluster.

A similar situation to that discussed above for amorphous silicon should exist in the vanadate glasses. The basic structural unit in V-O glasses is known to be a vanadium ion surrounded by six oxygen ions in octahedral coordination. From the macroscopic standpoint, the oxygen ions form a densely packed structure (in the crystalline vanadium oxides, the oxygen ions form a close-packed structure, distorted slightly by the vanadium ions), with vanadium ions distributed in octahedral interstices to satisfy charge requirements. The difference between a V^{4+} and a V^{5+} ion is therefore best distinguished by the vanadium ion radial distribution function. In the glasses under study, the existence of other ions (K, P) with different charges and coordination modifies this simple interpretation.

As in silicon, it seems probable that if a mistake occurs which causes a V^{5+} site to have the vanadium ion coordination of a V^{4+} site [which we shall designate $(V^4)^{5+}$], then a number of surrounding sites will have the same error leading to clusters. Note that long-range charge neutrality can be met by having the surrounding region vanadium deficient. Because of the excess positive charge in the vicinity of $(V^4)^{5+}$ sites, the

localized states at the bottom of the conduction band (assuming one exists) will be peaked on these sites.

As in silicon, the clustering of mistakes would lead to $\omega^{0.8}$ and ω^{2} A.C. conductivity. The observed difference in activation energy between the two regions of ω dependence (Figs. 3 and 4) suggests that there is a variation in the average energy levels of the clusters. In other words, there appears to be a small variation in the energy levels of a single cluster. However, if the energy levels within each cluster are averaged, then there will be a larger variation in these averages. Thus, as the temperature is increased, hops become possible between more clusters, yielding a higher activation energy than for hops within a cluster. This variation in levels between clusters could conceivably result from the P_2O_5, K_2O, or V^{4+} impurity ions in the glass.

The foregoing is summarized in the qualitative electronic structure illustrated in Fig. 9 for the glass heat treated one-half hour at 288°C.

A radiation dosage of 5×10^{16} nvt in the one-half hour heat treated glass results in only a small change in the σ_o activation energy (Figs. 3, 4 and 5). This corresponds to a decrease in the energy difference between the Fermi level and the band edge. The effect of this level of radiation is to continue the process begun by the heat treatment. There is also a small increase in the magnitude of σ_o. This has been previously shown through Co^{60} γ-ray experiments to be due to γ-ray ionization of carriers through Compton scattering.

Further irradiation to a dosage of 1×10^{17} nvt (Fig. 6) does change the A.C. conductivity, increasing both the ω^{2} and the $\omega^{0.8}$ conductivity. This would occur if the glass structure became more disordered, leading to the creation of more clusters. An increase in the number of donor V^{4+} ions participating also evidently occurs, resulting from the continuing γ-ray exposure, leading to the higher σ_o and part of the increased A.C. conductivity. The σ_o activation energy may also change when

the dosage is increased to 2.1×10^{17} nvt, the clusters of mistakes evidently become more disordered, leading to a further decrease in the ω^2 conductivity, and a decrease in the $\omega^{0.8}$ conductivity. The band edge energy E_c also increases due to the increased disorder, causing more localized states to exist, resulting in a decrease in σ_o.

In the quenched glass (Fig. 2), the disorder is evidently sufficiently great that radiation causes the glass to approach the random hopping center model; that is, the clusters become sufficiently disordered that the number of hops contributing to the $\omega^{0.8}$ conductivity greatly increases.

The 30.8 hour heat treated glass presents a different picture (Fig. 7). If the clusters of mistakes are large and well separated, then the A.C. conductivity will be proportional to ω^2 as observed. These clusters may be large enough to be recognized as a separate phase as indicated by x-ray diffraction results. Radiation apparently first increases the number of clustered regions. Since they remain well separated, this results mainly in an increase in the ω^2 conductivity. Further irradiation then produces a splitting up of the clusters, resulting in the appearance of $\omega^{0.8}$ conductivity. That the lower frequency conductivity is proportional to $\omega^{1.3}$ may have one of two explanations: (1) Since the glass is electrically heterogeneous, if one phase has a conductivity proportional to $\omega^{0.8}$ and the other to ω^2, then the composite conductivity when the conductivities of the two phases are about equal will be given by:

$$\sigma_{A.C.}(\omega) = C\omega^n$$

where

$$n = v_c(0.8) + (1-v_c)2$$

with v_c the volume fraction of the precipitate phase, and assuming the precipitate phase has ω^2 conductivity. With v_c = 0.4,

$$n = 1.5$$

which is about what is observed. (2) An alternative explanation is that as new clusters are created, they are not randomly distributed but are clustered together. This means that shorter relaxation times are more numerous than in the random cluster distribution model, resulting in a frequency coefficient greater than 0.8, but less than 2.

Summary

1. Due to the existence of structural organization in amorphous semiconductors, there exists a threshold radiation dosage above which changes in electrical properties are observed. For the vanadate glasses in the system 33 KPO_3-67 V_2O_5 this level is 5×10^{16} nvt.

2. The ω^2 conductivity is attributed to electron hops within clusters of structural mistakes, that is, within regions of the glass where the atomic coordination deviates markedly from the crystalline coordination.

3. The observed changes in the A.C. and D.C. conductivity can be attributed to changes in donor concentration as a result of Compton scattering from γ-rays and from changes in atomic structure resulting from neutron-induced damage.

References

1. B. E. Warren and R. L. Mozzi, Acta Cryst., 21, 459 (1966).

2. C. V. Gokularathnam, R. W. Gould and L. L. Hench, Nucleation and Crystallization Revisited, Special Tech. Pub. of Amer. Ceram. Soc., 1971, L. L. Hench and S. W. Freiman, eds.

3. R. Grigorovici, J. Non-Cryst. Solids, 1, 303 (1969).

4. J. Chang, "Structure of Amorphous Ge Films," M.S. Thesis, University of Florida, 1970.

5. L. L. Hench, J. Non-Cryst. Solids, 2, 250 (1970).

6. L. L. Hench, W. D. Tuohig and A. E. Clark, Proceedings of Conf. on Ceramics in Severe Environments, North Carolina State University, December 1970, Plenum Press, New York (to be published).

7. L. L. Hench, H. F. Schaake and A. E. Clark, Proceedings of 4th Internat'l Symposium on Amorphous and Liquid Semiconductors, August 1971 (to be published).

8. L. L. Hench, A. E. Clark and H. F. Schaake, to be published

9. H. F. Schaake, "Heterogeneous Semiconductors," in Physics of Electronic Ceramics, L. L. Hench and D. B. Dove, eds., Marcel Dekker, New York (in press).

10. Proceedings of 4th Internat'l Symposium on Amorphous and Liquid Semiconductors, August 1971 (in press).

11. M. Rollach and T. H. Geballe, Phys. Rev., 122, 1742 (1961).

Figure Captions

Fig. 1 - Total conductivity versus frequency for a 33 mole% KPO_3-67 mole% V_2O_5 glass heat treated 30.8 hours. σ_o is as described in the text.

Fig. 2 - A.C. conductivity ($\sigma_{A.C.}$) of quenched glass for various radiation doses.

Fig. 3 - A.C. conductivity ($\sigma_{A.C.}$) of glass heat treated 0.5 hour. No irradiation.

Fig. 4 - A.C. conductivity ($\sigma_{A.C.}$) of glass heat treated 0.5 hour. Dosage 5×10^{16} nvt.

Fig. 5 - σ_o versus reciprocal temperature for glass heat treated 0.5 hour.

Fig. 6 - A.C. conductivity ($\sigma_{A.C.}$) of glass heat treated 0.5 hour for various doses.

Fig. 7 - A.C. conductivity ($\sigma_{A.C.}$) of glass heat treated 30.8 hours for various doses.

Fig. 8 - Proposed electronic structure for glass heat treated 0.5 hour. Energies indicated are approximate, and in electron-volts. E_F is the Fermi level; E_c the critical energy separating band and localized states.

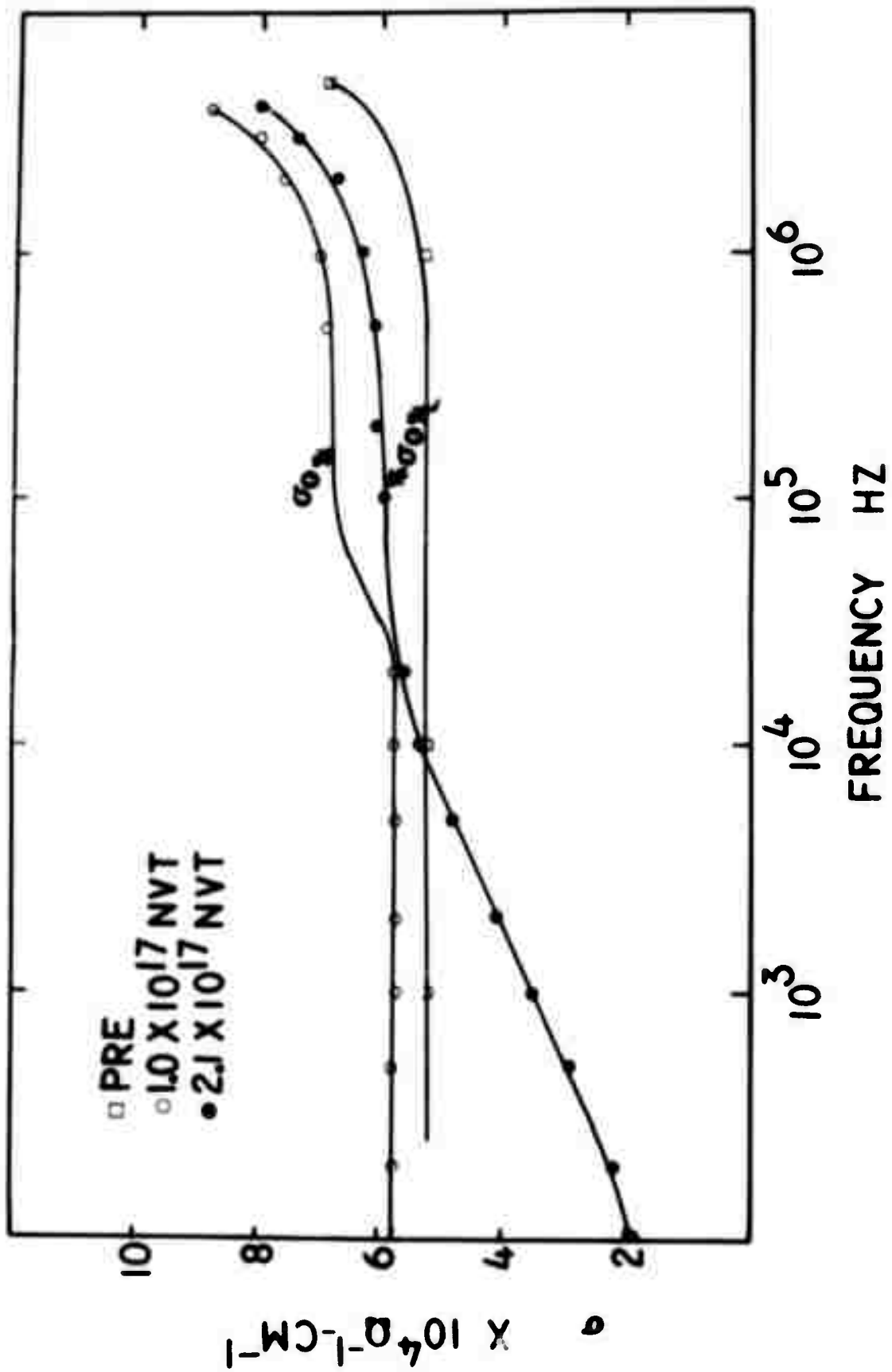
□ PRE
○ 1.0 X 10^17 NVT
● 2.1 X 10^17 NVT
σ X 10^4 Ω^-1-CM^-1
10
8
6
4
2
10^3
10^4
10^5
10^6
FREQUENCY HZ

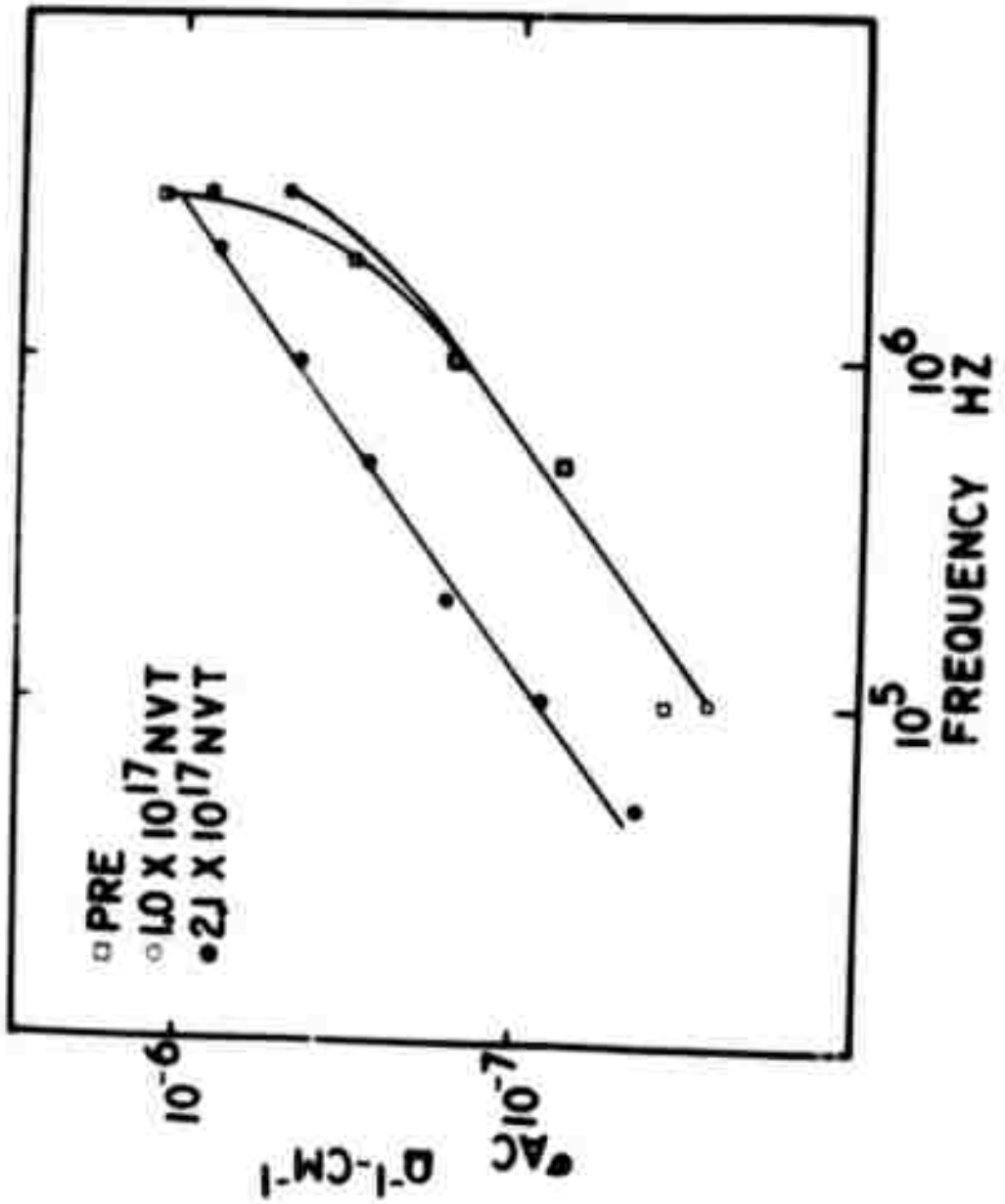
□ PRE
○ 1.0 X 10^17 NVT
● 2.1 X 10^17 NVT
10^-6
10^-7
Ω^-1-CM^-1
σAC
10^5
10^6
FREQUENCY HZ

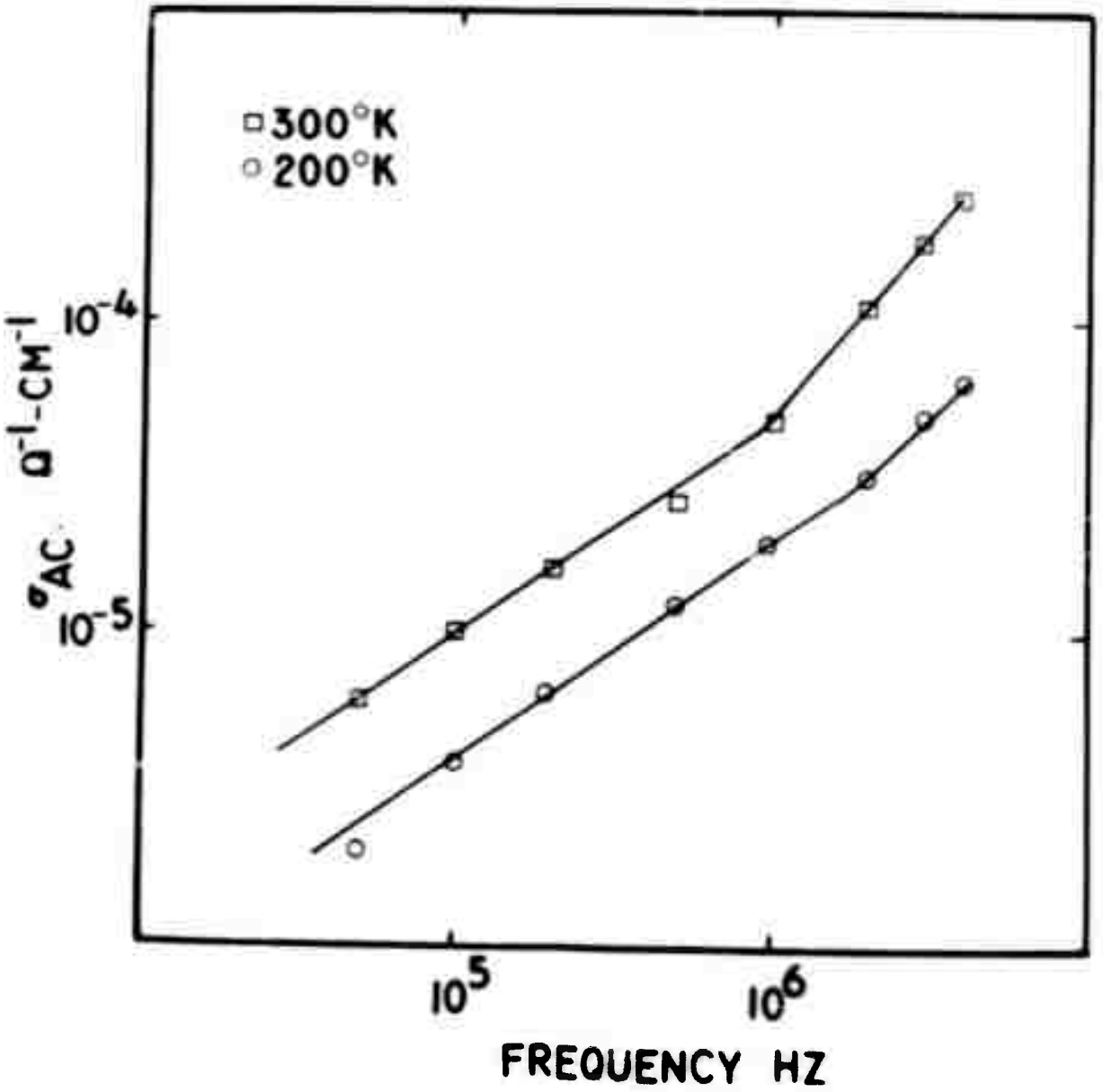
□300°K
○200°K
σ_{AC} Ω^{-1}-CM^{-1}
10^{-4}
10^{-5}
10^{5}
10^{6}
FREQUENCY HZ

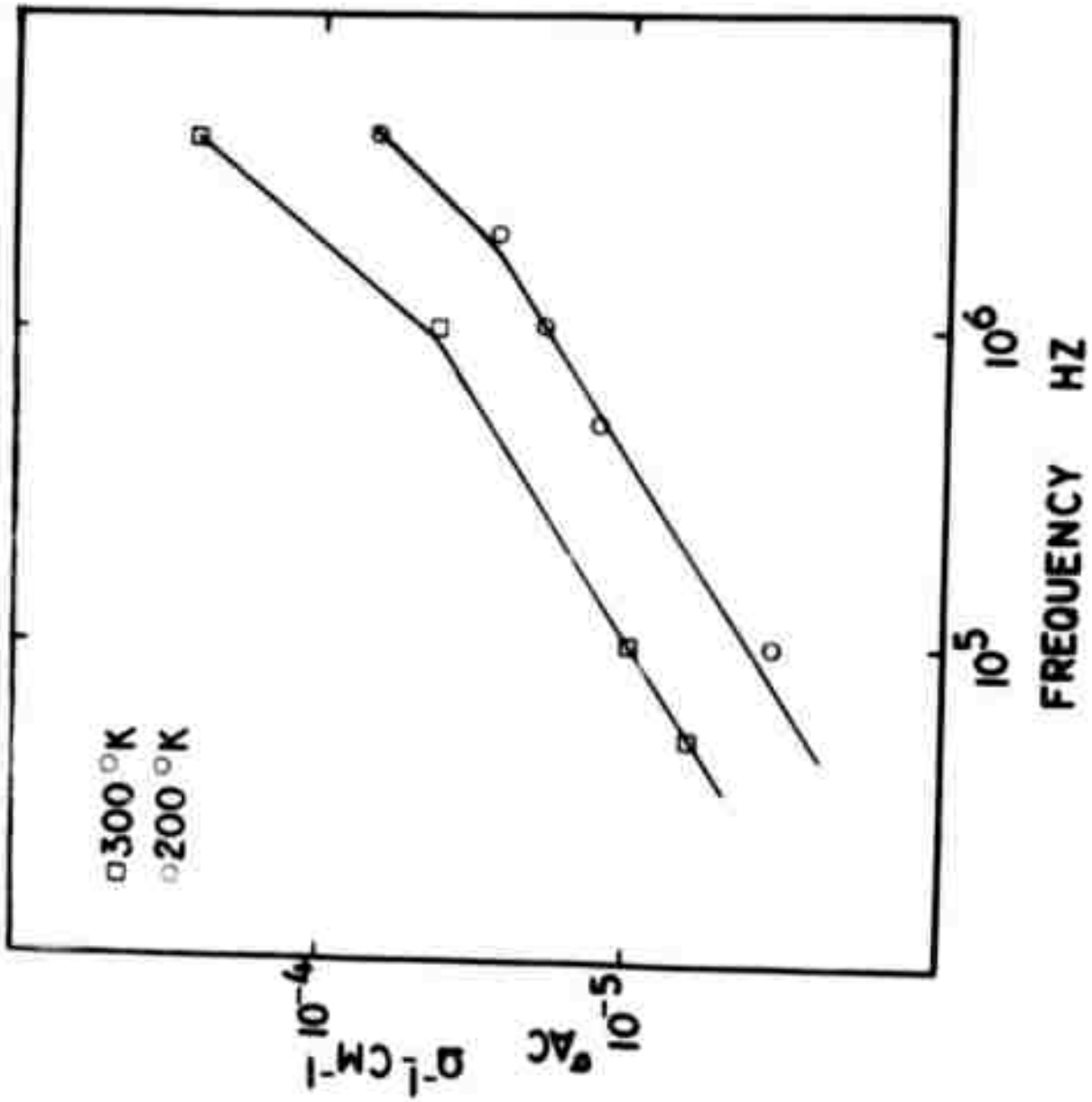
□300 °K
○200 °K
10^{-4}
10^{-5}
σ_{AC} Ω^{-1} CM^{-1}
10^{5}
10^{6}
FREQUENCY HZ

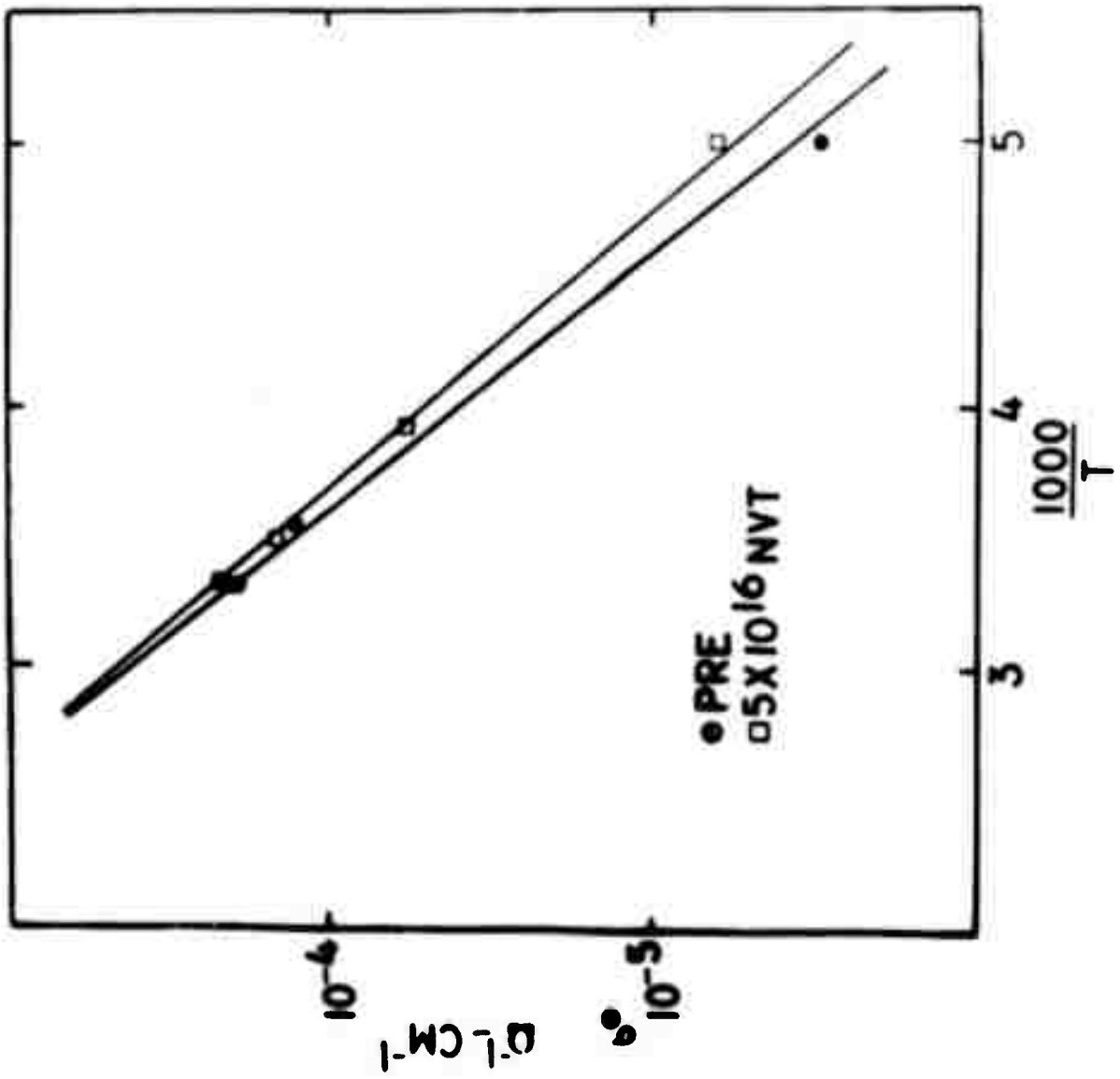
σ, Ω⁻¹ CM⁻¹
10⁻⁴
10⁻⁵
3
4
5
1000/T
●PRE
□5X10¹⁶ NVT

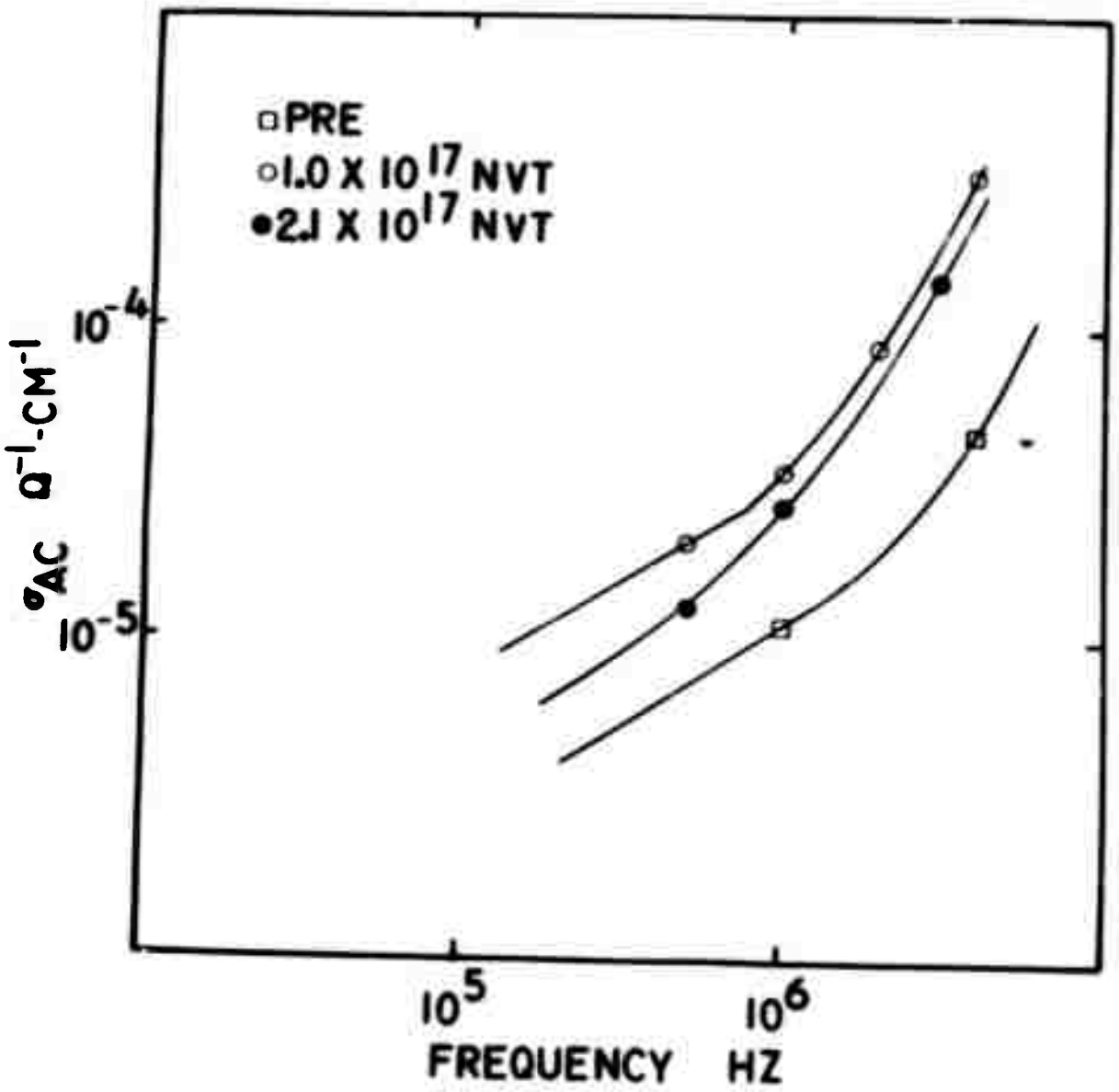
□PRE
○1.0 X 10^17 NVT
●2.1 X 10^17 NVT
10^-4
10^-5
σAC Ω^-1-CM^-1
10^5
10^6
FREQUENCY HZ

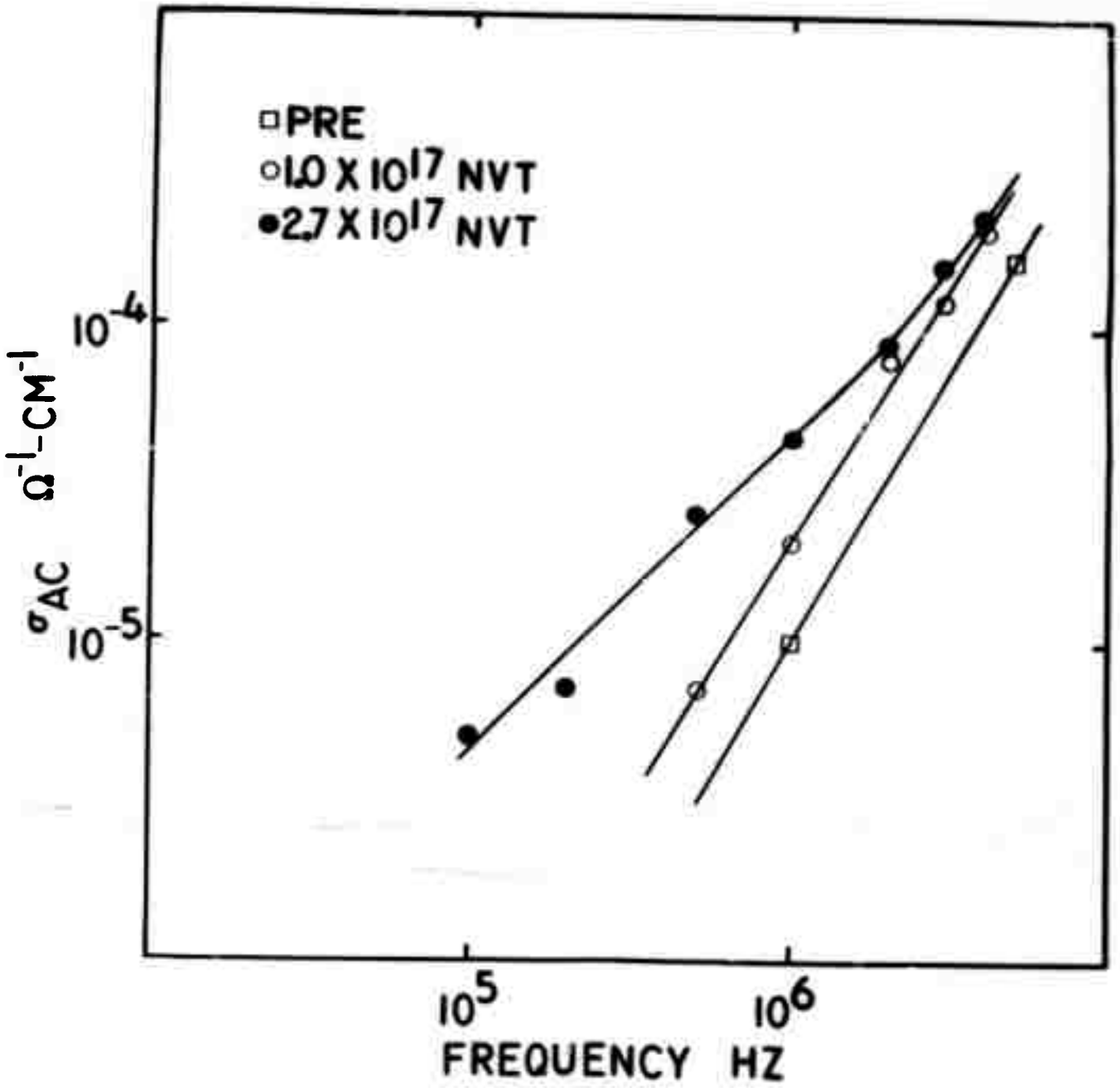
□PRE
○1.0 X 10^17 NVT
●2.7 X 10^17 NVT
10^-4
10^-5
σAC Ω^-1-CM^-1
10^5
10^6
FREQUENCY HZ

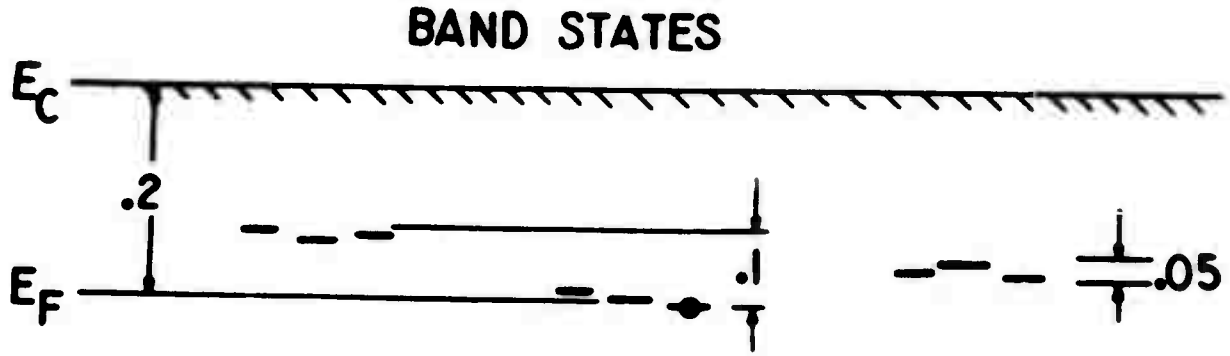
BAND STATES
E_C
.2
E_F
.1
.05

B. EFFECTS OF MICROSTRUCTURE ON THE RADIATION STABILITY OF AMORPHOUS SEMICONDUCTORS

(L. L. Hench, A. E. Clark and H. F. Schaake)

Introduction

Because of the structural randomness of amorphous semiconductors they offer the promise of radiation insensitive electronic properties. Studies have demonstrated that there is only minor alteration of the electrical properties of non-crystalline V_2O_5-P_2O_5 and K_2O-V_2O_5-P_2O_5 amorphous semiconductors at fast neutron fluences of 4×10^{17} nvt and γ-ray dosages of 1.2×10^8 rads.[1,2]

However, it has been shown for both oxide[2,3] and chalcogenide[4,5] amorphous semiconductors that structural heterogeneities are present in many compositional systems. The data indicate that heterogeneities result from: 1) microcrystallization during quenching of bulk or thin films; 2) glass-glass phase separation; 3) nucleation and growth of crystals from a glassy phase; and 4) compositional fluctuations. Can such structural heterogeneities influence the radiation sensitivity of these materials? Several recent reports[6-9] show chalcogenide thin film switching devices, which contain filamentary heterogeneities, are stable up to fluences of 10^{16} n/cm^2 and 3.3×10^7 R of fission γ-rays. However, heterogeneous vanadia

based amorphous semiconductors in bulk form exhibit marked changes in electronic behavior at fluences of 1×10^{17} nvt and above.[2,10]

Consequently, one objective of the present paper is to extend the range of the previous work by reporting the extent of radiation sensitivity of a 33 mole % KPO_3, 67 mole % V_2O_5 glass when crystallized to a large volume fraction, ~0.4. Secondly, a basis for selecting compositions for improved irradiation stability is suggested.

Experimental Procedure

The glasses were melted in air in Pt and melt cast at 900°C into graphite molds. The 1.8 cm diameter discs were heat treated at 288°C for 30.8 hours in air after polishing.[2] Previous studies[2,11,12] of thermal treatment of glasses in the K_2O-P_2O_5-V_2O_5 system have shown that a 90 Å phase separation is enhanced by a thermal treatment for 1/2 hour at 288°C. The matrix appears to order during heating with the D.C. conductivity increasing by 10^4. Longer treatments at 288°C result in the precipitation of P_2O_5-$2(V_2O_5)$ crystallites until at 30.8 hours ~0.4 volume fraction of crystals are present. D.C. conductivity increases during this process to a 25°C value of 5×10^{-3} $ohm^{-1}cm^{-1}$. Evaporated double guard ring gold electrodes were annealed at 150°C for 1/2 hour. Measurements were made as described elsewhere.[13]

Irradiation was done in the Wright-Patterson Air Force Base test reactor having a fast neutron flux capability of 1.5×10^{13} n/cm^2 (>0.1 meV). Cadmium wrapping protected the gold electrodes. The sample temperature was maintained near 50°C during the run. Samples held at 50°C without radiation showed no property changes.

Results

The conductivity frequency dependence at 25°C of the 288°C/30.8 hour sample is shown in Fig. 1 before and after

cumulative exposures of 1.0×10^{17} nvt and 2.1×10^{17} nvt. The total conductivity first increases with nvt and then decreases. The conductivity increase is similar to that seen in the quenched and heat treated glasses previously studied.[1,2] The decrease in σ_{tot} at higher nvt was also observed in the 288°C/0.5 hour glasses at nvt $>2 \times 10^{17}$.[11]

The A.C. conductivity, $\sigma_{AC}(\omega) = \sigma_{meas}(\omega) - \sigma_a$, before and after irradiation is shown to be a function of ω^2 in Fig. 2. σ_{AC} of the multiphase material is considered to be the average of the A.C. conductivities of the phases and σ_o is defined as shown in Fig. 1. There is no detectable $\omega^{0.8}$ conductivity in any samples. A fluence of 1×10^{17} nvt causes the ω^2 conductivity to increase by a factor of 2. Further radiation to 2.1×10^{17} results in no change in the ω^2 conductivity, but does introduce a new low frequency dependence of $\omega^{1.3}$. The behavior of σ_o is as follows:

Pre-irradiation	$\sigma_o = 5.2 \times 10^{13}$ ohm^{-1}cm^{-1}
1×10^{17} nvt	$\sigma_o = 6.8 \times 10^{-3}$ ohm^{-1}cm^{-1}
2.1×10^{17} nvt	$\sigma_o = 5.9 \times 10^{-3}$ ohm^{-1}cm^{-1}

The loss angle of the material is greatly increased with 1×10^{17} nvt, as shown in Fig. 3. After 2.1×10^{17} a large loss peak appears in the tanδ-frequency plot.

Discussion

The results show that fast neutron irradiation affects: 1) σ_{DC} magnitude, 2) σ_{AC}-ω dependence, and 3) tanδ peaks. The increases in σ_{DC} may be attributed to an increase in mobile carrier concentration due to γ-ray ionization processes. As shown[1] γ-ray dosages of 1.2×10^8 rads produce a 15% increase in σ_{DC} in V_2O_5-P_2O_5 glasses. A disordering of the glass matrix, reversing the thermal treatment effects, is proposed for the conductivity decrease after 2.1×10^{17} nvt. The matrix

disordering would isolate high conductivity crystallites providing barriers suitable for Maxwell-Wagner-Willars (MWS) peaks which appear at 2.1×10^{17} nvt.

Explanations for the variations in ω dependence are more speculative. Localized state pairs may be present in the heterogeneous material which would result in an ω^2 dependence via adiabatic hopping.[14] The irradiation may produce a sufficient redistribution of nearest neighbors, as reported for fused silica[15] that a complex $\omega^{1.3}$ behavior produced. It is also possible that excess carrier generation or other effects could produce an electrode barrier behavior altering the dependence.

The nvt threshold for degradation of electrical properties related to heterogeneities is plotted as a function of softening point* for heterogeneous K_2O-V_2O_5-P_2O_5 and Li_2O-$2SiO_2$ glasses[19,16] in Fig. 4. In both systems the onset of changes in the MWS loss peaks is taken as nvt threshold. The threshold for significant structural change of fused silica and crystalline quartz is used for the SiO_2 data point[17] since partially devitrified SiO_2 has not been studied.

Figure 4 shows that as the softening point increases the threshold for damage to heterogeneities increases. This is reasonable since the softening point is related to the magnitude of bond energies in the material. Thus a larger cumulative number of events is requires to damage the boundaries and crystallites of higher bond energy materials.

Extrapolation of the plot in Fig. 4 indicates that damage to ordered heterogeneities in chalcogenide systems, e.g., on-state filaments, may occur at $>5 \times 10^{16}$ nvt. The higher threshold for glasses with larger crystallites[10] indicates that the damage threshold of devices may be increased as the on-state filament diameter is increased. The correlation

---

*Although other criteria might be used for comparison, e.g., T_x, T_g, T_m, an advantage of the softening point is that it is sensitive to previous thermal history and heterogeneities in the material.

shown in Fig. 4 suggests that another way to improve radiation tolerance is to increase the softening points of amorphous semiconductors by compositional modification.

Acknowledgements

The authors would like to gratefully acknowledge the financial support of the Advanced Research Projects Agency of the Department of Defense monitored by the ARCRL under Contract No. F-19628-68-8-0058 and AROD Contract No. DAHC04-70-C-0024.

The continuing assistance of Lt. B. Wilson, Major F. Buoni, and Mr. A. Bauer of the Wright-Patterson Reactor Facility is also acknowledged.

BIBLIOGRAPHY

1. L. L. Hench and G. A. Daughenbaugh, J. Nuclear Materials, 25, 58-63 (1968).

2. L. L. Hench, J. Non-crystalline Solids, 2, 250-277 (1970).

3. D. L. Kinser, J. Electrochem. Soc., 117 [4] 546 (1970).

4. B. G. Bagley and W. R. Northover, J. Non-crystalline Solids, 2, 161 (1970).

5. This Conference, papers HB1, HB3, BA4, DB4, BA5.

6. S. R. Ovshinsky, E. J. Evans, D. L. Nelson and H. Fritzsche, "Radiation Hardness of Ovonic Devices," IEEE Trans. on Nuclear Science, December 1968.

7. a. R. R. Shanks, J. H. Helbers and D. L. Nelson, "Ovonic Computer Circuits Development," Technical Report AFAL-TR-69-309, June 1970.

   b. R. R. Shanks, D. L. Nelson, R. L. Rowler, H. C. Chambers and D. J. Neihaus, "Radiation Hardening Circuitry Using New Devices," Technical Report AFAL-TR-70-15, March 1970.

8. E. J. Evans, "A Feasibility Study of the Applications of Amorphous Semiconductors to Radiation Hardening of Electronic Devices," Picatinny Arsenal Technical Report 3698.

9. R. B. Nicolaides and W. Doremus, this Conference, paper HB8.

10. L. L. Hench, W. D. Tuohig and A. E. Clark, "Fast Neutron Effects in Glass-Ceramics and Amorphous Semiconductors," Ceramics in Severe Environments Conference, North Carolina State Univ., December 1970, Kreigl and Palmour, eds., Plenum Press.

11. L. L. Hench, D. L. Kinser and S. R. Bates, "Microstructural Effects in a K_2O-V_2O_5-P_2O_5 Amorphous Semiconductor,"to be published.

12. A. Fuwa, "Electrical Properties of Glasses and Crystals in the K_2O-V_2O_5-P_2O_5 System," M.S. Thesis, University of Florida, 1970.

13. L. L. Hench, "Dielectric Relaxation in Materials Analysis," Society of Aerospace Materials and Process Engineers, Proceedings of the 14th Annual Symposium, Cocoa Beach, November 1968; reprinted as Technical Paper 428, Engineering Progress at the University of Florida, Gainesville.

14. H. F. Schaake, "Heterogeneous Semiconducting Glasses," in Physics of Electronic Ceramics, L. L. Hench and D. B. Dove, eds., M. Dekker, Inc. 1971.

15. C. V. Gokularathnam, "X-ray Diffraction Studies of Structural Changes in Vitreous SiO_2," Ph.D. Thesis, University of Florida, 1971.

16. W. D. Tuohig and L. L. Hench, J. Nuclear Materials, 31, 86-92 (1969).

17. H. Bale, R. E. Shepler and G. W. Gibbs, J. Appl. Phys., 41 [1] 241 (1970).

Figure Captions

1 Effect of fast neutron irradiation on the total conductivity of a 33 mole % K_2PO_3 - 67 mole % P_2O_5 glass previously heat treated for 30.8 hours at 288°C.

2 Change in A.C. conductivity of a heat treated vanadia-phosphate glass with fast neutron irradiation.

3 Influence of fast neutron irradiation on the loss tangent of a partially crystallized vanadia-phosphate glass.

4 A correlation between the dilatometric softening point of glasses with the threshold fluence for fast neutron structural changes.

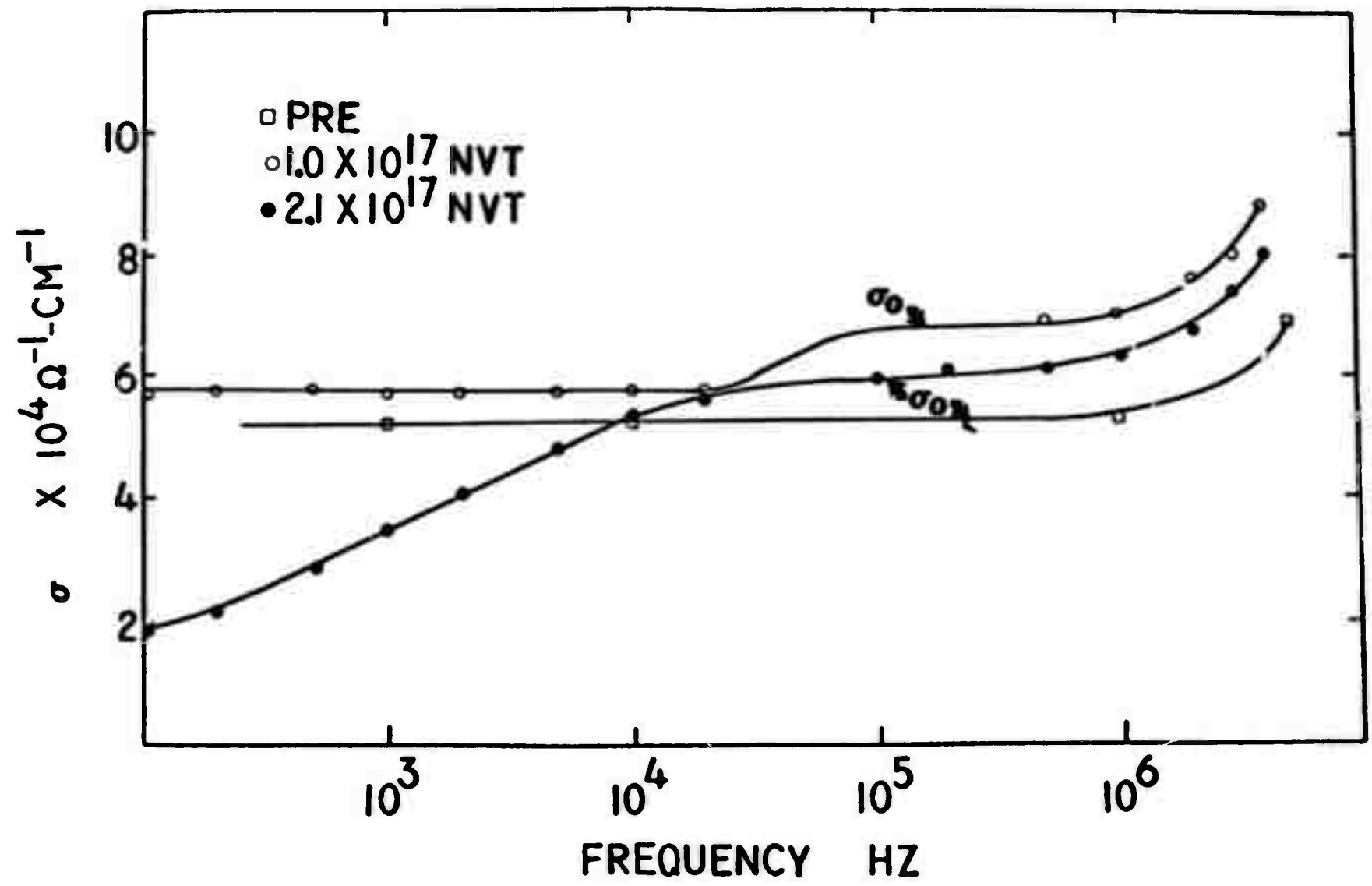
□ PRE
○ 1.0 X 10^17 NVT
● 2.1 X 10^17 NVT
σ X 10^4 Ω^-1-CM^-1
10
8
6
4
2
10^3
10^4
10^5
10^6
FREQUENCY HZ

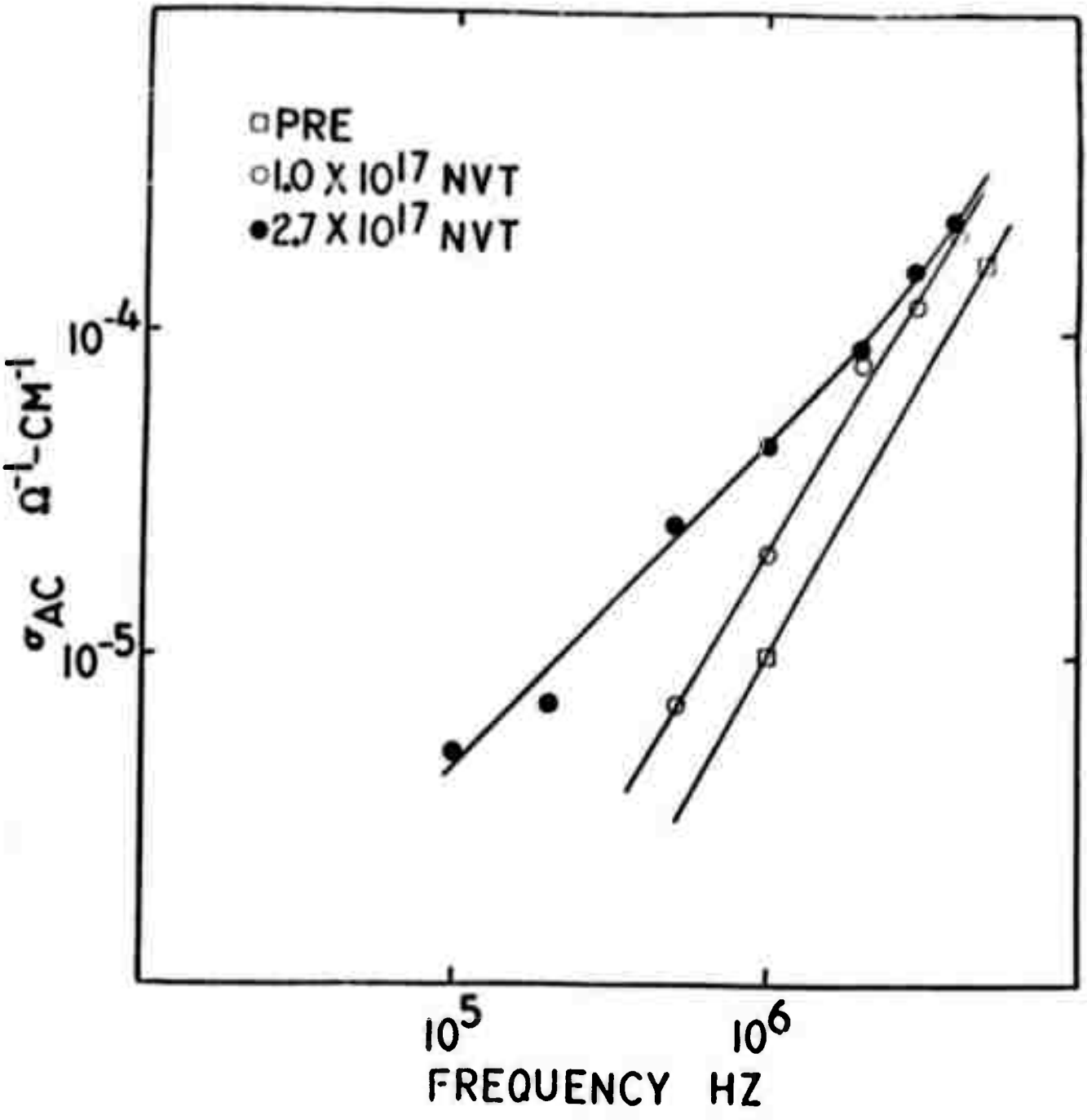
□PRE
○1.0 X 10^17 NVT
●2.7 X 10^17 NVT
10^-4
10^-5
σAC Ω^-1-CM^-1
10^5
10^6
FREQUENCY HZ

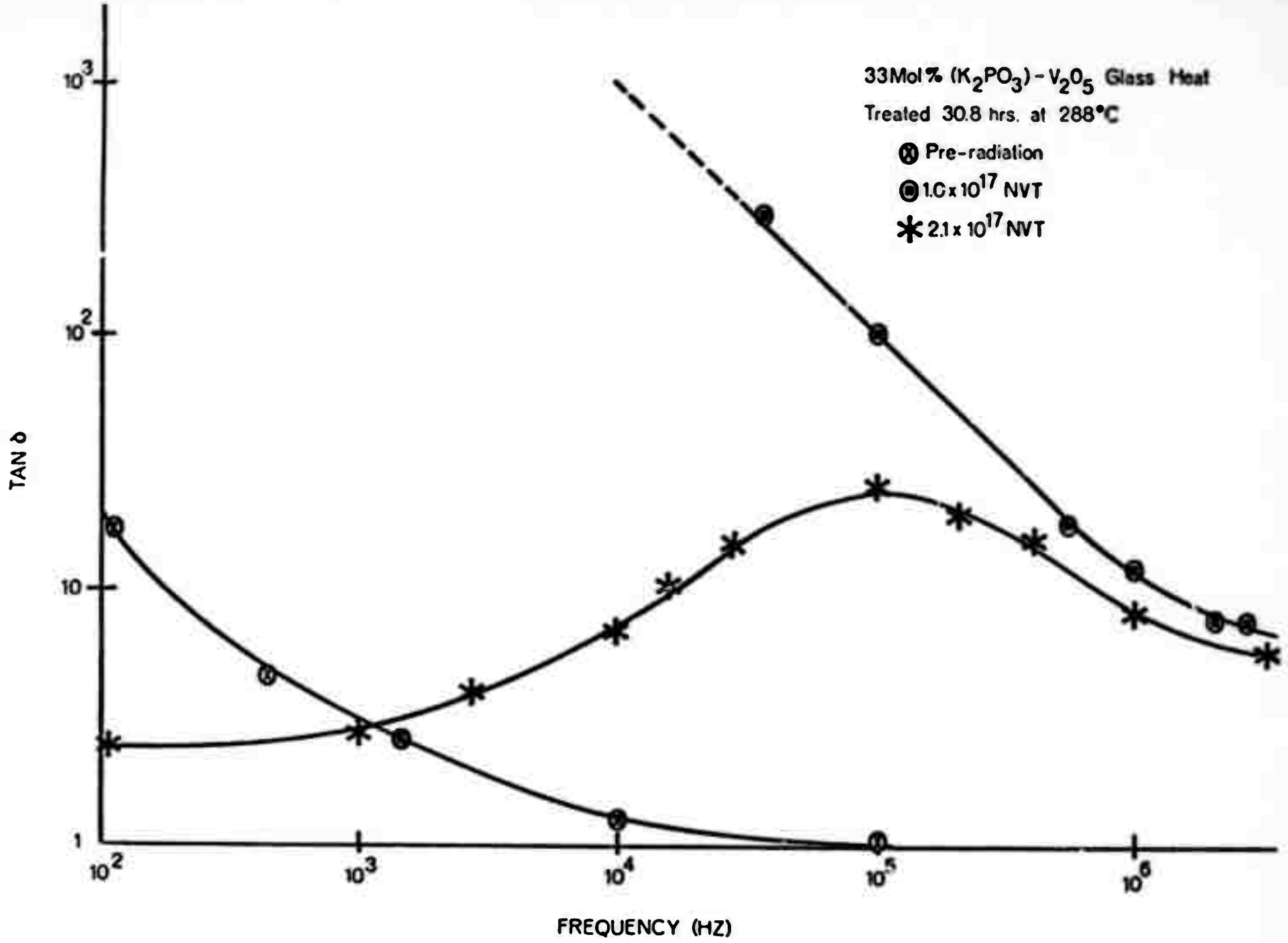
33Mol% $(K_2PO_3)-V_2O_5$ Glass Heat
Treated 30.8 hrs. at 288°C
Pre-radiation
1.0×10^{17} NVT
2.1×10^{17} NVT
TAN δ
10^3
10^2
10
1
10^2
10^3
10^4
10^5
10^6
FREQUENCY (HZ)

Glass Softening Point vs Fast Neutron Damage

Threshold for Structural Change (nvt)

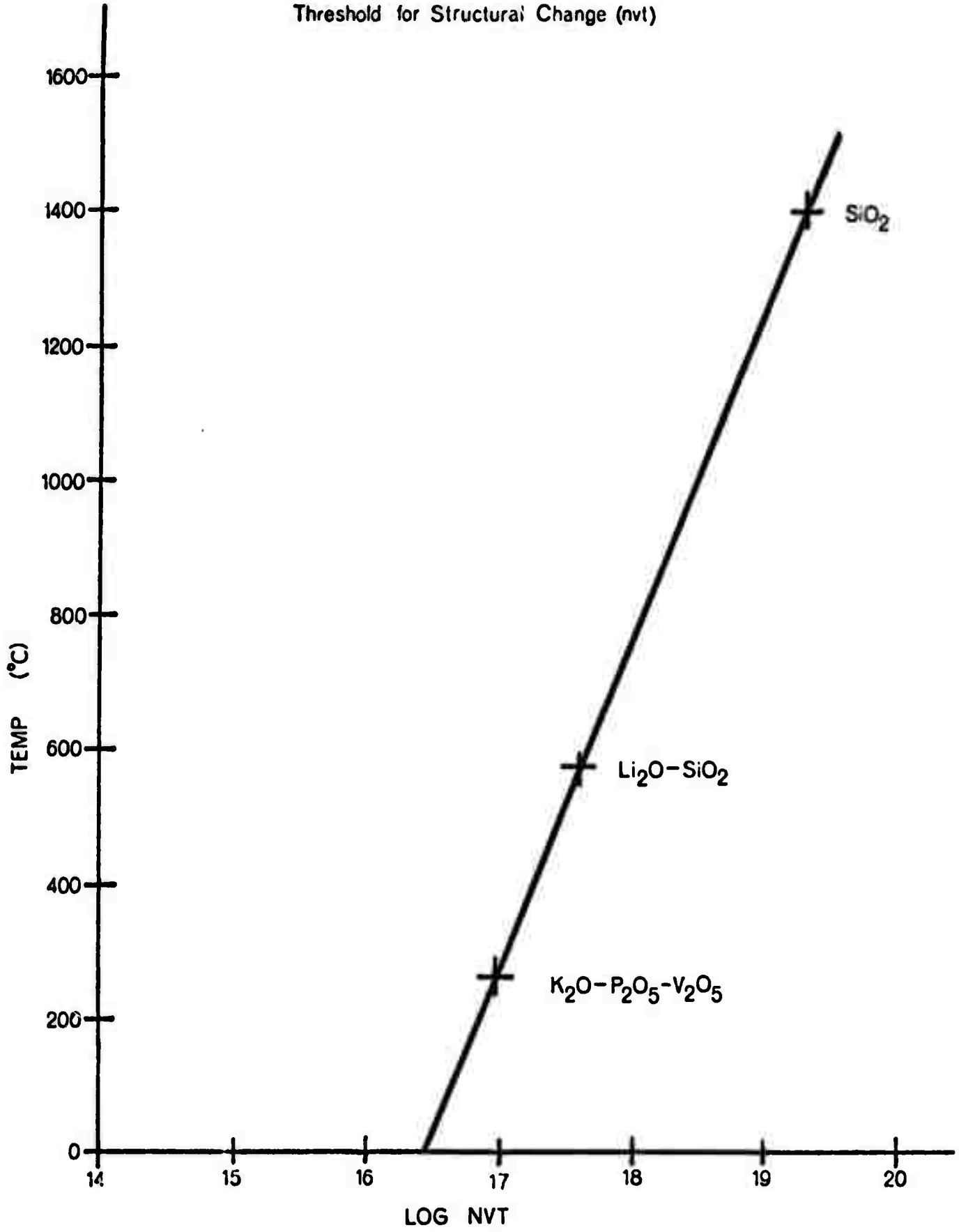

C. ELECTRONIC MATERIALS INTERFACIAL CHARACTERIZATION PROGRAM
(G. J. Scott and L. L. Hench)

Introduction

Previous research reported in this contract program demonstrated that the dielectric properties of electronic substrates, radomes, and window materials are strongly influenced by relative humidity and temperature. This behavior was attributed to penetration of water vapor along grain boundaries and micropores forming a polar condensate which contributes to interfacial and dipolar losses in the dielectric properties of the material.

A review study presented in the last progress report of this program discussed a variety of means suitable for characterizing the surface of ceramic powders. Understanding powder surfaces is an especially important concern of electronic ceramics processors and users today. This is because it has been shown that agglomeration of powders controls the microstructural heterogeneity of fine-grained sintered ceramics such as insulator substrates, ferrites, ferroelectrics, etc. Agglomeration of powders is a surface phenomena which is very poorly understood. Consequently, only by obtaining a more fundamental understanding of powder surfaces will it be possible to control

agglomeration and eliminate heterogeneous sintered microstructures and thereby improve the reliability and performance of a variety of thin film and bulk devices requiring ceramic components.

It was shown in the review study that indirect means of powder surface characterization are the only practical tools available for bulk studies at the present time. Two of the most powerful indirect methods for surface characterization are differential thermal analysis adsorbtion isotherms and dielectric adsorbtion isotherms. We have recently completed an experimental facility which couples these two techniques together for surface characterization studies. One of the consequences of the combined surface analytical approach is having to analyze the formidable amount of data collected in such a study. Data are accumulated for eleven parameters and variables. Calculations must be made on the data and a large number of cross-plots constructed in order to interpret the significance of the results.

In order to make such an undertaking tractable, a computer program has been written, debugged, and operated. The following is a description of that program.

Overview

1. The "DIEL" set of programs gives graphical results of complete studies, including temperature dependence, of dielectric property response, on a single sample. The five programs are designed to accommodate data collected

a. at up to five temperatures,

b. during adsorptive or desorptive modes (and hereafter mode refers to the ad- or desorptive run of an experiment at a given temperature),

c. up to 20 relative humidities per temperature and mode combination (hereafter T-MC),

d. and up to 25 frequencies per relative humidity and T-MC.

2. These programs can plot up to 16,200 points on nine types of cuts through an eleven-dimensional space, with up to 24,200 specified data values, on up to 270 sets of axes.

3. The plots are of nine types:

a. 1→3: loss tangent, charging permittivity, and loss permittivity as ordinates versus log frequency as the abscissa, parametrically at up to three relative humidities, for a given T-MC. The usual symbolic names for the ordinate variables are tan del, ε', and ε'' respectively.

b. 4→9: charging and loss permittivity and capacitance change are plotted against the quantity of water adsorbed. Symbolic names are respectively ε', ε'', Δc, and milligrams per gram. The parameter for these graphs is the set of six special frequencies -- data for type 4, 6 and 8 graphs is taken at high frequency, viz., 1 MHz, 500 KHz, 100 KHz; for types 5, 7 and 9 at lower frequency, 20 KHz, 5 KHz and 500 Hz.

4. There are five programs in the set. Their names and functions are:

a. DIELPNCH - data reduction; punch a deck for reading data and calculated values into a direct access storage unit.

b. DIELCELL - arrange data according to the temperature, mode, relative humidity and frequency breakdown, explained above, into the data cell (a magnetic chip-on-disc memory unit) or into a magnetic tape.

c. REPAIR - change several isolated data values in the data cell, as necessary.

d. D1 - draw the graph of types 1 through 3.

e. D2 - same for types 3 to 9.

5. Detailed explanations of these programs, construction rules for their data decks, and listings of the programs follow. An explanation of the job control language ("JCL") cards required for access to the programs' software is an appendix.

6. Five subprograms, which do the actual work of putting the graphs on paper,* are shared by D1 and D2. We will refer to them as they are referred to during operation of D1, so that they will physically separate D1's description from D2's.

DIELPNCH

1. Purpose - to produce a printout of the raw data and resulting calculated information, and punch a data deck suitable for reading graph-drawing data into the data cell.

2. Input - a manually key punched deck containing the samples, dimensions, partial pressures of water, weight in vacuum and a humid atmosphere, and frequency-conductivity-capacitance-vacuum capacitance data.

3. Output - the printout and deck referred to above.

4. Operation

a. Allocate storage for use by the subroutine which adds vacuum capacitance data for entries lacking it. Read the "vacuum data" frequencies and corresponding capacitances from the appropriate number of cards. Then read a "case heading" card. Calculate the values of those variables particular to each case. Then print out, and have the machine punch cards containing "heading" values, punching only those essential to graph drawing. Read the first of the several cards containing the frequency-dependent data of each case. Test to determine the signaling effect of the frequency, capacitance and vacuum capacitance values just read, and call the routine which calculates or recalls the vacuum capacitance, if none was read. Then for F>5, i.e., a data value, the frequency-dependent variables are calculated. If the vacuum-to-humid capacitance change turns out to be less than zero (a physically unrealistic event), then the capacitance change is assigned

*From the practical standpoint.

a zero value. The output is completed by printing and punching the frequency-dependent data.

b. If the frequency value is >5, then the program's control is transferred to reproducing the frequency card just read, propagating the appropriate signal to "DIELCELL." If the frequency value equals five, then execution is ended, after printing the list of frequencies and vacuum capacitances read and/or calculated.

5. Variables names, in order of appearance:

FD - The set of data frequencies at which a vacuum capacitance has been experimentally determined.

CVD - The set of vacuum capacitances experimentally determined.

WR - The number of milligrams of water adsorbed from the atmosphere per gram of sample weight, the Weight Ratio.

LØGPPØ - The logarithm to the base 10 of the ambient partial pressure of water divided by the saturated partial pressure of water, at the sample temperature.

IVS - The reciprocal of the capillary volume squared.

NFR - The number of frequencies for which vacuum capacitance data has been experimentally determined.

T - The sample thickness.

D - The sample diameter.

P - Ambient partial pressure of water.

PØ - Saturated partial pressure of water at the sample temperature.

W - Weight of the sample in the ambient atmosphere.

WØ - Weight of the sample after baking out in vacuum.

TEMP - The sample temperature.

SAMPLE - The sample number.

CØ - The theoretical or "geometric" capacitance of the sample.

RH - The relative humidity of the atmosphere.

V - The capillary volume of the sample, equal to the number of cc occupied by the adsorbed water.

F - The frequency of alternating current applied to the sample, generally 100 to 1 million hertz, inclusive.

G - The conductance (micro-ohms) of the sample at the above frequency.

C - The capacitance (picofarads) at the given frequency.

CV - The vacuum capacitance appropriate to the particular frequency.

TD - The loss tangent, commonly called "tan del."

EP - ε', the charging permittivity.

EDP - ε'', the loss permittivity of the sample.

DC - The change of capacitance on adsorption of water from the atmosphere.

6. Data deck.

Card type	Format	Columns (inclusive)	Variable code name	Remarks
1	I2	1 & 2	NFR	The number of frequencies at which vacuum capacitance data has been taken.
2	8F10.0	1-10	FD(1)	The highest of the above frequencies.
		11-20	FD(2)	The next highest frequency.
		21-30	FD(3)	Continue punching frequencies in decreasing order until all "NFR" frequencies are punched. Use as many cards as necessary.
		.	.	
		.	.	
		.	.	
3	8F10.0	1-10	CVD(1)	The vacuum capacitance for the highest frequency.
		11-20	CVD(2)	Carry on punching vacuum capacitances until each vacuum capacitance corresponding to the respective frequency is recorded on a type 3 card or cards.
		.	.	
		.	.	
		.	.	

Card type	Format	Columns (inclusive)	Variable code name	Remarks
4	8F10.5	1-10	T	"Case heading" card.
		11-20	D	
		21-30	T	
		31-40	TØ	
		41-50	W	
		51-60	WØ	
		61-70	TEMP	
		71-80	SAMPLE	
5	F20.10	1-20	F	This is the frequency-dependent card, normally having the frequencies arranged in decreasing order. There are usually 10-15 of these cards per case.
		21-40	G	
		41-60	CV	
		61-80	CV	

DIELCELL

1. Purpose - to arrange the calculated data punched by the DIELPNCH program, in the data cell, such that all temperature, mode, relative humidity and frequency sequential correspondences are maintained; to establish the values of other quantities needed as data distinguishers or by the CALCØMP plotting routines.

2. Input - the deck from DIELPNCH preceded by cards containing the axis names, the number of temperatures, the humidities at each temperature and mode, and interleaved with the sequence numbers of the special frequencies (section 3-b above) specific to each case (temperature, mode, and relative humidity combination).

3. Output

a. A printout of the number of frequencies for each case and an optional (5300 line) namelist printout of the contents of the data cell, as arranged therein.

b. Properly arranged data sets designed for convenient use by the drawing programs.

4. Operation

a. Allocate storage in the configuration which will be used for the drawing programs. Establish namelists containing the variables used by each of the drawing programs. Set all data spaces equal to zero, to eliminate uncontrolled and undesired information from the data set. Read 18 cards with the axis titles centered in the first 20 spaces, then another card with the number of temperatures at which data has been taken. Read a card on which is punched the number of relative humidities appropriate to each temperature-mode combination ("T-MC"). This set of numbers must be determined by inspection of the printout of DIELPNCH.

b. The program reads two "case heading" cards. The first contains the sequence numbers of the "special" frequencies which are the parameters for drawing the type 4-9 graphs. The value of the case's relative humidity and the number of milligrams per gram are then read from the following card, which was the first card per case punched by DIELPNCH. We next have the machine establish the count of frequency cards for each case. After counting the current frequency's sequence number, the values of frequency, capacitance change, ε', ε'' and tan del are read in sequence. As before, the value of F in comparison with 5 is used to control the next operation. If F is greater than 5, hence a data value, the particular space in storage involved is filled with the logarithm to the base 10 of the frequency, other data values are stored, the frequency counter is stepped by one, and another frequency card is read. Eventually, the program encounters a card whose frequency is less than or equal to 5. At the end of each case except the last, an F value of zero is encountered. This causes the program to store the number of frequencies that are in the case and to print out the temperature, mode and relative humidity indices, the number

of frequencies and the relative humidity value just calculated. Then the program adjusts the index for relative humidity, mode or temperature, as appropriate, and returns to read the two case heading cards and more frequency cards. If, at the end of the data deck punched by DIELPNCH, an F value of 5 is encountered, then the number of frequencies for the last case is entered in storage and the last printing of the above indices, number of frequencies and relative humidity is made.

c. The next job that the program undertakes is to calculate the set of origin location values, giving the x and y coordinates of each origin in sequence. (See page 7, the TD program write-up, Report No. 7.) Then the entire set of data calculated and recorded in this program is transferred, array by array, from the machine's core into the data cell for use by the drawing programs. Then a card bearing a signal as to whether to print the namelist containing the data (as it appears in the data cell) is read. If this signal equals zero, then the namelist, consisting of some 5300 lines of printout, is not printed out, and execution is ended. However, if the signal is not equal to zero, then the namelists are printed before execution is ended.

5. Variable names, in order of appearance, not already named above.

TITLE - the set of axis titles arranged according to graph type and axis.

LSP - the set of "special frequency" sequence numbers specific to the graph 4→9 parameter frequencies and specific to a case.

KM - the set of maximum number of cases per T-MC.

NF - the number of frequencies per each case.

Ø - the set of origin locations with respect to the one preceding.

I - the index which marks a temperature's sequence number. Maximum value is 5.

J - the index which marks the mode's sequence number. Maximum value is 2. A set of values of I and J identifies a T-MC.

K - the index which marks the relative humidity sequence number, per T-MC. Maximum value is 20. A set of values of I, J and K identifies a case.

L - the index which marks the frequency sequence number within each case. Maximum value is 25.

NSP - the index identifying one of the six special frequencies, the parameters for graph types 4 through 9.

NT - the number of temperatures at which data has been taken for a particular specimen.

NRH - the number of relative humidities, specific to a given T-MC.

ØX - the number of inches in the x direction to the next origin's location.

ØY - the same for the y direction.

N1,N2 - integers assisting set-up of the origin location array.

QPRINT - the indicator of whether to print namelists.

6. Data deck

Card type	Format	Columns (inclusive)	Variable code name	Remarks
1	5A4	1-20	Title (1,1,1→5)	The first "1" means that this title refers to an x axis, the second means that it refers to a type 1 graph, and 1→5 refers to each block of four alphabetic characters contained therein. The actual content of this title is "Log Frequency," centered on the first 20 space block.
	5A4	1-20	Title (1,2,1→5)	"Log frequency" for plotting against ε', whereas the above title was for plotting against tan del.

Card type	Format	Columns (inclusive)	Variable code name	Remarks
	5A4	1-20	Title (2,9,1→5)	"Delta capacitance," for use on the vertical axis of the last graph type.
2	I1	1	NT	The number of temperatures for which data has been taken.
3	24I3	1-3 4-6 7-9 . . .	KM(J,F) J=1,2 I=1,NT	This is the maximum number of relative humidities appearing per T-MC. Note that the entries must be right-justified in the 3-column block that each of these variables uses.
4	6I3 . . .	1-3	LSP (1,K,J,I)	The sequence number of the first special frequency, i.e., 1MHz.
			LSP (2,K,J,I)	Sequence number at which 500 KHz is found.
		16-18	LSP (6,K,J,I)	Sequence number of the last special frequency, 500 Hz, for the K^{th} relative humidity of the $I\text{-}J^{th}$ T-MC. The indices for the case may be punched as a guide to easy handling of the deck, are any columns beyond 18.
5	19X,5.1 6X,F6.2	20-25	RH	This case's relative humidity, for printout only.
		31-37	WR (K,J,I)	The mg/g value which is to be plotted for this case. This card is the case heading card punched by DIELPNCH.

Card type	Format	Columns (inclusive)	Variable code name	Remarks
6	5F12.3	1-12	F (L,K,J,I)	The particular frequency value identified with the "L" position in the sequence for the case identified with the Kth relative humidity and/or milligraws per gram value, the Jth mode, and the Ith temperature.
		13-24	DC (L,K,J,I)	
		25-36	EP (L,K,J,I)	
		37-48	EDP (L,K,J,I)	
		49-60	TD (L,K,J,I)	
				This is the frequency-dependent card punched by DIELPNCH.
Several groups of types 4, 5 and 6 cards form the bulk of the data deck for DIELCELL.				
7	79X,F1.0	80	OPRINT	If the value of OPRINT is zero, then no name-list will be printed out.

REPAIR

1. Purpose - to do the software manipulating required to change isolated values or groups of values of the data in the data cell.

2. Input - the changed values, both by name and proper magnitude. See this paragraph for subroutine CHANGE, immediately following.

3. Output

a. The revised values to the proper location in the data cell.

b. Optional printout of the old and new values. Details are discussed in the section for CHANGE.

4. Operation - establish blocks of main core storage for use by both REPAIR and CHANGE. Read the entire contents of the data sets designed for the D1 and D2 programs' use. Call the subroutine which actually changes the values, CHANGE. Upon return from CHANGE, rewind the data sets, write the proper values therein, and finish execution.

5. Variable names are the same as in the DIELCELL data deck.

CHANGE

1. Purpose - assign proper values to spaces in the data set which were given incorrect contents when established during the operation of DIELCELL. Manipulation of the data set (in the magnetic disc "data cell" or a magnetic tape) is done by the REPAIR main routine above.

2. Input - this may be done:

a. by direct arithmetic assignment statements,

b. calculated arithmetic assignment statements, or

c. reading exact or functionally related values from cards.

3. Output - the revised values automatically placed in the main core storage shared with REPAIR.

4. Method of operation - the possibilities are best described through an example. Suppose errors in transcribing data from notebooks to data coding sheets, misreading of instrument ranges, keypunch errors, or system malfunctions have resulted in the following errors:

a. The 7th through 12th milligrams/gram values for the second temperature, adsorption mode run are 0.312 mg/g too high.

b. The values for the ε' and ε'' for the third temperature, the desorption mode and the ninth relative humidity and sixth frequency in sequence are missing. That ε' value is hand-calculated to be 27.372, and the

value of TD (6,9,2,3) appears, is checked and found to be correct. Note we also know that tan del = ε"/ε'.

c. All 24 log frequencies for the seventh relative humidity and the first temperature adsorption run are nonsystematically incorrect.

d. To correct these errors a satisfactory procedure would be:

(1) use iterative arithmetic assignment statements to subtract 0.312 from WR (7 12,1,2).

(2) assign-by-equation, ε" (6,9,2,3) = 27.372 TD (6,9,2,3).

(3) read the correct frequencies from a card deck and store their (common) logarithms. The part of the original deck, extracted for this job, containing the proper frequencies would be suitable, and eliminate any need for additional key printing.

e. Since it is advisable to have visible assurance that the changes actually took place, the old and new values of interest should be printed out.

5. Variable meanings - the same as in DIELCELL.

6. Data deck - it is understood that the data deck structure listed here refers to the above example only. The needs of other jobs may result in no data deck or data decks of several hundred cards.

Card type	Format	Columns (inclusive)	Variable code name	Remarks
1	F20.10	1-20	F (L,7,1,1)	Listed from the proper place in the DIELCELL data deck, 24 cards required.

D1

1. Purpose - to draw report-ready graphs of tan del, ε', ε", at various T-MC's, drawing three parametric curves at three relative humidities.

2. Input - the above data set; a single card to control an optional printout of the data.

3. Output

a. Up to 210 report-ready graphs.

b. A printout to show the progress (and propriety) of execution.

4. Operation - there are seven subroutines, which do the following jobs:

a. MAIN (the name will be used interchangeably with "D1") controls the allocation of storage, the temperature-mode flow through the data, and the flow through the three graph types for each T-MC. MAIN also initializes the graphing sheet, the three sets of points (nascent curves) for each graph, and sets the position of the origin for the next graph.

b. SETF3 converts the dielectric quantities into abscissa and ordinate variables for graphing. All further manipulations of the data will be made in terms of curve number, first through third, and point number along the curve.

c. JUSTFY determines whether there is data adequate to justify continuing on to draw a graph. It also determines the range of the data values for the present curves.

d. SCALE adjusts the range of the variables to make drawn axes both efficient and easy to read displayers of the data. That this is done for a set of curves is the main difference between the TD programs and the DIEL (see Report No. 7 for TD program). This routine is a much amplified version of the TD "SCALIN" routine.

e. PREP, as in TDDRAW, draws titled and scaled axes, and calculates and prints enough tic values to implement easy readability.

f. POINT sets the curves on the axes, by drawing a triangle centered on the curve 1's points, a square on curve 2's, and a diamond on curve 3's.

g. SHFL arranges the sequence of point drawings to reduce graph drawing time.

h. Details of the operation of D1 are:

(1) allocate storage, then read a card which contains a signal whether to print out the contents of the data set used by the program. If the last column of the data card is blank or contains a zero, the data set's contents will not be printed out. Initialize the CALCØMP package, the graphing sheet, the graph position number (equal to zero) and the graph position advancing criterion number (equal to one).

(2) establish and iterate the temperature and mode indices so that all temperature-mode combinations are used in order (i.e., T_1 adsorption, T_1 desorption, T_2 adsorption, T_2 desorption, etc.). Initialize the graph type number (equal to zero), and assign a scalar value to the maximum number of relative humidities proper to this T-MC. If there are no relative humidities, iterate the temperature and/or mode index and start again at the second sentence of this paragraph. For a finite number of relative humidities, add one to the graph type number, and set the per-graph relative humidity control index to zero.

(3) if the graph position advancing criterion number is not zero, a new set of axes needs to be drawn, and the graph position number is stepped by one. In case the advancing criterion number had previously been set to zero, it is now reset to one, since we assume that a new graph position will be used the next time through. Then, the data from previous sets of points is wiped out by setting the number of points index-for-each-of-the-three-succeeding-curves, and all 75 available abscissa and ordinate values equal to zero. Then, the origin is moved to its next location.

(4) if the graph-advancing-criterion is zero (and here we glimpse the functioning of the later routines), the preceding steps have been taken, but a graph has not been drawn, due to there being no data to plot. Therefore, the old graph position and the zeroing of the curve-point-location variables suffices for the present case.

(5) write a message in the printout showing the values of the graph type index, the graph position number, and the temperature-mode indices. Then call SETF3, sending the appropriate array (TD, EP or EDP) for use as ordinate values for the graph about to be drawn, according to the graph type number.

(6) as seen in (4), there can be a "good" return from SETF3 or a "bad" one, depending upon whether the graph has been drawn or not. A "bad" return causes the T-M indices to be iterated. "Good" returns from type 1 and 2 graphs are handled by testing whether the curves have been drawn for all relative humidities. If yes, then control is sent back to where the graph type index is stepped (last sentence of paragraph (2) above), so that it eventually becomes three. A "good" return from SETF3 after drawing the type 3 graph again elicits the test for having drawn curves at all relative humidities. A "no," meaning that there are more graphs to be drawn, sends control back to the top of (4).

(7) when graphs for all T-MC have been drawn, the CALCØMP package is emptied and closed, and the program stops execution, writing a message in the Operating System Monitor's log file, showing that the program has ended according to design.

5. List of symbols not already introduced.

S - the set of tic spacings.

ZS - the set of scale factors.

SD - the set of units of axis variable per tic division, henceforth called "tic division."

NPR - the ordinal number of tics between those which are marked, i.e., print a label every "NPRth" tic.

X - the array containing the values of the abscissas for each point on each curve.

Y - the similar array for the ordinates.

ZMAX - starts out being the largest data value to the graph, per axis.

ZMIN - similarly, except the smallest.

NPTS - the array containing the number of points on each of the three curves for each graph.

NG - the graph position sequence number, or merely "graph number." Maximum value = 210.

NGADVQ - the index which controls the advancing of the graph position sequence number. Mnemonic with the question "Should NG advance?"

NTP - the index for the type of graph.

KST - the relative humidity sequence number which starts the parametric curves on a given graph.

KND - likewise, except the end.

NS - the curve number on a particular graph.

6. Data deck

Card type	Format	Columns (inclusive)	Variable code name	Remarks
1	79X,F1.0	80	QPRINT	If the value of QPRINT is zero, no namelist will be printed out.

Subroutine SETF3

1. Purpose - to fill generalized abscissa and ordinate variables with those values of tan del, ε', ε", and log F, which will draw a maximum of three distinguishable curves on the set of prepared axes.

2. Input - arguments in the subroutine list.

a. The ordinate array.

b. The sequence number of the starting relative humidity.

c. The current graph number.

d. The type number of the graph.

e. The temperature sequence number.

f. The mode sequence number.

g. A dummy, not used on input, variable.

h. The number of relative humidities pertaining to this T-MC.

i. A dummy variable.

j. Also implied as input are the various scaling and graph drawing variables which are in the common storage shared by all subroutines of D1. The SETF3 common block of storage implicitly makes input of the log frequency set of values, and the number of frequencies-per-case values.

3. Output - the normal method of operation makes the output of SETF3 go to subroutine JUSTFY. Output to this routine includes the graph sequence number, the graph number, the total number of curves which are to be drawn. On return to MAIN, however, if the number of frequencies should be zero, then the last numerical argument in the argument list is given a value of zero, while the first dummy argument (the seventh argument in the argument list) is given the sequence number of the last relative humidity which was used in curve drawing.

4. Operation - the first time through per T-MC; the starting relative humidity sequence number is given a value of 1 and the finishing relative humidity sequence number is given a value which is the least of three or the number of relative humidities. However, on the second and subsequent times through, the starting relative humidity sequence number is increased by 3. The ending relative humidity sequence number is given a value which is the least of three greater than the

value it had the last time or the total number of relative humidities for the T-MC. Then the curve number index is set at zero, the number of curves is calculated and for each relative humidity, the curve sequence number is increased by 1. The number of points are in the NS^{th} curve and the abscissa and ordinate point locations are filled, the abscissas with the proper value of log frequency and the ordinate with the proper value of the input ordinate-type array. After the required number of curves has had its abscissa-ordinate locations determined, the program writes a message giving the range of the relative humidity sequence numbers and the number of curves, then the program is sent to subroutine JUSTFY.

5. List of symbols not already named.

ØRD - a dummy array name set up to receive the values of one of the ordinate arrays as named in MAIN.

M - a dummy variable whose value is given to NGADVQ on return to MAIN.

NCVS - the number of curves to be drawn on a specific graph.

NPNTS - the number of points to be drawn on a particular curve.

Subroutine JUSTFY

1. Purpose - JUSTFY is designed to justify carrying on to do the work which is required to scale and draw ticked and labeled axes. The specific justification criterion is that at least one of the points have a nonorigin location, inferring that there is indeed data to be plotted. In the process, JUSTFY determines the largest and smallest values of both the abscissa and ordinate variables.

2. Input

a. The graph position sequence number, the graph type number, and the number of curves which are to be drawn.

b. The ten arrays in that block of storage common to all other routines.

3. Output

a. Normal operation - JUSTFY sends to subroutine SCALE the values of NG, NTP and NCVS, as well as the largest and smallest data values per axis via the block of blank common storage.

b. "Bad" operation - if no data is found by JUSTFY, control returns to the statement in subroutine SETF3, which sets the graph-number-advancing-criterion integer equal to zero.

4. Operation - allocate storage. For the x axis, initialize the range-end variables so that they are certain to be changed by a data value. Determine the highest and lowest values of x for the three curves. Repeat this process for the variables on the y axis. The justification for proceeding is that both axis maximum values be different from zero (see paragraph b,(4) of section D1). If justification succeeds, write the largest and smallest data values per axis, and proceed to subroutine SCALE. If justification fails, write a failure message and return to MAIN by the route which precludes advancing the graph position number.

5. Flowchart

Subroutine SCALE

1. Purpose - SCALE selects interval bounds which minimize both dead space on the axis and distraction by unusual, overly significant tic markings.

2. Input - the numbers of the current graph, its type and the number of curves.

3. Output - proper values of the scaling variables (the first four of the blank common blocks), as well as revised values of the high- and low-end variables for each axis.

4. Operation

a. To the storage allocations which have been used so far, add those for the array of axis lengths. Then, for each axis in turn, convert the maximum and minimum array values to scalars for speedier referencing. Determine the order of magnitude of the bounding data values and their ratio. If the minimum data value should be zero, assign the maximum data value to be the ratio (as though the minimum data value was one). Next, determine what fraction of the order-of-magnitude is used by the maximum axis value and assign a proper upper bound, from a selection of six. Similarly, select an appropriate value for the lower bound of the axis.

b. The work of scaling the current axis is done in the following order:

(1) calculate the number of axis variable units per tic division, then the number of tics between labels. Assure that the axis bounding values are integral multiples of the tic division.

(2) test to see that more than six tics will be drawn. If not, halve the tic division, and check to be sure that the axis range is nonzero. If it should be, return to SETF3 on a second "bad" route. When both these tests are passed, the Scale factor and the number of inches of actual tic spacing may be calculated. When both axes have been scaled, the success message, showing the axis bounds and the scaling variables values, is printed out. Control then goes to PREP.

5. Symbols not already introduced.

R - The set of axis lengths.

NAX - The axis number; "1" for abscissas, "2" for ordinates.

ZX - A specific value for the maximum value on an axis.

ZN - The similar minimum.

A - The order of magnitude one greater than the maximum data value.

B - The similar for the minimum data value.

RATIO - The maximum data value divided by the minimum data value.

N - An integer which assists in determining the fraction of its order of magnitude that the data variable actually occupies.

NTHI - The number of tics required to exceed by one the maximum data value.

NTLØ - The number of tics required to bound the minimum data value on the low side.

RANGE - The actual magnitude of the axis variable which is to be on the axis.

Subroutine PREP

1. Purpose - to cause CALCØMP drawing of a set of ticked and labeled axes, printing enough tic values for easy readability.

2. Input

a. The graph number, type and the number of curves.

b. The variables in the blank common block.

3. Output

a. The ticked and labeled axes on the graph sheet.

b. Passing subroutine PØINT the number of curves, as well as the abscissa and ordinate variable values in the blank common block.

4. Operation

a. Allocate storage as before, with additional storage for a one-dimensional array containing the contents of a specific title. For each axis in turn, assign scalar values to array variables. Assign values to variables which locate the titles, and control axis and title drawing angles. Next draw the axis (subrcutine AXIS2), then write out the axis title.

b. Then the tic labeling parameters are determined. The origin tic value and the number of tics are calculated and the tic at which labeling is to start is assumed to be the first to be labeled. The origin tic value is tested as to whether it is an integer multiple of both the tic division and the labeling ordinal. If not, the second or subsequent tic value is determined and the same test is given to it. Each time this process is repeated the tic number at which ticking is to be started is increased by one. Eventually the program finds a value which is an integral multiple of both tic division and labeling ordinal and so the tic number for starting labeling takes its value for that graph.

c. If, however, the first tic will be more than one-third the way down the axis, the tic division parameter is halved, and the other scaling parameters are adjusted. Then the scaling process is repeated. A message is written, telling of the change. Next, depending on the value of the tic division parameter, the labeling ordinal is fixed, i.e., NPR↔(NAX) or NMARK = 5 means "print/mark" every fifth tic's label.

d. The tic labeling iteration parameters having been determined, at each appropriate tic

(1) determine the tic values.

(2) convert the numeric tic value to an alphabetic label, for use by the label drawing routine.

(3) determine the location of the tic value according to its value, axis and number of characters, so that the tic label will be centered upon its proper tic.

(4) the program branches here to accommodate the printing of short tic labels (four characters or less) or long ones (five to eight characters). When all tics on both axes are drawn, then the program proceeds to subroutine PØINT. The PREP success message gives the value of the last tic label on the y axis.

5. Symbols not already named:

TL - A one-dimensional array containing a specific title.

SDE - Scalar value for a particular axis' tic division value.

NP - Scalar value of the number-between-printed-tic-values array ("labeling ordinals" array) for the particular axis.

SE - Tic spacing for the particular axis.

R - Lengths of the particular axis.

A - Angle at which the axis is to be drawn.

XST - Abscissa value of the lower left hand corner of the block on the paper which contains the title.

YST - The similar ordinate value.

AL - The angle at which the lettering in the title is placed.

NHALVE - The number of times the program has had to halve the tic division, so as to allow for an adequate number of marked tics.

TVØ - The tic value at the origin or other first-labeled-tic.

NTICS - The number of tics on the axis, disregarding the tic which is placed at the origin.

NSTCNG - The Number of tic at which to StarT tiC labeliNG.

Q - The test variable which determines whether a tic value is an intege. multiplier of the tic division value and the printing ordinal.

NQ - The value to which noninteger Q's are rounded down.

NMARK - The scalar tic labeling ordinal.

N - The sequence number of tics to be labeled.

M - The number away from the origin of a tic which is to be labeled.

TV - The value represented by a particular tic, stored in a floating point form.

ITV - The tic value rounded down to the next lowest integer.

NC - The number of characters in a tic label.

ITVHI - That portion of an integer tic value between 10,000 and 99,999,999.

CTR - The distance a tic label has to be displaced in the -x direction, so that the value is centered on the tic. This is proportional to the number of characters.

X1,Y1 - The abscissa and ordinate values of the lower left hand corner of the block of paper which is occupied by the tic label.

LAB - The alphabetic (binary coded digital) content of a tic label.

LABHI,LABLØ - The respective portions of a tic label greater and less than 10,000.

Subroutine PØINT

1. Purpose - PØINT marks the position of the data points on the prepared set of axes.

2. Input

a. From PREP - the number of curves.

b. From the block of blank common storage, the values of the abscissa and ordinate variables, and their scale factors, and origin values.

3. Output is the set of points, arranged in up to three curves, distinguished by using different symbols for the points of each curve.

4. Operation - Storage allocation consists of the block of blank common. For each curve in sequence, check to determine if its points should be reversed in order. (See subroutine SHFL.) Determine the CALCØMP symbol number and height appropriate to the curve number, then calculate the actual x and y coordinates (in inches) of the center of a point about which the symbol will be drawn. The symbol for the first curve

is a triangle; for the second, a square; and for the third, diamonds. Actual execution of the drawing is done by the CALCØMP routine "TPRINT." A running total of the number of points is kept, and after all three curves are drawn, the success message gives the number of points actually drawn.

After the third graph is completed, a CALCØMP message is drawn on the graph sheet, showing the order of drawing the curves.

5. Symbols not already named:

NSY - The symbol number, as given in the CALCØMP repertoire.

HT - The height of the symbol.

A,B - The abscissa and ordinate of the center of the point.

NPT - The total number of points drawn.

Subroutine SHFL

1. Purpose - SHFL changes the order in which points are drawn, greatly reducing the total distance that the CALCØMP pen must travel.

2. Input - SHFL uses the curve number as given to it by subroutine PØINT, and the values in the NPTS array (of blank common) so as to properly interchange the x and y array values.

3. Output - SHFL returns a revised sequence of x and y array values to PØINT.

4. Operation - This is a classic algorithm in which one of the values to be interchanged is assigned to a holding variable. Then the value of the other variable is given to the first, after which the value of the holding variable is assigned to the second. This process is cut off before the middle or farther point in the original sequence is changed, and control is returned to PØINT.

5. Symbols not already named:

M - The sequence number of the "low-end" point.

NHI - Same for the "high-end" point.

T1,T2 - The ordinate and abscissa, respectively, holding variable.

D2, MAIN

1. Purpose - to draw report ready graphs of ε', ε'', and Δ capacitance vs. mg/g (the WR (K,J,I)) array at all possible T-MC's. Graphs are drawn parametrically at 1 MHz, 500 kHz and 100 kHz; then 20 kHz, 5 kHz and 500 Hz.

2. Input - The data set established by DIELCELL, plus a single card to control an optional printout of the data.

3. Output

a. Up to 60 report ready graphs.

b. A printout to show the progress (and propriety) of execution.

4. Operation - There are seven subroutines, two of which (PREP and SHFL) are identical with their counterparts in D1. Three others are virtually the same as in D1. The main and setup routines are, of course, quite different.

The details of D2 MAIN's operation are: allocate storage, and establish a namelist. Read the data from the data set and, if desired, write its contents, depending upon the just-read value of QPRINT. Initialize the CALCØMP package, the graph sheets and the control indices. Determine the appropriate temperature-mode combination, iterating the temperature and mode indices so as to cover all T-MC's.

Set and/or step the graph-type index, and set a new origin when indicated by a nonzero value of NGADVQ. Print a message identifying each graph. Eliminate unessential and uncontrolled numbers from the graph drawing block of storage. A computed "GO TO" statement directs the program to set up one of the last six graph types, according to the value of the graph-type

index. Note that provision for two types of returns from subroutine SETL6 is made. After all T-MC's have been graphed, the CALCØMP package is emptied and closed, and the program stops execution, writing a message in the Operating System Monitor's Log File, showing that the program has ended according to design.

Subroutine SETL6

1. Purpose - to fill generalized abscissa and ordinate variables with those values of ε', ε'', Δc and milligrams per gram needed to draw curves at three high or three low frequencies on a set of prepared axes.

2. Input - arguments in the subroutine statement's list:

a. 1) a generalized ordinate array, which can hold the contents of any of the above four-dimensional arrays; 2) the starting-special-frequency-number; 3) the current graph number; 4) the type number of the graph; 5) the temperature; 6) mode sequence numbers; and 7) dummy variables not used on input.

b. Other implicit inputs are in the SET49 and blank common blocks.

3. Output - the normal method of operation makes the output of SETL6 go to Subroutine JUSTFY. Output to this routine includes the graph sequence number, the graph number, the total number of curves which are to be drawn. On return to MAIN, however, if the case's number of frequencies was zero, then the last numerical argument in the argument list is assigned a value of zero.

4. Operation - allocate storage and initialize. Test to determine that there is a nonzero number of relative humidities, i.e., cases, at this T-MC. If so, for each of the special frequencies entered, whether of the high frequency or the low frequency group, and for all the relative humidities, test to assure that data have been taken for at least one of those frequencies. If not, write a message (only once per T-MC)

that there is no data. If no relative humidity for the T-MC has data for the frequency group, return so as to change only the graph type.

If there is at least one case, and at least one point of data, assign the proper values for the particular frequency applicable to the case. Form the sum of abscissa and ordinate as a check. If there is at least one curve with at least one nonorigin point to be drawn, proceed to Subroutine JUSTFY.

5. Variables not already named:

Z - The sum of data point coordinate values.

KBAD - The count of relative humidities for which no high (usually) frequency data has been taken.

NSP1,NSP2 - These values are the remaining values in the set of special frequency indicating numbers.

```
//DIELPNCH JOB (XXXX,XX,010,06,3000),'$$$BUDRAYGER$$$',CLASS=S
/*PASSWORD
// EXEC F4GCXS
//FORT.SYSIN DD *
CCCCCCCCCCCCCCCCCCCCCCCCCCCCCCCCCCCCCCCCCCCCCCCCCCCCCCCCCCCCCCCCCCCC
C                                                                     C
C         DIELPNCH CALCULATES ALL QUANTITIES FOR COMPLETE             C
C         DIELECTRIC ANALYSIS OF A SAMPLE, THEN PRINTS AND            C
C         PUNCHES THEM IN THE FORM REQUIRED FOR DIELCELL.             C
C         THERE IS NO LIMIT ON THE AMOUNT OF DATA WHICH CAN           C
C         BE HANDLED.                                                 C
C                                                                     C
C         TO USE DIELPNCH--                                           C
C              KEYPUNCH A CARD CONTAINING THE COUNT OF FRE-           C
C         QUENCY VALUES FOR WHICH VACUUM CAPACITANCE VALUES           C
C         HAVE BEEN DETERMINED. KEYPUNCH (A) CARDS CONTAI-            C
C         NING ALL THE FREQUENCY VALUES APPEARING IN THAT             C
C         LIST, BEING SURE THEY ARE IN DECREASING ORDER.              C
C         THESE FREQUENCIES SHOULD BE PUNCHED EIGHT TO A CARD         C
C         IN TEN SPACE BLOCKS, TILL ALL ARE RECORDED. KEYPUNCH        C
C         THE CORRESPONDING VALUES OF VACUUM CAPACITANCE              C
C         IN ANOTHER SET OF CARDS. PLACE THESE CARDS                  C
C         IN FRONT OF THE CASE-HEADING AND FREQUENCY-DEPENDENT        C
C         CARDS, PUNCHED FROM THE DATA CODING SHEETS.                 C
C                                                                     C
CCCCCCCCCCCCCCCCCCCCCCCCCCCCCCCCCCCCCCCCCCCCCCCCCCCCCCCCCCCCCCCCCCCC
C
C         ALLOCATIONS
C
      COMMON FD(100),CVD(100),NFR
      REAL LOGPPO,IVS
C
C         READ THE VACUUM CAPACITANCE DATA.
C
      READ(5,1)NFR
    1 FORMAT(I2)
      READ(5,2)(FD(N),N=1,NFR)
    2 FORMAT(8F10.0)
      READ(5,2)(CVD(N),N=1,NFR)
C
C         READ A CASE HEADING CARD, AND CALCULATE THE QUAN-
C         TITIES PARTICULAR TO EACH CASE.
C
    3 READ(5,4)T,D,P,PO,W,WO,TEMP,SAMPLE
    4 FORMAT(8F10.5)
      CO=8.854E-14*D*D*3.14159/4./(2.54*T)
      RH=100.*P/PO
      LOGPPO=ALOG10(P/PO)
      WR=1000.*(W-WO)/WO
      V=100.*WR
      IVS=1./V*V
```

```
C
C         PRINT OUT THE CASE-PARTICULAR QUANTITIES, AND
C         WRITE COLUMN HEADINGS FOR AC FREQUENCY-DEPENDENT DATA.
C
      WRITE(6,5)TEMP,P,RH,WR,SAMPLE,LOGPPO,V,IVS
    5 FORMAT(1H1///' TEMPERATURE='F5.1,'  PARTIAL PRESSURE H2O='
     $F6.2,'  RELATIVE HUMIDITY ='F5.1,'  MG PER G ='F6.2/'AND',
     1'SAMPLE IS NUMBER'F5.1,'LOG P/PO = 'F6.3,'CAPILLARY VOLUME'
     2,'='F6.4,'  IVS = 'F8.1////3X,4HFREQ,5X,5HOMEGA,7X,4HCOND,
     36X,3HCAP,6X,7HCAP VAC,3X,9HDELTACAP,2X,10HEPS PRIME ,
     411HEPS DBL PRM,2X,7HTAN DEL)
     47X,7HTAN DEL)
C
C         PUNCH THOSE ESSENTIAL TO GRAPH DRAWING.
C
      WRITE(7,6)TEMP,P,RH,WR
    6 FORMAT(' T='F4.1,' +='F5.2,' RH='F5.1,'   WR='F6.2)
C
C         READ A FREQUENCY-DEPENDENT CARD.
C
    7 READ(5,8)F,G,C,CV
    8 FORMAT(4F20.10)
C
C         DETERMINE THE SIGNAL APPROPRIATE TO THE FREQUENCY
C         AND CAPACITANCE VALUES.
C
      IF(F-5.)15,15,9
    9 IF(C)7,7,10
C
C         RETRIEVE OR INTERPOLATE UNPUNCHED VACUUM CAPACITANCES
C         BY USING ADDCV.
C
   10 IF(CV)12,11,12
   11 CALL ADDCV(F,CV)
C
C         CALCULATE, ...
C
   12 O=2.*3.14159*F
      TD=1.E6*G/O/C
      EP=1.E-12*C/CO
      EDP=EP*TD
      DC=C-CV
      IF(DC.LT.0.)DC=0.
C
C         ...PRINT OUT, AND...
C
      WRITE(6,13)F,O,G,C,CV,DC,EP,EDP,TD
   13 FORMAT(/2F10.1,7F11.3)
```

```
C
C        ...PUNCH THE FREQUENCY-DEPENDENT VARIABLES, AND RE-
C        TURN TO READ ANOTHER FREQUENCY-DEPENDENT CARD.
C
      WRITE(7,14)F,DC,EP,EDP,TD
   14 FORMAT(5F12.3)
      GO TO 7
C
C        FOR F LESS THAN OR EQUAL TO 5, THE CASE HAS ENDED.
C        THE SIGNAL IS PROPAGATED TO DIELCELL BY THIS
C        PUNCH COMMAND.
C
   15 WRITE(7,8)F,G,C,CV
C
C        THE PROGRAM IS SENT FOR ANOTHER CASE CARD WITH F
C        LESS THAN 5, OR TO THE END OF EXECUTION FOR F = 5,
C        AFTER PRINTING THE VACUUM DATA.
C
      IF(F-1.) 3,3,16
   16 PRINT,17  (FD(N),CVD(N),N=1,NFR),NFR
   17 FORMAT(5(F10.0,F8.3))
      STOP 1
      END
```

```
//DIELCELL JOB (XXXX,XX,010,10,1000),'$$$LARRAYGER$$$',CLASS=M
/*PASSWORD
// EXEC F4GCXM
//FORT.SYSIN DD *
CCCCCCCCCCCCCCCCCCCCCCCCCCCCCCCCCCCCCCCCCCCCCCCCCCCCCCCCCCCCCCCCCCCCCCC
C                                                                      C
C         DIELCELL SETS UP THE DATA PUNCHED BY DIELPNCH INTO           C
C         THE FORM USED BY THE DRAWING PROGRAMS. TWO MAG-              C
C         NETIC-MEMORY DATA SETS HOLD THE DRAWING PROGRAMS'            C
C         DATA.                                                        C
C                                                                      C
CCCCCCCCCCCCCCCCCCCCCCCCCCCCCCCCCCCCCCCCCCCCCCCCCCCCCCCCCCCCCCCCCCCCCCC
C
C         ALLOCATIONS.
C
      INTEGER TITLE
      COMMON LSP(6,20,2,5),KM(2,5),TD(25,20,2,5),EP(25,20,2,5),
     $EDP(25,20,2,5),DC(25,20,2,5),F(25,20,2,5),WR(20,2,5),
     1NF(20,2,5),O(2,210),TITLE(2,9,5)
      NAMELIST/ONE/NT,KM,NF,F,TD,EP,EDP,O,TITLE
      NAMELIST/TWO/NT,KM,LSP,WR,EP,EDP,DC,O,TITLE
C
C         CLEAR THE DATA STORAGE OF UNCONTROLLED, UNDESIRED
C         INFORMATION.
C
      DO  2 I=1,5
      DO  2 J=1,2
      KM(J,I)=0
      DO  2 K=1,20
      DO  1 NSP=1,6
    1 LSP(NSP,K,J,I)=0
      NF(K,J,I)=0
      WR(K,J,I)=0.
      DO  2 L=1,25
      TD(L,K,J,I)=0.
      EP(L,K,J,I)=0.
     EDP(L,K,J,I)=0.
      DC(L,K,J,I)=0.
    2   F(L,K,J,I)=0.
C
C     FOR THE NEXT FOUR COMMENTS , THE PROGRAM READS THE ...
C
C           ...EIGHTEEN AXIS TITLES, A PERMANENT PART OF THIS
C         PROGRAM'S DECK.
C
      READ(5,3)(((TITLE(NAX,NTP,N),N=1,5),NTP=1,9),NAX=1,2)
    3 FORMAT(5A4)
C
C           ...NUMBER OF TEMPERATURES, AND THE NUMBER OF RELA-
C         TIVE HUMIDITIES FOR EACH TEMPERATURE-MODE COMBINATION.
C
```

```
      READ(5,4) NT
    4 FORMAT(I1)
      READ(5,5)((KM(J,I),J=1,2),I=1,NT)
    5 FORMAT(10I3)
      DO 15 I=1,NT
      DO 15 J=1,2
      NRH=KM(J,I)
      IF(NRH)14,14,6
    6 DO 14 K=1,NRH
C
C          ...THE TWO CASE-HEADING CARDS. THE PRECEEDING THREE
C        CARDS CONTENTS RESULT FROM INSPECTING THE DIELPNCH
C        PRINTOUT.
C
      READ(5,7)(LSP(NSP,K,J,I),NSP=1,6)
    7 FORMAT(6I3)
      READ(5,8) RH, WR(K,J,I)
    8 FORMAT(19X, F5.1,6X,F6.2)
      L=0
C
C        COUNT THE NUMBER OF FREQUENCIES PER CASE.
C
    9 L=L+1
C
C        REAC A FREQUENCY-DEPENDENT CARD, AND EVALUATE
C        ITS SIGNAL.
C
      READ(5,10)F(L,K,J,I),DC(L,K,J,I),EP(L,K,J,I),
     $EDP(L,K,J,I),TD(L,K,J,I)
   10 FORMAT(5F12.3)
      IF(5.-F(L,K,J,I))11,16,12
C
C        FOR F GREATER THAN 5, I. E., A DATA VALUE, STORE ITS
C        COMMON LOGARITHM, AND READ ANOTHER CARD.
C
   11 F(L,K,J,I)=ALOG10(F(L,K,J,I))
      GO TO 9
C
C        IF F IS LESS THAN 5, THIS CASE ENDS, BUT OTHERS
C        FOLLOW.
C
   12 NF(K,J,I)=L-1
      WRITE(6,13)  I,J,K,NF(K,J,I),RH
   13 FORMAT(10X,'FOR I,J,  K = 'I2,2(', 'I2),', NF = 'I2,
     $'  AND RH = 'F5.1,' ')
   14 CONTINUE
   15 CONTINUE
C
C        WHEN F EQUALS FIVE, NO MORE DIELCTRICS INFORMATION
```

```
C         FOLLOWS.
C
   16 NF(K,J,I)=L-1
      PRINT,13 I,J,K,NF(K,J,I),RH
C
C         THIS LOOP CALCULATES THE LOCATIONS OF THE ORIGINS.
C
      OX=0.
      OY=8.5
      DO 17 N=1,210,3
      N1=N+1
      N2=N+2
      O(1,N)=OX
      O(1,N1)=0.
      O(1,N2)=0.
      O(2,N)=0.
      O(2,N1)=OY
      O(2,N2)=OY
      OX=11.
   17 OY=-OY
C
C         WRITE THE DATA INTO THE DATA CELL, IN SETS DESIGNED
C         FOR USE BY D1 AND D2.
C
      WRITE(1) NT,KM,O,TITLE,NF,FTD,EP,EDP
      WRITE(2) NT,KM,O,TITLE,LSP,WR,EP,EDP,DC
C
C         READ THE CARD WHICH DETERMINES WHETHER THE NAME-
C         LISTS ARE TO BE PRINTED.
C
      READ(5,18)QPRINT
   18 FORMAT (79X,F1.0)
      IF(QPRINT.EQ.0.) STOP 1
      WRITE(6,ONE)
      WRITE(6,19)
   19 FORMAT(1H1)
      WRITE(6,TWO)
      STOP 2
C
C         THE TITLE CARDS AND JCL BELOW ARE AN UNVARYING PART
C         OF THIS PROGRAM'S DECK.
C
      END
/*
```

```
//GO.FT01F001 DD DSN=THREE.DAY.FOR.D1,UNIT=2321,
//  SPACE=(CYL,(10,5)),VOL=SER=DCELL1,DISP=(NEW,KEEP)
//GO.FT02F001 DD DSN=THREE.DAY.FOR.D2,UNIT=2321,
//  SPACE=(CYL,(10,5)),VOL=SER=DCELL1,DISP=(NEW,KEEP)
               OR IF TAPES SHOULD BE REQUIRED, ESTABLISH
               THEM WITH THE FIRST FOUR CARDS BELOW, BUT
               FOR SUBSEQUENT REFERENCES, BY REPAIR, D1 OR
               D2, REPLACE THE 2ND AND 4TH CARDS BY, RES-
               PECTIVELY, THE 5TH AND 6TH, USING THE
               VOLUME SERIAL NUMBER SUPPLIED BY THE
               COMPUTING CENTER.
//GO.FT01F001 DD UNIT=TAPE9,DCB=(DEN=2),LABEL=(1,SL),
//  DSN=DRAW.ONE.TAPE,DISP=(NEW,KEEP)
//GO.FT02F001 DD UNIT=TAPE9,DCB=(DEN=2),LABEL=(1,SL),
//  DSN=DRAW.TWO.TAPE,DISP=(NEW,KEEP)
//  DSN=DRAW.ONE.TAPE,DISP=(OLD,KEEP),VOL=SER=02XXXX
//  DSN=DRAW.TWO.TAPE,DISP=(OLD,KEEP),VOL=SER=02XXXX
//GO.SYSIN DD *
    LOG FREQUENCY            NAX AND NTP ARE 1,1, RESPECTIVELY.
    LOG FREQUENCY                            1,2
    LOG FREQUENCY                            1,3
    MG H2C PER G                             1,4
    MG H2C PER G                             1,5
    MG H2O PER G                             1,6
    MG H2O PER G                             1,7
    MG H2O PER G                             1,8
    MG H2C PER G                             1,9
      TAN DELTA                              2,1
    EPSILON PRIME                            2,2
EPSILON DOUBLE PRIME                         2,3
    EPSILON PRIME                            2,4
    EPSILON PRIME                            2,5
EPSILON DOUBLE PRIME                         2,6
EPSILON DOUBLE PRIME                         2,7
  DELTA CAPACITANCE                          2,8
  DELTA CAPACITANCE                          2,9
*************************************************************
*                                                           *
*                THE REST OF THE DATA DECK.                 *
*                                                           *
*************************************************************
THE 1 IN COLUMN 80 CAUSES DATA PRINTOUT.                     1
/*EOJ
```

```
      SUBROUTINE ACDCV(A,B)
CCCCCCCCCCCCCCCCCCCCCCCCCCCCCCCCCCCCCCCCCCCCCCCCCCCCCCCCCCCCCCCCCCCC
C                                                                     C
C        ACDCV PROVIDES A VALUE FOR VACUUM CAPACITANCE WHERE          C
C        NONE HAVE BEEN PUNCHED. THE VALUE MAY EITHER BE RE-          C
C        CALLED FROM THE ORIGINAL SET, OR CALCULATED BY               C
C        LINEAR INTERPOLATION.                                        C
C                                                                     C
CCCCCCCCCCCCCCCCCCCCCCCCCCCCCCCCCCCCCCCCCCCCCCCCCCCCCCCCCCCCCCCCCCCC
C
C        ALLOCATIONS
C
      COMMON FD(100),CVD(100),NFR
      DO 3 N=1,NFR
C
C        THE INPUT FREQUENCY, CALLED ''A'' BY THIS ROUTINE, IS
C        REPEATEDLY COMPARED WITH THE LIST OF DECREASING-OR-
C        DERED FREQUENCIES, UNTIL ONE SMALLER OR EQUAL IS FOUND.
C
      IF(FD(N)-A) 1,2,3
C
C        FOR THE ''SMALLER'' CASE, THE APPROPRIATE VALUE OF
C        VACUUM CAPACITANCE IS CALCULATED BY LINEAR INTERPO-
C        LATION.
C
    1 B=CVD(N-1)-(CVD(N-1)-CVD(N))*(FD(N-1)-A)/(FD(N-1)-FD(N))
      B=FLOAT(IFIX(B*1000.))/1000.
      GO TO 4
C
C        FOR THE EQUALITY CASE, THE VACUUM CAPACITANCE IS
C        THE CORRESPONDING ORIGINAL ONE.
C
    2 B=CVD(N)
      RETURN
    3 CONTINUE
C
C        PUT INTERPOLATED VALUES INTO THEIR PLACE IN THE LIST.
C
    4 P=FD(N)
      R=CVD(N)
      FD(N)=A
      CVD(N)=B
      DO 5 M=N,NFR
      Q=FD(M+1)
      S=CVD(M+1)
      FD(M+1)=P
      CVD(M+1)=R
      P=Q
    5 R=S
```

```
C
C         SINCE THE LIST HAS BEEN INCREASED IN LENGTH BY ONE,
C         THE INCREASE IS MADE EXPLICIT HERE.
C
      NFR=NFR+1
      RETURN
      END
```

```
//REPAIR JOB (XXXX,XX,010,01,0000),'*$$BUDRAYGER$$$',CLASS=M
/*PASSWORD
// EXEC F4GCXM
//FORT.SYSIN DD *
CCCCCCCCCCCCCCCCCCCCCCCCCCCCCCCCCCCCCCCCCCCCCCCCCCCCCCCCCCCCCCCCCCCCCC
C                                                                     C
C        REPAIR DOES THE MANIPULATION OF THE MAGNETIC                 C
C        DATA SETS WHILE SMALL- OR LARGE-SCALE ALTERATIONS            C
C        OF THEIR CONTENTS ARE MADE.                                  C
C                                                                     C
CCCCCCCCCCCCCCCCCCCCCCCCCCCCCCCCCCCCCCCCCCCCCCCCCCCCCCCCCCCCCCCCCCCCCC
C
C        ALLOCATIONS.
C
      INTEGER TITLE
      COMMON LSP(6,20,2,5),KM(2,5),TD(25,20,2,5),EP(25,20,2,5),
     $EDP(25,20,2,5),DC(25,20,2,5),F(25,20,2,5),WR(20,2,5),
     1NF(20,2,5),O(2,210),TITLE(2,9,5),NT
C
C        READ THE CONTENTS OF THE DATA SETS.
C
      READ (1) NT,KM,O,TITLE,NF,F,TD,EP,EDP
      READ (2) NT,KM,O,TITLE,LSP,WR,EP,EDP,DC
C
C        ''CHANGE'' IS UNIQUE TO EVERY RUN, AND CORRECTS ONLY
C        THOSE PORTIONS OF THE DATA SET REQUIRED.
C
      CALL CHANGE
C
C        REWIND AND REFILL THE DATA SETS.
C
      REWIND 2
      REWIND 3
      WRITE(1) NT,KM,O,TITLE,NF,F,TD,EP,EDP
      WRITE(2) NT,KM,O,TITLE,LSP,WR,EP,EDP,DC
      STOP
      END
```

```
      SUBROUTINE CHANGE
CCCCCCCCCCCCCCCCCCCCCCCCCCCCCCCCCCCCCCCCCCCCCCCCCCCCCCCCCCCCCCCCCCCC
C                                                                     C
C        CHANGE PERFORMS THE OPERATIONS REQUIRED TO COR-              C
C        RECT BAD PORTIONS OF THE DATA IN THE DATA SET.               C
C                                                                     C
C        THE OPERATIONS OF THE PROGRAM LISTED BELOW ARE AN            C
C        EXAMPLE ONLY, MEANT TO SHOW THE OPTIONS AVAILABLE.           C
C                                                                     C
CCCCCCCCCCCCCCCCCCCCCCCCCCCCCCCCCCCCCCCCCCCCCCCCCCCCCCCCCCCCCCCCCCCC
C
C        ALLOCATIONS
C
      COMMON LSP(6,20,2,5),KM(2,5),TD(25,20,2,5),CP(25,20,2,5),
     $EDP(25,20,2,5),DC(25,20,2,5),F(25,20,2,5),WR(20,2,5),
     1NF(20,2,5),O(2,210),TITLE(2,9,5),NT
C
C        PRINT OUT THE INCOMING VALUES.
C
      WRITE(6,1)
    1 FORMAT (' ON ENTRY--')
      WRITE(6,2)(WR(K,1,2),K=1,20),(F(L,7,1,1),L=1,25),
     $EDP(6,9,2,3)
    2 FORMAT(' WR(K,1,2) = '/4(5G24.5)//'F(L,7,1,1) = '/
     $5(5G24.5)//'EDP(6,9,2,3) = 'F20.10/////)
C
C        CHANGE THE VALUES.
C
      DO 3 K=7,12
    3 WR(K,1,2)=WR(K,1,2)-0.312
      EDP(6,9,2,3)=27.372*TD(6,9,2,3)
      DO 5 L=1,24
      READ(5,4) A
    4 FORMAT(F20.10)
    5 F(L,7,1,1)=ALOG10(A)
C
C        PRINT OUT THE CORRECTED VALUES.
C
      WRITE(6,6)
    6 FORMAT(' AFTER CORRECTION')
      WRITE(6,2)(WR(K,1,2),K=1,20),(F(L,7,1,1),L=1,25),
     $EDP(6,9,2,3)
      RETURN
```

```
C
C         JCL FOR REPAIR/CHANGE.

      END
/*
//GO.FT01F001 DD DSN=THREE.DAY.FOR.D1,UNIT=2321,
//      VOL=SER=DCELL1,DISP=OLD
//GO.FT02F001 DD DSN=THREE.DAY.FOR.D2,UNIT=2321,
//      VOL=SER=DCELL1,DISP=OLD
//GO.SYSIN  DD *
                    *****THE DATA DECK*****
/*EOJ
```

```
//D1 JOB (XXXX,XX,035,06,1000),'$$BUDRRAYGER$$$',CLASS=M
/*PASSWORD
// EXEC F4GCXM
//FORT.SYSIN DD *
CCCCCCCCCCCCCCCCCCCCCCCCCCCCCCCCCCCCCCCCCCCCCCCCCCCCCCCCCCCCCCCCCCCCCCC
C                                                                      C
C        D1 DRAWS REPORT-READY GRAPHS OF THE PERMITTIVITIES            C
C        AND LOSS TANGENT VS. LOG FREQUENCY, SCALING THE               C
C        AXES FOR EACH GRAPH.                                          C
C                                                                      C
C                                                                      C
C        THE MAIN PROGRAM READS THE DATA, AND CONTROLS THE             C
C        FLOW THROUGH ALL THE RELATIVE HUMIDITIES OF EACH              C
C        TEMPERATURE-MODE COMBINATION, DRAWING ALL GRAPHS              C
C        OF A GIVEN TYPE (VIZ., WITH A GIVEN ORDINATE),                C
C        BEFORE PROCEEDING TO THE NEXT TYPE.                           C
C        TO USE D1--                                                   C
C        DETERMINE WHETHER THE DATA PRINTOUT IS DESIRED.               C
C        PUNCH THE DATA CARD ACCORDINGLY. USUALLY, NO PRINT-           C
C        OUT IS NEEDED, CALLING FOR A BLANK OR A ZERO IN THE           C
C        DATA CARD'S LAST COLUMN.                                      C
C                                                                      C
CCCCCCCCCCCCCCCCCCCCCCCCCCCCCCCCCCCCCCCCCCCCCCCCCCCCCCCCCCCCCCCCCCCCCCC
C
C        ALLOCATIONS
C
      INTEGER TITLE,KM(2,5)
      REAL ORD(25,20,2,5),TD(25,20,2,5),EDP(25,20,2,5),EP(25,20,2
     $,5),O(2,210),R(2)
      COMMON S(2),ZS(2),SD(2),NPR(2),X(3,25),Y(3,25),ZMAX(2),ZMIN
     $(2),TITLE(2,9,5),NPTS(3)
      COMMON /SET13/F(25,20,2,5),NF(20,2,5)
      NAMELIST /ONE/NT,KM,NF,F,TD,EP,EDP,O,TITLE
C
C        READ THE DATA FROM THE DATA CELL, AND PRINT THE
C        CONTENTS IF DESIRED.
C
      READ (1) NT,KM,O,TITLE,NF,F,TD,EP,EDP
      READ (5,1) QPRINT
    1 FORMAT (79X,F1.0)
      IF(QPRINT.NE.0.) WRITE(6,ONE)
C
C        INITIALIZE THE CALCOMP PACKAGE, THE GRAPH SHEETS, AND
C        THE CONTROL INDICES.
C
      CALL PLSTRT(1111,11)
      CALL PLOT(3.,1.50,-3)
      NG=0
      NSP=0
      NGADVQ=1
```

```
C
C         FOR EACH TEMPERATURE-MODE COMBINATION, TEST TO SEE IF
C         THE NUMBER OF CASES IS GREATER THAN ZERO, AND STEP
C         THE GRAPH TYPE INDEX.
C
      DO 14 I=1,NT
      DO 14 J=1,2
      NTP=0
      NRH=KM(J,I)
      IF(NRH) 14,14,2
    2 NTP=NTP+1
      KST=0
C
C         SET A NEW ORIGIN WHEN NECESSARY.
C
    3 IF(NGADVQ)4,6,4
    4 NG=NG+1
      NGADVQ=1
C
C         ELIMINATE ALL UNESSENTIAL AND/OR UNCONTROLLED NUMBERS
C         FROM THE BLOCK OF STORAGE WHICH WILL BE FILLED WITH
C         GRAPH DRAWING INFORMATION.
C
      DO 5 NS=1,3
      NPTS(NS)=0
      DO 5 N=1,25
      X(NS,N)=0.
    5 Y(NS,N)=0.
      CALL PLOT(O(1,NG),O(2,NG),-3)
C
C         PRINT A MESSAGE IDENTIFYING EACH GRAPH.
C
    6 WRITE(6,7)NTP,NG,I,J
    7 FORMAT('0',' NTP ='I2,', NG = 'I3,', I = 'I2,', J = 'I2)
    8 IF(NTP-2) 9,10,12
C
C         PROCEED WITH SETTING UP THE GRAPH OF THE PRESENT TYPE,
C         WITH THE PROPER ORDINATE ARRAY (FIRST ARGUMENT) AND
C         FREQUENCY RANGE (SECOND ARGUMENT).
C
    9 CALL SETF3(TD,KST,NG,NTP,I,J,KND,NRH,NGADVQ, 14, 11)
   10 CALL SETF3(EP,KST,NG,NTP,I,J,KND,NRH,NGADVQ, 14, 11)
   11 IF(KND-NRH) 3,2,2
   12 CALLSETF3(EDP,KST,NG,NTP,I,J,KND,NRH,NGADVQ, 14, 13)
   13 IF(KND-NRH) 3,14,14
   14 CONTINUE
      CALL PLTEND
      STOP  111
```

```
C
C              *****CHOOSE ONE OF THE SAMPLE DATA CARDS BELOW*****
C
C               ************************************************
C               *****THE JOB CONTROL LANGUAGE CARDS BELOW*****
C               *****    BETWEEN ''/*'' AND ''/*EOJ''    *****
C               *****ARE PLACED BEHIND THE DECK FOR SUB- *****
C               *****ROUTINE SHFL WHEN ACTUALLY RUNNING  *****
C               ***** THE PROGRAM.                       *****
C               ************************************************
C
      END
/*
//GO.FT01F001 DD DSN=THREE.DAY.FOR.D1,UNIT=2321,
//      VOL=SER=DCELL1,DISP=OLD
//GO.FT18F001 DD UNIT=TAPE7,DCB=(RECFM=U,BLKSIZE=1440,DEN=1,TRTCH=ET),
//             DISP=OLD,LABEL=(,BLP),VOL=SER=OUTPT,DSN=CALCOMP
//GO.SYSIN DD *
A BLANK IN COLUMN 80 DELETES DATA PRINTOUT.
THE 1 IN COLUMN 80 CAUSES DATA PRINTOUT.                          1
/*EOJ
```

```
      SUBROUTINE SETF3(ORD,KST,NG,NTP,I,J,KND,NRH,M,*,*)
CCCCCCCCCCCCCCCCCCCCCCCCCCCCCCCCCCCCCCCCCCCCCCCCCCCCCCCCCCCCCCCCCCCCC
C                                                                     C
C         SETF3 DETERMINES WHICH TRIO OF RELATIVE HUMIDITIES'         C
C         DATA IS TO BE GRAPHED, AND FILLS THE THREE CURVES'          C
C         ORDINATE AND ABSCISSA ARRAYS.                               C
C                                                                     C
CCCCCCCCCCCCCCCCCCCCCCCCCCCCCCCCCCCCCCCCCCCCCCCCCCCCCCCCCCCCCCCCCCCCC
C
C         ALLOCATIONS.
C
      COMMON S(2),ZS(2),SD(2),NPR(2),X(3,25),Y(3,25),ZMAX(2),ZMIN
     $(2),TITLE(2,9,5),NPTS(3)
      COMMON /SET13/F(25,20,2,5),NF(20,2,5)
      REAL ORD(25,20,2,5)
C
C         DETERMINE THE SEQUENCE NUMBERS OF THE STARTING AND
C         FINISHING RELATIVE HUMIDITIES, ACCORDING TO HOW
C         MANY HAVE BEEN GRAPHED BEFORE.
C
      IF(KST-1)1,2,2
    1 KST=1
      KND=MIN0(3,NRH)
      GO TO 3
    2 KST=KST+3
      KND=MIN0(KND+3,NRH)
    3 NS=0
      NCVS=KND-KST+1
C
C         FILL THE ORDINATE AND ABSCISSA-VALUE ARRAYS FOR EACH
C         RELATIVE HUMIDITY'S CURVE WITH DATA VALUES.
C
      DO 4 K=KST,KND
      IF(NF(K,J,I).EQ.0) GO TO 6
      NS=NS+1
      NPNTS=NF(K,J,I)
      NPTS(NS)=NPNTS
      DO 4 L=1,NPNTS
      X(NS,L)=F(L,K,J,I)
    4 Y(NS,L)=ORD(L,K,J,I)
```

```
C
C         THIS MESSAGE IDENTIFIES THE ORDINALS OF THE RELATIVE
C         HUMIDITIES TO BE GRAPHED, AND THE NUMBER OF CURVES.
C
      WRITE(6,5) KST,KND,NCVS
    5 FORMAT('  K  RANGES FROM' I3,' TO ' I3,'.'I4,' CURVES WILL'
     $,'BE DRAWN.')
C
C         GO ON TO JUSTIFY GRAPH DRAWING.
C
      CALL JUSTFY (NG,NTP,NCVS, 6, 7, 2)
C               *****   IN D2, USE THIS FORM--  *****
      CALL JUSTFY(NG,NTP,NCVS, 6, 7)
    6 M=0
      RETURN 1
    7 RETURN 2
      END
```

```
      SUBROUTINEJUSTFY(NG,NTP,NCVS,*,*,*)
C             *****   IN D2, USE THIS FORM--  *****
      SUBROUTINE JUSTFY(NG,NTP,NCVS,*,*)
CCCCCCCCCCCCCCCCCCCCCCCCCCCCCCCCCCCCCCCCCCCCCCCCCCCCCCCCCCCCCCCCCCCCCCC
C                                                                      C
C        THIS ROUTINE DETERMINES THAT AT LEAST ONE OF THE              C
C        POINTS SENT TO IT HAS A NON-ORIGIN LOCATION, INFER-           C
C        RING THAT THERE IS INDEED DATA TO BE PLOTTED, AND             C
C        THUS THAT DRAWING TICKED AND LABELLED AXES IS JUS-            C
C        TIFIED.                                                       C
C                                                                      C
CCCCCCCCCCCCCCCCCCCCCCCCCCCCCCCCCCCCCCCCCCCCCCCCCCCCCCCCCCCCCCCCCCCCCCC
C
C        ALLOCATIONS.
C
      INTEGER TITLE
      COMMON S(2),ZS(2),SD(2),NPR(2),X(3,25),Y(3,25),ZMAX(2),ZMIN
     $(2),TITLE(2,9,5),NPTS(3)
C
C        FOR THE X-AXIS, INITIALIZE THE RANGE-END VARIABLES SO
C        THAT THEY ARE CERTAIN TO BE CHANGED BY A DATA OR
C        ASSIGNED VALUE.
C
      ZX=-9.9E70
      ZN=+9.9E70
C
C        CHECK ALL THREE CURVES FOR THE HIGHEST AND LOWEST X-
C        VALUES.
C
      DO 1 NS=1,NCVS
      NPNTS=NPTS(NS)
      DO 1 N=1,NPNTS
      ZX=AMAX1(ZX,X(NS,N))
    1 ZN=AMIN1(ZN,X(NS,N))
      ZMAX(1)=ZX
      ZMIN(1)=ZN
C
C        REPEAT THESE TWO PROCEDURES FOR THE Y-AXIS.
C
      ZX=-9.9E70
      ZN=+9.9E70
      DO 2 NS=1,NCVS
      NPNTS=NPTS(NS)
      DO 2 N=1,NPNTS
      ZX=AMAX1(ZX,Y(NS,N))
    2 ZN=AMIN1(ZN,Y(NS,N))
      ZMAX(2)=ZX
      ZMIN(2)=ZN
```

```
C
C         A VALUE OF FALSE FOR THIS TEST IS THE JUSTIFICATION
C         FOR PROCEEDING, AND PRINTING OUT THE RANGE OF DATA
C         VALUES.
C
      IF (ZMAX(1).EQ.0..OR.ZMAX(2).EQ.0.) GO TO 4
C
C         IF JUSTIFICATION FAILS, THE ''BAD'' RETURN ROUTE
C         IS ENTERED AFTER THE FAILURE MESSAGE PRINTOUT.
C
      WRITE (6,3) ZMAX,ZMIN
    3 FORMAT(' THE LARGEST DATA VALUES PER AXIS ARE' 2G12.3,
     $', WHILE THE SMALLEST ARE'2G12.3)
      CALL SCALE(NG,NTP,NCVS, 8, 7)
C               *****   IN D2, USE THIS FORM--  *****
      CALL SCALE(NG,NTP,NCVS, 7)
    4 PRINT,5 NG
    5 FORMAT(' THERE IS NO DATA FOR THE GRAPH WHICH WOULD HAVE'
     $,' BEEN THE 'I2,'TH. CONTROL IS RETURNED TO MAIN .')
    6 RETURN 1
    7 RETURN 2
    8 RETURN 3
      END
```

```
      SUBROUTINE SCALE(NG,NTP,NCVS,*,*)
C              *****   IN D2, USE THIS FORM--  *****
      SUBROUTINE SCALE(NG,NTP,NCVS,*)
CCCCCCCCCCCCCCCCCCCCCCCCCCCCCCCCCCCCCCCCCCCCCCCCCCCCCCCCCCCCCCCCCCCCCCC
C                                                                     C
C        SCALE SELECTS INTERVAL BOUNDS WHICH MINIMIZE BOTH            C
C        DEAD SPACE ON THE AXES, AND DISTRACTION BY OVERLY            C
C        SIGNIFICANT, MENTALLY UNCOMFORTABLE, AXIS MARKINGS.          C
C                                                                     C
CCCCCCCCCCCCCCCCCCCCCCCCCCCCCCCCCCCCCCCCCCCCCCCCCCCCCCCCCCCCCCCCCCCCCCC
C
C        ALLOCATIONS.
C
      INTEGER TITLE
      COMMON S(2),ZS(2),SD(2),NPR(2),X(3,25),Y(3,25),ZMAX(2),ZMIN
     $(2),TITLE(2,9,5),NPTS(3)
      DIMENSION R(2)
      DATA R/8.,5./
C
C        FOR EACH AXIS IN TURN ...
C
      DO 20 NAX=1,2
      ZX=ZMAX(NAX)
      ZN=ZMIN(NAX)
C
C        DETERMINE THE ORDER OF MAGNITUDE OF THE BOUNDING DATA
C        VALUES, AND THEIR RATIO.
C
      A=10**(1+IFIX(ALOG10(ZX)))
      IF(ZN) 2,2,1
    1 B=10**(1+IFIX(ALOG10(ZN)))
      RATIO=ZX/ZN
      GO TO 3
    2 B=0.
      RATIO=ZX
C
C        DETERMINE WHAT FRACTION OF ITS ORDER IS USED BY THE
C        MAXIMUM AXIS VALUE, AND SET THE UPPER BOUND ACCOR-
C        DINGLY.
C
    3 DO 6 N=2,10,2
      IF(N-10) 5,4,4
    4 ZX=A
      IF(ZX.LT.0.78*A) ZX=0.80*A
      IF(ZX.LT.0.62*A) ZX=0.60*A
      GO TO 8
```

```
    5 IF(ZX.LT.A/FLOAT(10-I)) GO TO 7
    6 CONTINUE
    7 IF(N.EQ.8) ZX=A/2.
      IF(N.EQ.6) ZX=A/4.
      IF(N.EQ.4) ZX=A/5.
      IF(N.EQ.2) ZX=A*0.15
C
C        ASSIGN AN APPROPRIATE VALUE TO THE LOWER BOUND.
C
    8 IF(RATIO.GT.1000..AND.ZN.LT.100.) ZN=0.
      IF(RATIO.GT.1000.) GO TO 13
      IF(A-10.) 9,9,10
    9 ZN=0.
      GO TO 13
   10 DO 11 N=2,8,2
      IF(ZN.GT.B/FLOAT(N)) GO TO 12
   11 CONTINUE
   12 IF(N.LE.4) ZN=B/FLOAT(N)
      IF(N.EQ.6) ZN=0.15*B
      IF(N.GE.8) ZN=B/10.
C
C        CALCULATE THE NUMBER OF VARIABLES (''TIC DIVISION''),
C        AND THE NUMBER OF TICS, BETWEEN LABELS.
C
   13 SD(NAX)=A/50.
      NPR(NAX)=5
      IF(RATIO.GT.8.)SD(NAX)=A/20.
      IF(RATIO.GT.8.)NPR(NAX)=4
C
C        ASSURE THAT THE AXIS BOUNDS BECOME AN INTEGER MUL-
C        TIPLE OF THE TIC DIVISION.
C
   14 NTHI=1+IFIX(ZX/SD(NAX))
      NTLO=IFIX(ZN/SD(NAX))
      IF((NTHI-NTLO).LE.10)NPR(NAX)=2
C
C        IF LESS THAN SIX TICS WOULD RESULT, HALVE THE TIC DI-
C        VISION.
C
      IF(NTHI-NTLO-6)15,15,16
   15 SD(NAX)=SD(NAX)/2.
      GO TO 14
   16 ZMAX(NAX)=NTHI*SD(NAX)
      ZMIN(NAX)=NTLO*SD(NAX)
C
C        ASSURE THAT THERE IS A NONZERO AXIS RANGE. IF THERE
C        SHOULD BE, RETURN D1 TO SETF3, TO TRY THE NEXT TRIO
C        OF RH'S. IN D2, RETURN TO MAIN AND CHANGE GRAPH
C        TYPES.
C
```

```
      RANGE=ZMAX(NAX)-ZMIN(NAX)
      IF (RANGE) 17,17,19
   17 WRITE (6,18)ZMAX(NAX),ZMIN(NAX),(TITLE(NAX,NTP,N),N=1,5)
   18 FORMAT(' ZMAX = 'G12.3,', WHILE ZMIN = 'G12.3,' SO THAT'
     $,' THERE IS APPARENTLY A NEGATIVE OR ZERO RANGE FOR ',
     1'PLOTTING '/T20,5A4)
      RETURN 1
C
C        CALCULATE THE SCALE FACTOR, AND THE NUMBER OF INCHES
C        ACTUAL TIC SPACING.
C
   19 ZS(NAX)=R(NAX)/RANGE
      S(NAX)=ZS(NAX)*SD(NAX)
   20 CONTINUE
C
C        PRINT OUT THE SUCCESS MESSAGE, SHOWING THE BOUNDS AND
C        THE SCALING VARIABLES' VALUES.
C
      WRITE(6,21)NG,(TITLE(2,NTP,N),N=1,5),(TITLE(1,NTP,N),N=1,5)
     $,((S(NAX),SD(NAX),ZMAX(NAX),ZMIN(NAX)),NAX=1,2)
   21 FORMAT(' FOR GRAPH   'I3,', OF '5A4,' VS '5A4/T10,
     $'  ON THE X-AXIS  S = 'G12.3,', SD = 'G12.3,', ZMAX = '
     1G12.3,', ZMIN = 'G12.3/T7,' AND ON THE Y-AXIS '6X,G12.3,
     27X,G12.3,2(9X,G12.3))
C
C        GO ON TO DRAW THE TICKED AND LABELLED AXES.
C
      CALL PREP(NG,NTP,NCVS)
      RETURN  2
      END
```

```
      SUBROUTINE PREP(NG,NTP,NCVS)
CCCCCCCCCCCCCCCCCCCCCCCCCCCCCCCCCCCCCCCCCCCCCCCCCCCCCCCCCCCCCCCCCCCC
C                                                                     C
C        PREP DRAWS THE TICKED AND LABELLED AXES IN PREPA-            C
C        RATION FOR CURVE DRAWING.                                    C
C                                                                     C
CCCCCCCCCCCCCCCCCCCCCCCCCCCCCCCCCCCCCCCCCCCCCCCCCCCCCCCCCCCCCCCCCCCCC
C
C        ALLOCATIONS
C
      INTEGER TITLE,TL
      COMMON S(2),ZS(2),SC(2),NPR(2),X(3,25),Y(3,25),ZMAX(2),ZMIN
     $(2),TITLE(2,9,5),NPTS(3)
      DIMENSION TL(20),R(2)
      DATA R/8.,5./
C
C        FOR EACH AXIS, ASSIGN SCALAR VALUES TO ARRAY VARI-
C        ABLES, FOR FASTER REFERENCE.
C
      DO 33 NAX=1,2
      SCE=SC(NAX)
      NP=NPR(NAX)
      SE=S(NAX)
      P=R(NAX)
C
C        ASSIGN VALUES TO TITLE AND AXIS-DRAWING VARIABLES.
C
      IF(NAX-1) 1,1,2
    1 A=0.
      XST=2.36
      YST=-0.656
      AL=0.
C
C        AXIS2 DRAWS THE AXIS, HERE THE ABSCISSA ...
C
      CALL AXIS2(0.,0.,P,A,SE)
      GO TO 3
    2 A=270.
      XST=-1.00
      YST=0.86
      AL=+90.
C
C        ... AND HERE THE ORDINATE.
C
      CALL AXIS2(0.,5.,P,A,SE)
C
C        WRITE OUT THE AXIS' TITLE.
C
    3 DO 4 N=1,5
    4 TL(N)=TITLE(NAX,NTP,N)
      CALL CPRINT(TL,20,XST,YST,.164,AL)
```

```
C
C          THE NEXT FIVE COMMENTS DEAL WITH DETERMINING THE
C          TIC LABELLING PARAMETERS.
C
      NHALVE=0
C
C          DETERMINE THE ORIGIN TIC VALUE, AND WHETHER IT IS
C          AN INTEGER MULTIPLE OF BOTH THE TIC DIVISION AND
C          THE LABELLING ORDINAL.
C
    5 TVC=ZMIN(NAX)
      NTICS=IFIX(P/SE) + 1
      NSTCNG=1
    6 C=TVC/SCE/FLOAT(NP)
      NC=IFIX(C+.0001)
      IF(C-FLOAT(NC)-1.E-4)8,8,7
C
C          IF NOT, SET UP TO DETERMINE WHETHER THE SECOND OR
C          SUBSEQUENT TIC MIGHT BE.
C
    7 NSTCNG=NSTCNG+1
      IF(NSTCNG.EQ.20) GO TO 11
      TVC=TVC+SCE
      GO TO 6
C
C          IF THE FIRST TIC WILL BE MORE THAN ONE THIRD THE WAY
C          DOWN THE AXIS, HALVE THE TIC DIVISION, AND ADJUST
C          THE OTHER SCALING PARAMETERS.
    8 IF(FLOAT(NSTCNG).LE.0.334*FLOAT(NTICS).AND.NTICS.GT.5)GO TO 10
      SCE=SCE/2.
      SE=SE/2.
      NTHI=1+IFIX(ZMAX(NAX)/SCE)
      NTLO=IFIX(ZMIN(NAX)/SCE)
      ZMAX(NAX)=SCE*FLOAT(NTHI)
      ZMIN(NAX)=SCE*FLOAT(NTLO)
      NTICS=NTHI-NTLO
      RANGE=ZMAX(NAX)-ZMIN(NAX)
      ZS(NAX)=R(NAX)/RANGE
      IF(NTICS.GT.10.AND.NP.GT.2)NP=NP/2
      IF(NP.GT.2) NP=NP/2
```

```
C
C         ... WRITE A MESSAGE DRAWING ATTENTION TO THE CHANGE,
C         AND REDETERMINE THE TIC LABELLING PARAMETERS.
C
      WRITE(6, 9) NAX,NTP,SE,SDE,NP
    9 FORMAT(30X,'S,SD,   NPR  SUB  ('I2,','I2,') HAVE BEEN HALVED.'/' T
     1HEIR VALUES ARE NOW '1PE10.2,','1PE10.2,',  'I2,' RESPECTIVELY.')
      NHALVE=NHALVE+1
      IF(NHALVE-5) 5,5,10
   10 IF(SDE.LT.1.) NMARK= IFIX(10.**(IFIX(ALOG10(SDE)))/SDE)
      IF(SDE.GE.1.) NMARK=NP
      IF(NMARK.GT.5) NMARK=5
      IF(NMARK) 33,33,11
   11 WRITE (6,12) NAX,NSTCNG,NTICS,NMARK
   12 FORMAT(T10,'FOR NAX ='I1,', NSTCNG, NTICS, AND NMARK ARE'I2,','I2,
     1', AND 'I2,', RESPECTIVELY')
      IF(NSTCNG.EQ.20) GO TO 33
C
C         AT EACH APPROPRIATE TIC ...
C
      DO 32 N=NSTCNG,NTICS,NMARK
      M=N-1
C
C         DETERMINE THE TIC VALUE.
C
      TV=SDE*FLOAT(M)+ZMIN(NAX)
      ITV=IFIX(TV+0.4)
      IF(ITV) 13,13,16
   13 IF(TV) 14,14,15
   14 ITV=0
      NC=1
C
C         CONVERT THE NUMERIC INFORMATION (ITV) TO ALPHABETIC
C         (LAB), AS REQUIRED BY THE TIC-LABEL DRAWING ROUTINE.
C
C
C         FOR SMALL LABELS ...
C
      CALL ZBCDIN(LAB,ITV)
      GO TO 21
   15 NC=1+IFIX(ABS(ALOG10(TV)))
      ITV=IFIX(TV*10.**(NC))
      CALL BCDINT(LAB,ITV)
      GO TO 21
   16 IF(ITV-10000) 17,18,18
   17 CALL ZBCDIN(LAB,ITV)
      GO TO 19
   19 ITVHI=ITV/10000
      ITVLO=ITV
```

```
C
C          ... OR LARGE.
C
      CALL ZBCDIN(LABHI,ITVHI)
      CALL BCDINT(LABLO, ITVLO)
   19 NC=IFIX(ALOG10(TV)) +1
   20 IF (ITV-10000) 21,27,27
   21 IF(NAX-1)  22,22,26
   22 IF(NC-3) 23,23,24
C
C          DETERMINE THE LOCATION OF THE LABEL WITH RESPECT TO
C          THE TIC, DEPENDING ON TIC VALUE AND AXIS.
C
   23 CTR=.362-.05*FLOAT(NC)
      GO TO 25
   24 CTR=0.
   25 X1=SE*FLOAT(M)-CTR
      Y1=-0.20
      GO TO 31
   26 X1=-.48
      Y1=SE*FLOAT(M)-.05
      GO TO 31
   27 IF (NAX-1) 28,28,29
   28 XHI=SE*FLOAT(M)-.05*FLOAT(NC)
      XLO=XHI+.1*4.
      Y1=-.20
      GO TO 30
   29 XHI=-.88
      XLO = -.48
      Y1=SE*FLOAT(M)-.05
C
C          DRAW THE TIC LABEL.
C
   30 CALL CPRINT(LABHI,4,XHI,Y1,0.10,0.)
      CALL CPRINT(LABLO,4,XLO,Y1,0.10,0.)
      GO TO 32
   31 CALL CPRINT(LAB, 4,X1,Y1,.10,0.)
   32 CONTINUE
   33 CONTINUE
      WRITE (6,34) ITV
   34 FORMAT('  THE LAST TIC LABEL ON THE Y-AXIS IS'I8)
C
C          PROCEED TO DRAW THE POINTS ON THE PREPARED AXES.
C
      CALL POINT(NCVS)
      RETURN
      END
```

```
      SUBROUTINE POINT(NCVS)
CCCCCCCCCCCCCCCCCCCCCCCCCCCCCCCCCCCCCCCCCCCCCCCCCCCCCCCCCCCCCCCCCCCC
C                                                                     C
C        POINT PLACES THE PROPER SYMBOL AT THE PROPER PLACE           C
C        WITH  RESPECT TO THE PREPARED AXES, AND COUNTS THE           C
C        NUMBER OF POINTS DRAWN ON THE GRAPH. IT ALSO DRAWS           C
C        A MESSAGE ON THE GRAPH SHEET, SHOWING THAT THE TRIA-         C
C        GLES MARK THE FIRST CURVE, SQUARES THE SECUND, AND           C
C        DIAMONDS THE THIRD.                                          C
C                                                                     C
CCCCCCCCCCCCCCCCCCCCCCCCCCCCCCCCCCCCCCCCCCCCCCCCCCCCCCCCCCCCCCCCCCCC
C
C        ALLOCATIONS.
C
      COMMON S(2),ZS(2),SD(2),NPR(2),X(3,25),Y(3,25),ZMAX(2),ZMIN
     $(2),TITLE(2,9,5),NPTS(3)
      NPT=0
      DO 4 NS=1,NCVS
C
C        REVERSE THE ORDER OF DRAWING POINTS SO AS TO
C        ELIMINATE WASTE PEN MOTION. FOR THE D2 PROGRAM,
C        THE RELATIONAL OPERATOR .NE. APPEARING BELOW IS
C        REPLACED BY .EQ..
C
      IF(NS.NE.2) CALL SHFL(NS)
      IF(NS-2) 1,1,2
    1 NSY=NS
      HT=0.1
      GO TO 3
    2 NSY=6
      HT=0.2
    3 NPNTS=NPTS(NS)
      DO 4 N=1,NPNTS
      IF(X(NS,N).EQ.0..AND.Y(NS,N).EQ.0.) GO TO 4
C
C        CALCULATE THE X AND Y COORDINATES, IN INCHES.
C
      A=(X(NS,N)-ZMIN(1))*ZS(1)
      B=(Y(NS,N)-ZMIN(2))*ZS(2)
C
C        TPRINT DRAWS THE PROPER SYMBOL, CENTERED ON (A,B),
C        OF HEIGHT HT.
C
      CALL TPRINT(NSY,A,B,HT)
      NPT=NPT+1
    4 CONTINUE
      WRITE(6,6) NPT
    6 FORMAT(T2,I3,' POINTS WERE DRAWN.')
```

```
C
C         THE REMINDER OF THE CURVE DRAWING ORDER IS DRAWN
C         ON THE GRAPH PAPER AFTER COMPLETING THE THIRD GRAPH.
C
      IF(NG-3) 8,7,8
    7 CALL TPRINT (1,0.,+8.0,0.1)
      CALL SPRINT('IS DRAWN FIRST',14,0.2,+8.0,0.1,0.)
      CALL TPRINT (2,1.70,+8.0,0.1)
      CALL SPRINT('SECOND AND', 10,1.90,+8.0,0.1,0.)
      CALL TPRINT(6,3.1,+8.0,0.2)
      CALL SPRINT ('THIRD',5,3.3,+8.0,0.1,0.)
    8 RETURN
      END
```

```
      SUBROUTINE SHFL(NS)
CCCCCCCCCCCCCCCCCCCCCCCCCCCCCCCCCCCCCCCCCCCCCCCCCCCCCCCCCCCCCCCCCCCC
C                                                                     C
C        SHFL CHANGES THE ORDER IN WHICH POINTS ARE DRAWN,            C
C        TO ELIMINATE NEEDLESS PEN TRAVEL.                            C
C                                                                     C
C        THE RESULTING DRAWING DIRECTIONS ARE--                       C
C                                                                     C
C                          D1          D2                             C
C              CURVE 1     R-L         L-R                            C
C              CURVE 2     L-R         R-L                            C
C              CURVE 3     R-L         L-R                            C
C                                                                     C
C        WITHOUT THE OPERATION OF SHFL, ALL CURVES WOULD BE           C
C        DRAWN FROM RIGHT TO LEFT.                                    C
C                                                                     C
CCCCCCCCCCCCCCCCCCCCCCCCCCCCCCCCCCCCCCCCCCCCCCCCCCCCCCCCCCCCCCCCCCCC
C
C        ALLOCATIONS.
C
      COMMON S(2),ZS(2),SD(2),NPR(2),X(3,25),Y(3,25),ZMAX(2),ZMIN
     $(2),TITLE(2,9,5),NPTS(3)
      NP= NPTS(NS)
C
C        ESTABLISH THE POINT NUMBERS TO BE INTERCHANGED, THE
C        M-TH AND THE NHI-TH.
C
      DO 1 M=1,NP
      NHI=NP-M+1
C
C        TEMPORARILY RENAME THE VALUE OF THE LOW-SEQUENCE-
C        NUMBER COORDINATES.
C
      T1=X(NS,M)
      T2=Y(NS,M)
C
C        PUT THE HIGH SEQUENCE NUMBER VALUE WHERE THE LOW FOR-
C        MERLY WAS.
C
      X(NS,M)=X(NS,NHI)
      Y(NS,M)=Y(NS,NHI)
C
C        GIVE THE HIGH END LOCATION THE RENAMED VALUE OF THE
C        LOW END VARIABLE.
C
      X(NS,NHI)=T1
      Y(NS,NHI)=T2
      IF((NP-M).GE.NP/2) RETURN
    1 CONTINUE
      RETURN
      END
```

```
//D2 JOB (XXXX,XX,035,06,1000,),'$$$BUDRAYGER$$$',CLASS=M
/*PASSWORD
// EXEC F4GCXM     FORT G COMPILE (NODECK), EXECUTE, CLASS M
//FORT.SYSIN DD *
CCCCCCCCCCCCCCCCCCCCCCCCCCCCCCCCCCCCCCCCCCCCCCCCCCCCCCCCCCCCCCCCCCCCCCC
C                                                                      C
C         D2 DRAWS REPORT-READY GRAPHS OF TYPES 4--9, OF               C
C         THE PERMITTIVITIES AND HUMID-CAPACITANCE CHANGE              C
C         VS. THE FRACTIONAL WEIGHT INCREASE BY ADSORPTION             C
C         OF AMBIENT WATER VAPOR. AXES ARE SCALED FOR EACH             C
C         GRAPH.                                                       C
C         THE MAIN PROGRAM READS THE DATA, AND CONTROLS THE            C
C         FLOW THROUGH THE TEMPERATURE-MODE COMBINATIONS,              C
C         DRAWING THE GRAPH OF EACH TYPE IN SUCCESION. EVEN            C
C         NUMBERED GRAPH TYPES HAVE CURVES FOR THREE SPE-              C
C         CIFIC HIGH FREQUENCIES, AND ODD TYPES FOR THREE              C
C         LOW FREQUENCIES.                                             C
C                                                                      C
CCCCCCCCCCCCCCCCCCCCCCCCCCCCCCCCCCCCCCCCCCCCCCCCCCCCCCCCCCCCCCCCCCCCCCC
C
C         ALLOCATIONS.
C
      INTEGER TITLE
      REAL R(2),EP(25,20,2,5),EDP(25,20,2,5),DC(25,20,2,5),O(2,201),
     1ORDNT(25,20,2,5)
      COMMON S(2),ZS(2),SD(2),NPR(2),X(3,25),Y(3,25),ZMAX(2),ZMIN
     $(2),TITLE(2,9,5),NPTS(3)
      COMMON/SET49/WR(20,2,5),LSP(6,20,2,5),KM(2,5)
      NAMELIST/TWO/NT,KM,LSP,WR,EP,EDP,O,TITLE
C
C         READ THE DATA FROM THE DATA SET.
C
      READ (2) NT,KM,O,TITLE,LSP,WR,EP,EDP,DC
C
C         IF DESIRED, WRITE ITS CONTENTS.
C
      READ (5,1) QPRINT
    1 FORMAT (79X,F1.0)
      IF(QPRINT.NE.0.) WRITE(6,TWO)
C
C         INITIALIZE THE CALCOMP PACKAGE, THE GRAPH SHEETS, AND
C         THE CONTROL INDICES.
C
      CALL PLSTRT(2222,22)
      CALL PLOT(3.,1.50,-3)
      NG=0
      NSP=0
      NGADVQ=1
```

```
C
C          T-MC'S ARE ITERATIVELY ESTABLISHED HERE.
C
      DO 13 I=1,NT
      DO 13 J=1,2
C
C          FOR EACH TEMPERATURE-MODE COMBINATION, SET AND/OR STEP
C          THE GRAPH TYPE INDEX.
C
      NTP=3
    2 NTP=NTP+1
C
C          SET A NEW ORIGIN WHEN NECESSARY.
C
      IF(NGADVQ) 3,4,3
    3 NG=NG+1
      CALL PLOT(O(1,NG),O(2,NG),-3)
C
C          PRINT A MESSAGE IDENTIFYING EACH GRAPH.
C
    4 WRITE (6,5) NTP,NG,I,J
    5 FORMAT('0',' NTP ='I2,', NG = 'I3,', I = 'I2,', J = 'I2)
C
C          ELIMINATE ALL UNESSENTIAL AND/OR UNCONTROLLED NUMBERS
C          FROM THE BLOCK OF STORAGE WHICH WILL BE FILLED WITH
C          GRAPH DRAWING INFORMATION.
C
      DO 6 NS=1,3
      NPTS(NS)=0
      DO 6 N=1,25
      X(NS,N)=0.
    6 Y(NS,N)=0.
      NGADVQ=1
C
C          PROCEED WITH SETTING UP THE GRAPH OF THE PRESENT TYPE,
C          WITH THE PROPER ORDINATE ARRAY (FIRST ARGUMENT), AND
C          FREQUENCY-RANGE-STARTING-INDEX (SECOND ARGUMENT).
C
      GO TO (7,7,7,7,8,9,10,11,12),NTP
    7 CALL SETL6( EP,1,NG,NTP,I,J,NGADVQ, 13, 2)
    8 CALL SETL6( EP,4,NG,NTP,I,J,NGADVQ, 13, 2)
    9 CALL SETL6(EDP,1,NG,NTP,I,J,NGADVQ, 13, 2)
   10 CALL SETL6(EDP,4,NG,NTP,I,J,NGADVQ, 13, 2)
   11 CALL SETL6( DC,1,NG,NTP,I,J,NGADVQ, 13, 2)
   12 CALL SETL6( DC,4,NG,NTP,I,J,NGADVQ, 13, 13)
   13 CONTINUE
      CALL PLTEND
      STOP 222
```

```
C              ************************************************
C              *                                              *
C              *****THE JOB CONTROL LANGUAGE CARDS BELOW******
C              *****BETWEEN ''/*'' AND ''/*EOJ''         *****
C              *****ARE PLACED BEHIND THE DECK FOR SUB-  *****
C              *****ROUTINE SHEL WHEN ACTUALLY RUNNING   *****
C              ***** THE PROGRAM.                        *****
C              *                                              *
C              ************************************************
      END
/*
//GO.FT02F001 DD DSN=THREE.DAY.FOR.D2,UNIT=2321,
//      VOL=SER=DCELL1,DISP=OLD
//GO.FT18F001 DD UNIT=TAPE7,DCB=(RECFM=U,BLKSIZE=1440,DEN=1,TRTCH=ET),
//             DISP=OLD,LABEL=(,BLP),VOL=SER=OUTPT,DSN=CALCOMP
//GO.SYSIN DD *
A BLANK IN COLUMN 80 DELETES DATA PRINTOUT.
THE 1 IN COLUMN 80 CAUSES DATA PRINTOUT.                        1
/*EOJ
```

```
      SUBROUTINE SETL6(ORDNT,NSPST,NG,NTP,I,J,M,*,*)
CCCCCCCCCCCCCCCCCCCCCCCCCCCCCCCCCCCCCCCCCCCCCCCCCCCCCCCCCCCCCCCCCCCC
C                                                                     C
C        SETL6 ENGAGES THE PROPER TRIO OF FREQUENCY-PARA-             C
C        METERS, AND FILLS THE THREE CURVES' ORDINATE AND             C
C        ABSCISSA ARRAYS.                                             C
C                                                                     C
CCCCCCCCCCCCCCCCCCCCCCCCCCCCCCCCCCCCCCCCCCCCCCCCCCCCCCCCCCCCCCCCCCCC
C
C        ALLOCATIONS.
C
      INTEGER TITLE
      REAL ORDNT(25,20,2,5)
      COMMON S(2),ZS(2),SD(2),NPR(2),X(3,25),Y(3,25),ZMAX(2),ZMIN
     $(2),TITLE(2,9,5),NPTS(3)
      COMMON/SET49/WR(20,2,5),LSP(6,20,2,5),KM(2,5)
C
C        INITIALIZE.
C
      Z=0
      KBAD=0
      NCVS =0
      NSPENC=NSPST+2
C
C        IF THERE IS NO DATA AT THIS TEMPERATURE-MODE COMBINA-
C        TION, RETURN TO MAIN AND ITERATE TO THE NEXT.
C
      IF(KM(J,I)) 7,7,1
C
C        FOR EACH OF THE SPECIAL FREQUENCIES IN TURN, ...
C
    1 DO 6 NSP=NSPST,NSPENC
      NS=NSP
      IF(NSP.GE.4) NS=NSP-3
      NRH=KM(J,I)
      NPTS(NS)=NRH
C
C        ... AND FOR ALL THE RELATIVE HUMIDITIES--
C
      DO 5 K=1,NRH
      IF(NCVS) 2,2,4
    2 NSP1=NSP+1
      NSP2=NSP+2
```

```
C
C         TEST TO ASSURE THAT DATA HAS BEEN TAKEN AT AT LEAST ONE
C         OF THE FREQUENCIES IN THE PRESENT GROUP. IF NOT, WRITE
C         A MESSAGE, ONLY ONCE PER T-MC, THAT THERE IS NO DATA.
C
      IF(LSP(NSP,K,J,I).EQ.0.AND.LSP(NSP1,K,J,I).EQ.0.AND.LSP(
     $NSP2,K,J,I).EQ.0.AND.NTP.LE.5) WRITE(6,3)I,J,K,NSPST
    3 FORMAT(' THERE IS A ZERO-TRIPLET OF LSP''S FOR I,J,K,',
     $'  STARTING NSP = '3(I3,','),'   'I2)
C
C         IF NO RELATIVE HUMIDITY FOR THE T-MC HAS DATA FOR THE
C         FREQUENCY GROUP, RETURN SO AS TO CHANGE ONLY THE GRAPH
C         TYPE.
C
      IF (LSP(NSP1,K,J,I).EQ.0) KBAD=KBAD+1
      IF(KBAD.EQ.NRH) RETURN 2
    4 IF(LSP(NSP,K,J,I) .EQ.0) GO TO 5
      X(NS,K)=WR(K,J,I)
      Y(NS,K)=ORDNT(LSP(NSP,K,J,I),K,J,I)
      Z=X(NS,K)+Y(NS,K)+Z
    5 CONTINUE
C
C         IF THE SUM OF ALL COORDINATE VALUES ON A CURVE IS
C         NOT ZERO, INCREASE THE EXPECTED NUMBER OF CURVES
C         BY ONE.
C
      IF(Z.GT.0) NCVS=NCVS+1
    6 CONTINUE
C
C         IF THERE ARE POSSIBLY SOME CURVES TO DRAW, PROCEED TO
C         SUBRCUTINE JUSTFY.
C
      IF(NCVS.GT.0) CALL JUSTFY (NG,NTP,NCVS, 7, 8)
    7 M=0
      RETURN  1
    8 RETURN 2
      END
```

IV. Discussion

The research of this eighth semi-annual period has yielded technical findings that bear on problems of interest to the Department of Defense. Moreover from this research has come the foundations upon which our future investigations will build.

The data reported here taken on dececters utilizing the PME and Dember effects in gold-doped silicon suggest that such devices may find use in special applications for photodetection in the visible and near infra-red regimes. Greater promise yet is shown by new detector structures to be described in the next Scientific Report. For example, gold-silicon Schottky barrier photodiode employing a new mask geometry in the form of a grating shows advantages in comparison with conventional silicon Schottky barrier photodiodes and most pn junction photodiodes now available. The relevant properties include the following: fast response time, high responsivity, flat spectral reponse between 0.4 and 1.0 microns, high quantum yield and low noise performance. These studies, together with those reported here describing fundamental electronic parameters in Cr-doped gallium arsenide and in n-type indium antiminide, all bear on the design of new types of detectors that potentially may be of interest in many military applications.

Transistors form the heart of the electronic systems used in numerous applications of interest to the Department of Defense: detection, telemetry, navigation, control, surveillance, medicine, etc. In this report we describe two studies critical to the design and optimum application of transistors. The first deals with an effect that can lower the breakdown voltage of a transistor, constituting a failure mode in some circuit applications. This effect, termed premature punch through, is described quantitatively with instructions given as to how it can be controlled or essentially eliminated. The second study deals with the incorporation of systematic model selection into the computer simulation of semiconductor circuit behavior. Compared with other procedures now available, the method described here simplifies computation, saves computational cost, and enables the simulation of larger circuits. It provoked sufficient interest among designers of circuits for radiation environments that the essentials of the method constituted one of five invited papers at the 1971 IEEE Nuclear and Space Radiation Effects Conference (Durham, N. H., July 1971).

Properties exhibited by amorphous semiconductors make them potentially useful in a variety of applications that may involve exposure to irradiation. From the research reported here has come some indications of the ultimate limits of performance to be expected from amorphous semiconductors. More comprehensive indications will appear in future Scientific Reports.